AD NUMBER

AD909220

NEW LIMITATION CHANGE

TO

Approved for public release, distribution unlimited

FROM

Distribution authorized to U.S. Gov't. agencies only; Test and Evaluation; Jan 1973. Other requests shall be referred to Commander, Naval Air Systems Command, Attn: AIR-310B, Washington, DC 20360.

AUTHORITY

USNASC ltr, 4 Sep 1973

REPORT NO. 2765.31/421
HAC REF. NO. C-4634

Contract N000 19-72-C-0212

CONFORMAL ANTENNA ARRAYS STUDY

FINAL REPORT

JANUARY 1972 TO JANUARY 1973

Prepared for the AIR SYSTEMS COMMAND
Department of the NAVY

Creating a new world with electronics

HUGHES

ANTENNA DEPARTMENT
AEROSPACE GROUP
HUGHES AIRCRAFT COMPANY
CULVER CITY, CALIFORNIA

Report No. 2765.31/421
HAC Ref. No. C4634

CONFORMAL ARRAY STUDY

CONTRACT N00019-72-C-0212

FINAL REPORT

January 1972 to January 1973

Prepared by

W. H. Kummer
A. F. Seaton
A. T. Villeneuve

Prepared for
Air Systems Command
Department of the Navy

Antenna Department
Equipment Engineering Divisions
AEROSPACE GROUP
Hughes Aircraft Company - Culver City, California

ACKNOWLEDGMENTS

The following personnel of the Hughes Radar Division contributed to the Conformal Antenna Arrays Study.

Dr. W. H. Kummer	Program Manager Radar Microwave Laboratory
A. F. Seaton	Antenna Department
Dr. A. T. Villeneuve	Antenna Department

The Technical Officer for this program is Mr. J. W. Willis (AIR-310B).

TABLE OF CONTENTS

LIST OF FIGURES

LIST OF FIGURES - Continued

LIST OF FIGURES - Continued

1.0 INTRODUCTION

Several topics relating to conformal arrays have received detailed attention in the last few years. These topics include pattern synthesis, types of appropriate radiating elements, and their impedance and mutual coupling characteristics, and wide angle scanning of linear arrays located on planar and conical surfaces.

Synthesis techniques for the far field patterns from current distributions on planar surfaces are well known. Since there are no proven techniques for synthesizing antenna patterns from arrays on conical surfaces, two different approaches have been pursued:

1. An equivalence principle was used to determine the distribution of sources on a cone to produce a prescribed pattern. Using this approach planar arrays are replaced by sources on a conformal surface. Thus, it is possible to generate patterns using well known synthesis techniques for planar surfaces. The equivalent sources are continuous functions on the cone. The practical validity of the method depends on the accuracy with which the continuous functions can be approximated by physically realizable radiators. Equivalent source distributions were computed at discrete points on a conical surface to approximate the patterns of a specific planar array.
2. The computation of approximate patterns from discrete radiators judiciously positioned on the cone was carried out. An optimiztion was performed to obtain the highest signal-to-noise ratio in the beam pointing direction.

In this report the work on both methods is continued. In the equivalence principle method, excitations and radiation patterns were computed for two particular beam pointing directions. These patterns were then compared to the equivalent far field pattern that would have been produced by the generating planar array. This technique is taken up in Section 2.

In the use of the heuristic method several layouts of readiating elements were considered as discussed in Section 3. Parameters such as variations of sidelobe levels, grating lobes and beamwidths were investigated.

The radiating elements used for all configurations assume that independent control of the polarization can be generated. A crossed slot with two orthogonal outputs is such an element. The element patterns were approximated to a better degree than previously.

The coordinates of all patterns were referenced to the IRIG Standard (Ref. No. 8). The detailed discussion is summarized in Section 4.

Suggestions for future investigations (Section 5) conclude the report.

2.0 PATTERN SYNTHESIS USING THE EQUIVALENCE PRINCIPLE

The field equivalence principle discussed in the Final Report on Contract N00019-69-C-0281 (Kummer, et al. 1970) has been used to synthesize beams from slots on a cone with a half-angle of 10 degrees. As discussed in that report, the planar array, whose pattern is to be approximated by that of the conical array, consisted of 24 half-wavelength slots on a circular groundplane. The slots were spaced at 0.7 wavelength intervals on a square grid as illustrated in Fig. 2-1. The calculated E-plane and H-plane patterns of the planar array are shown in Fig. 2-2.

The cone on which the equivalent sources were placed has an angle, θ_o, of 170 degrees and a base diameter of 5.08 wavelengths. The sources on the cone were short crossed-slots arranged in rings about the cone. The adjacent rings were separated 0.7 wavelength, with the first ring 0.7 wavelength from the tip. The azimuthal spacing of the crossed slots in the rings varied between 0.5 wavelength and 0.7 wavelength.

The pattern computation was performed in two steps. First, the equivalent sources on the cone were computed by determining the field of the planar array on the conical surface.* Then the pattern of these equivalent sources was computed. In the pattern computations the same approximate element pattern was used as has been used in all other pattern computations to date, i.e., if the slot is visible from the field point, the element pattern is that of a short slot in a groundplane tangent to the cone; if the element is not visible, the element pattern is zero.

Patterns were calculated for two cases:

a. the beam directed along the cone axis
b. the same beam directed 70° from the cone axis with vertical polarization.

A sample of the cone excitation along a generatrix and along one ring is illustrated for case (b) in Figures 2-3a and 2-3b.

---

*Due to an error in the computer program, the equivalent sources shown in Kummer, et al. (1970) are not correct. The program has been corrected and new equivalent sources were computed.

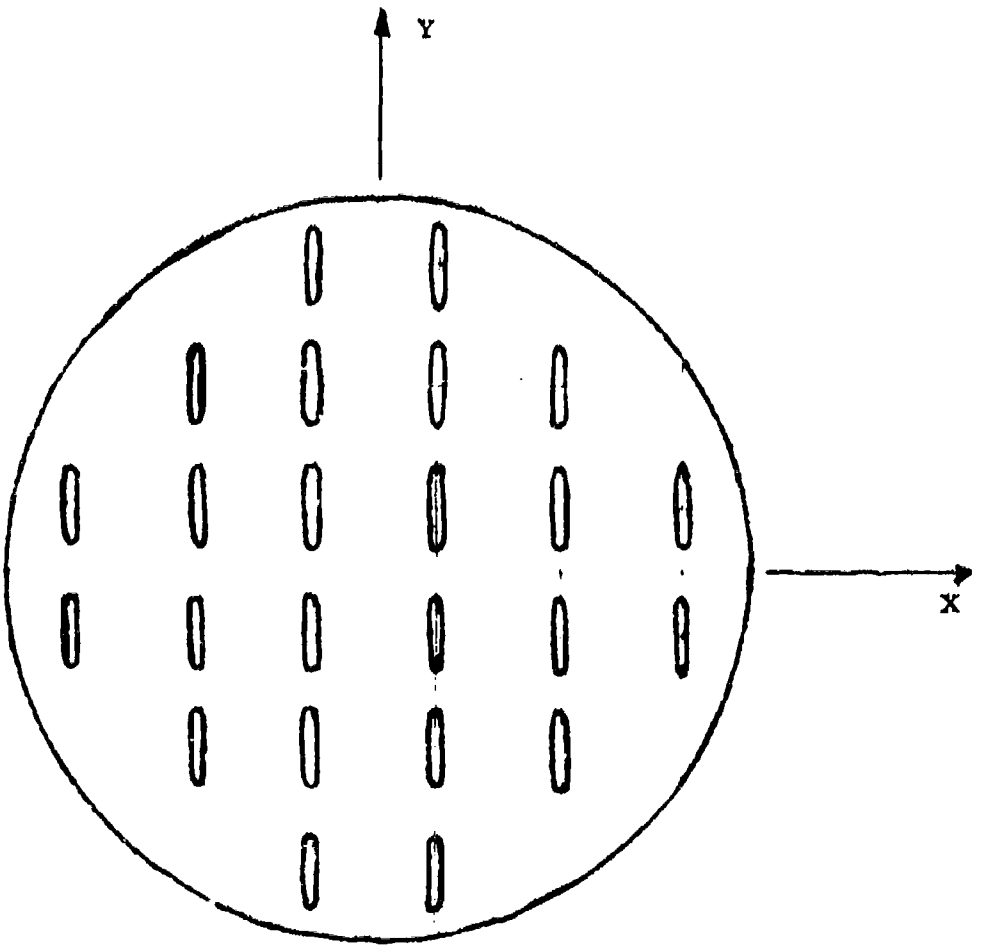

Figure 2-1. Reference Planar Array Slots are Half-Wavelength Long - Spacing is 0.7 Wavelength in X and Y Directions.

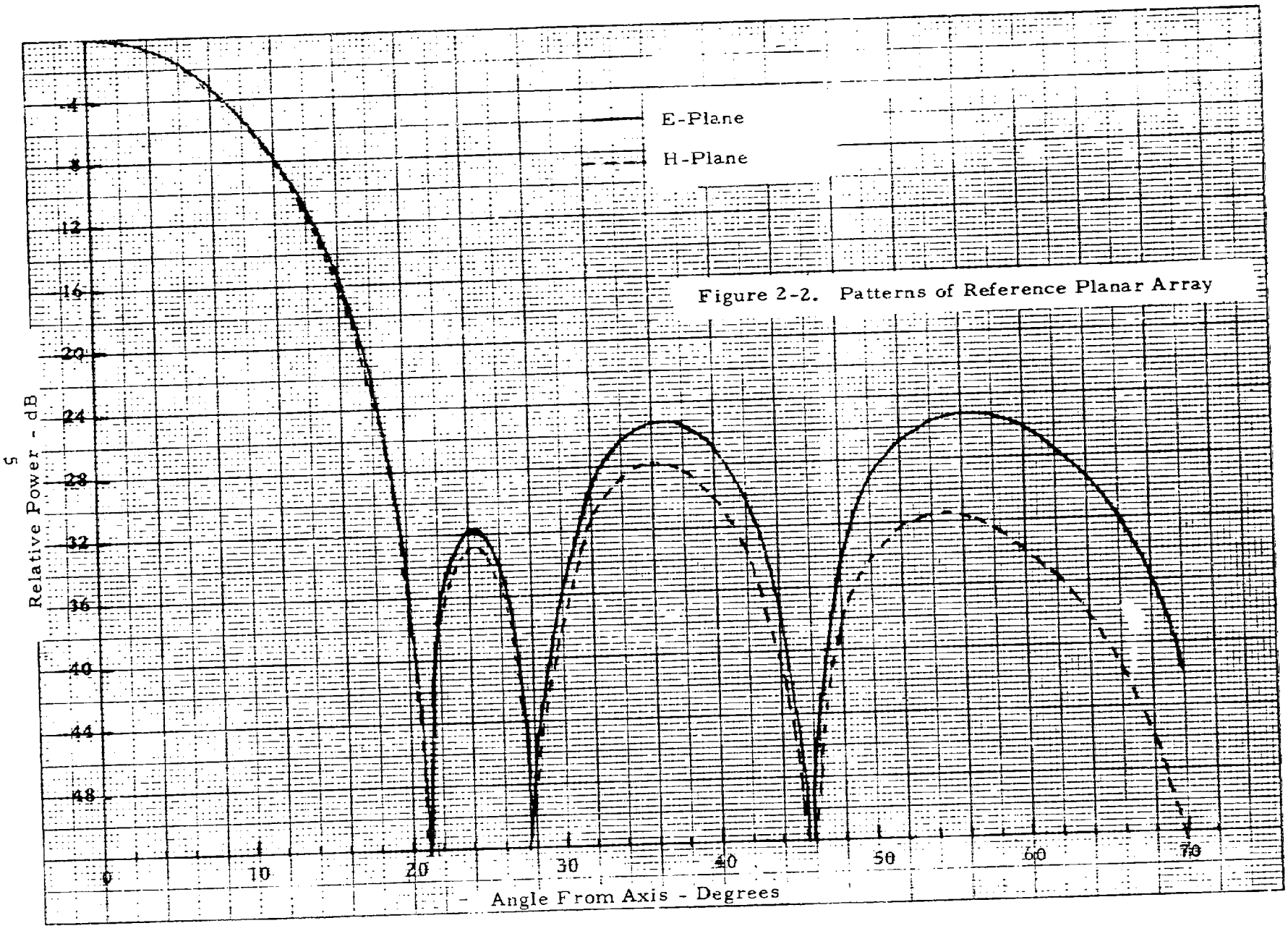

Figure 2-2. Patterns of Reference Planar Array

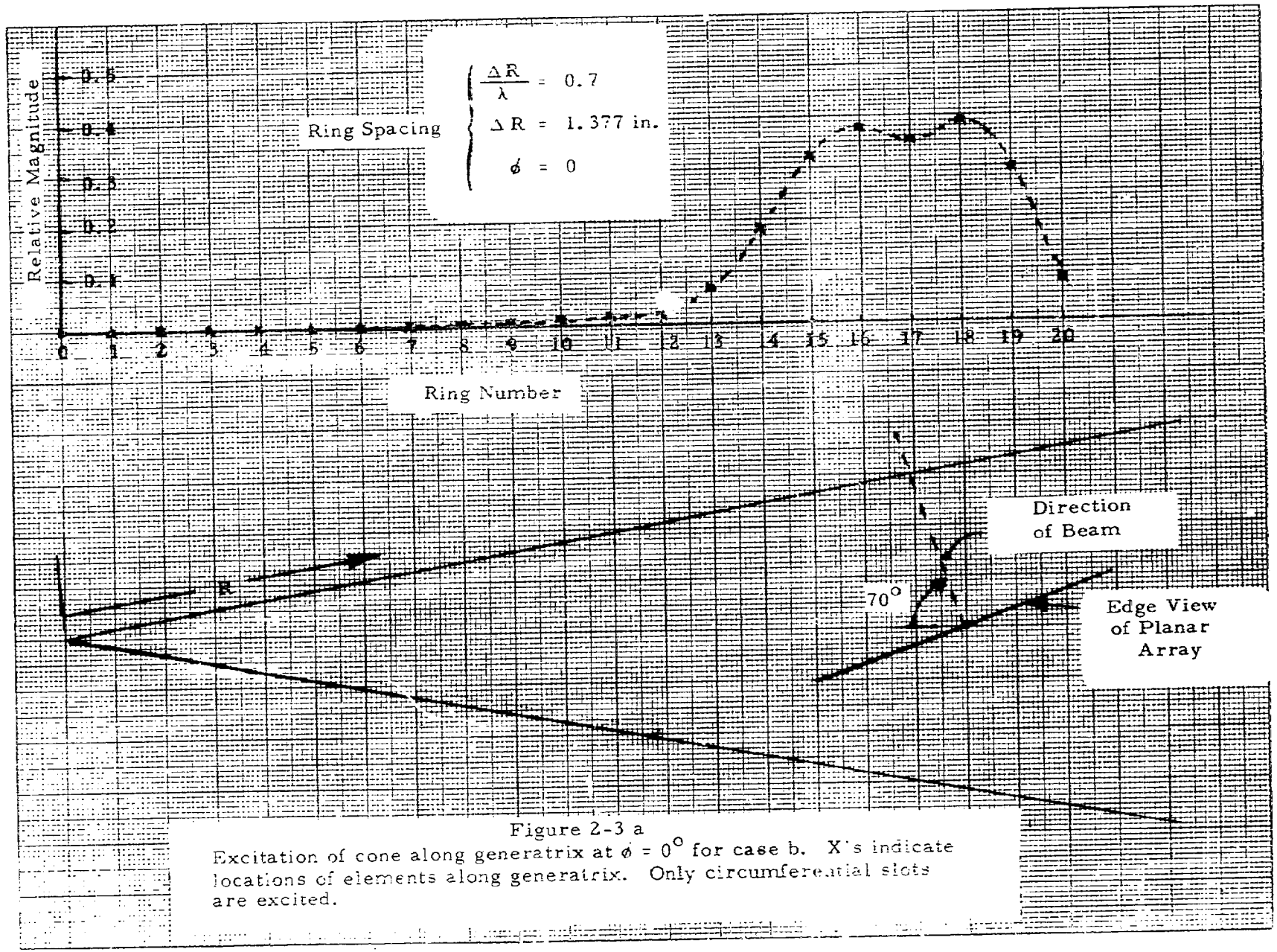

Figure 2-3 a

Excitation of cone along generatrix at $\phi = 0^{\circ}$ for case b. X's indicate locations of elements along generatrix. Only circumferential slots are excited.

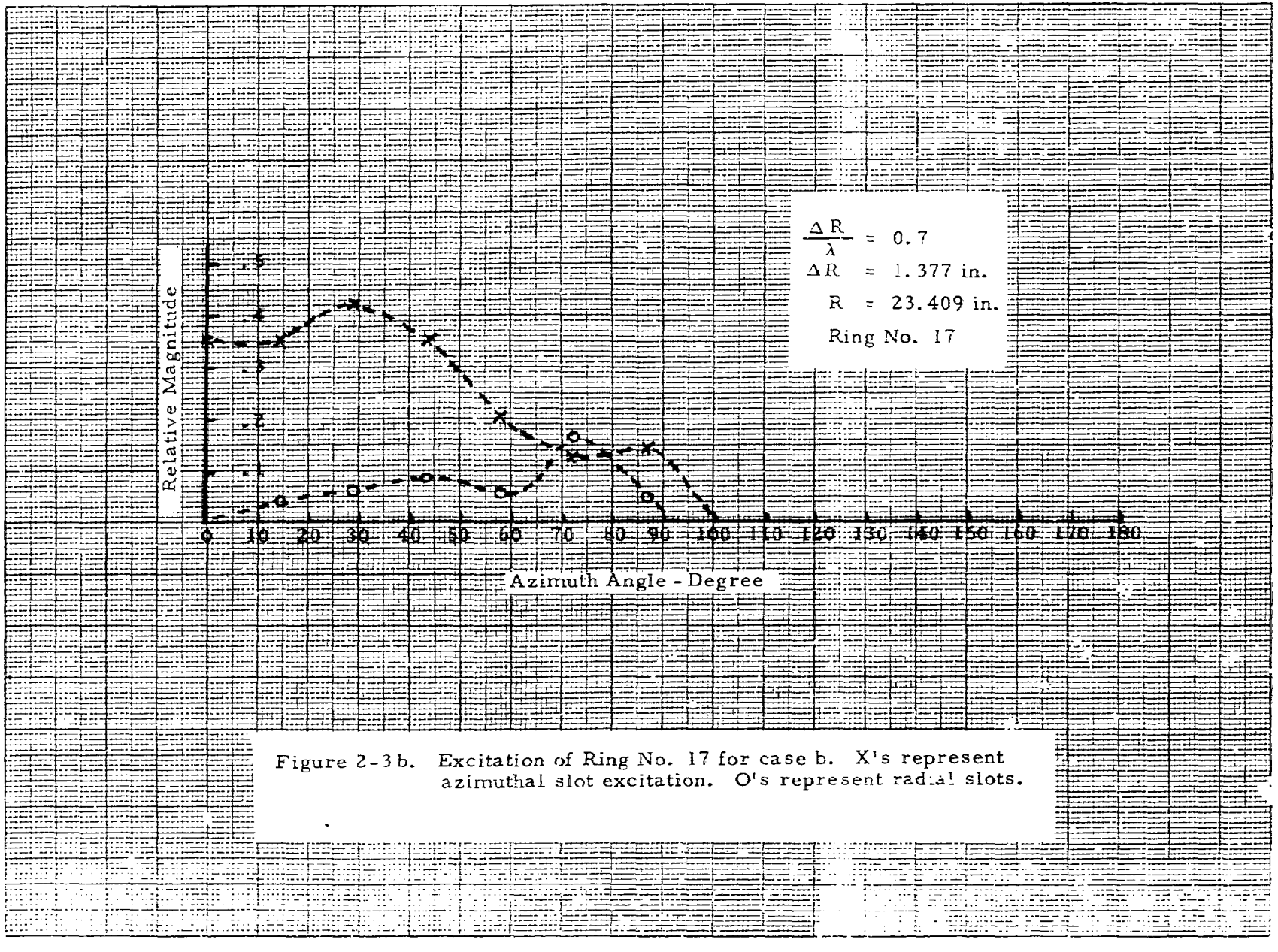

Figure 2-3b. Excitation of Ring No. 17 for case b. X's represent azimuthal slot excitation. O's represent radial slots.

The E-plane and H-plane patterns for case (a) are shown in Figs. 2-4a and 2-4 b. The coordinate system θ', ϕ' used to display the patterns, is oriented so that the beam pointing direction is $\theta' = 90^{\circ}$, $\phi' = 0^{\circ}$. The E-plane cut is taken through the beam with ϕ' held at 0°; the H-plane cut is taken through the beam with θ' held constant at 90°. It is apparent that the beamwidths agree well with those of the desired patterns, though in the region of the first sidelobe the synthesized pattern has a sidelobe only 16 dB down in the H-plane and 20 dB down in the E-plane, whereas the first sidelobe of the desired patterns is about 32 dB down in both planes. The remaining sidelobe levels are about the same for the synthesized patterns as for the desired patterns.

There are several reasons for the discrepancies between the desired patterns and the synthesized patterns. First, the sources of the synthesized patterns are discrete, whereas the required sources are continuous. Second, the element patterns used were only approximate patterns and do not account for the cone curvature or scattering by the cone tip. For the beam directed along the cone axis, the slots near the tip are strongly excited and tip scattering may be significant. The equivalence principle automatically includes these effects in determining the source distribtuions and, if they were accounted for in the element patterns, better agreement between synthesized patterns and desired patterns should result. When the beam is steered away from the cone axis the tip region is not strongly illuminated and the effects of tip scattering should not be so significant. This effect is illustrated in Figs. 2-5a and 2-5b, which show the synthesized patterns for case (b). The agreement between the desired patterns and the synthesized patterns is excellent. The main beams agree very closely and the sidelobe structures are also in good agreement. This agreement is especially good in the H-plane, since the element patterns used for computation in that plane are closer to the correct element patterns. It is evident that the cross-polarized patterns are at very low levels. In the E-plane the symmetry of the slot arrangement on the cone cancels out any cross-polarization. In the H-plane the symmetry is not maintained at points away from the beam peak, but the excitations as determined from the equivalence principle, keep the cross-polarized patterns at a low level.

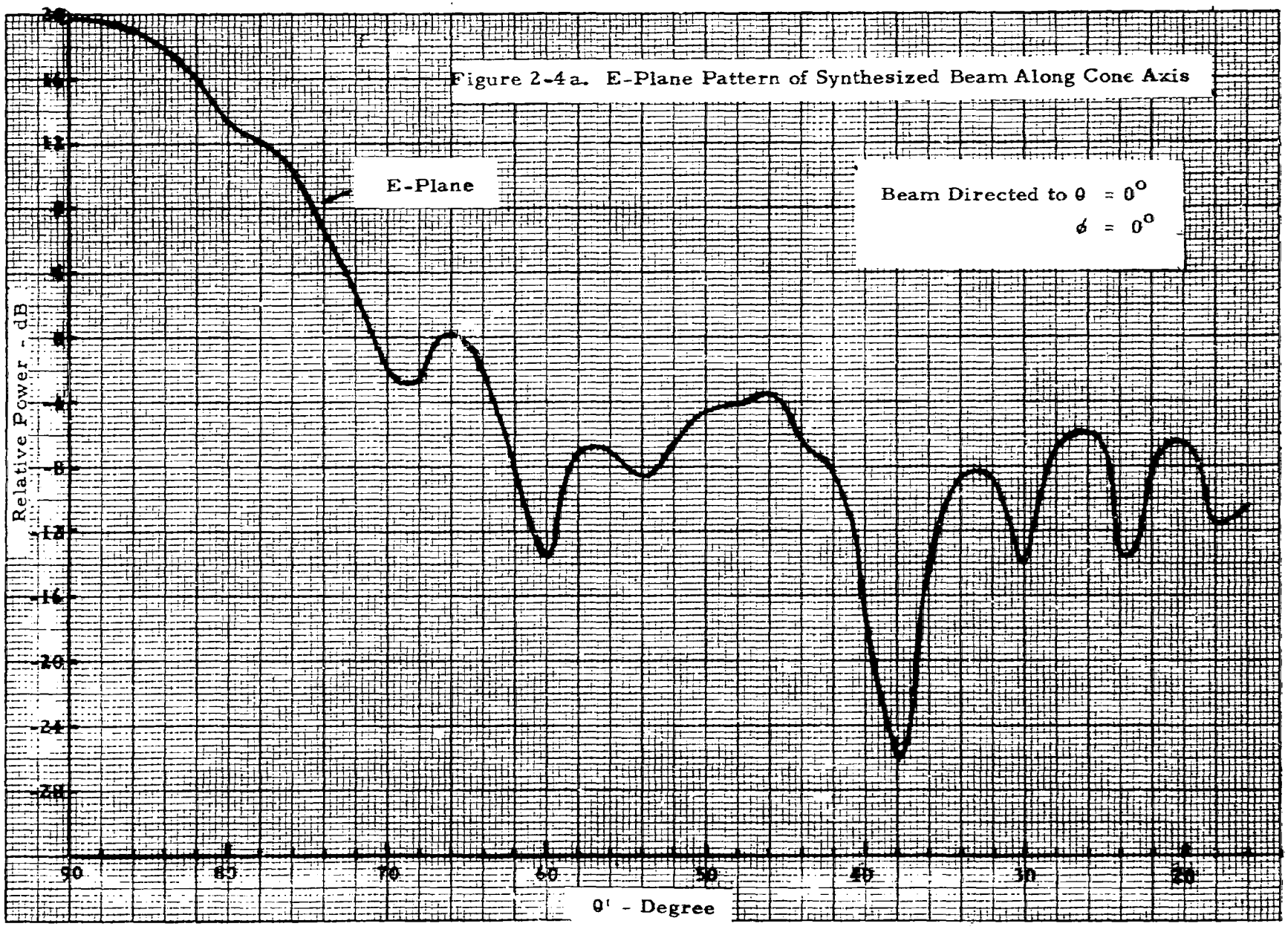

Figure 2-4a. E-Plane Pattern of Synthesized Beam Along Cone Axis

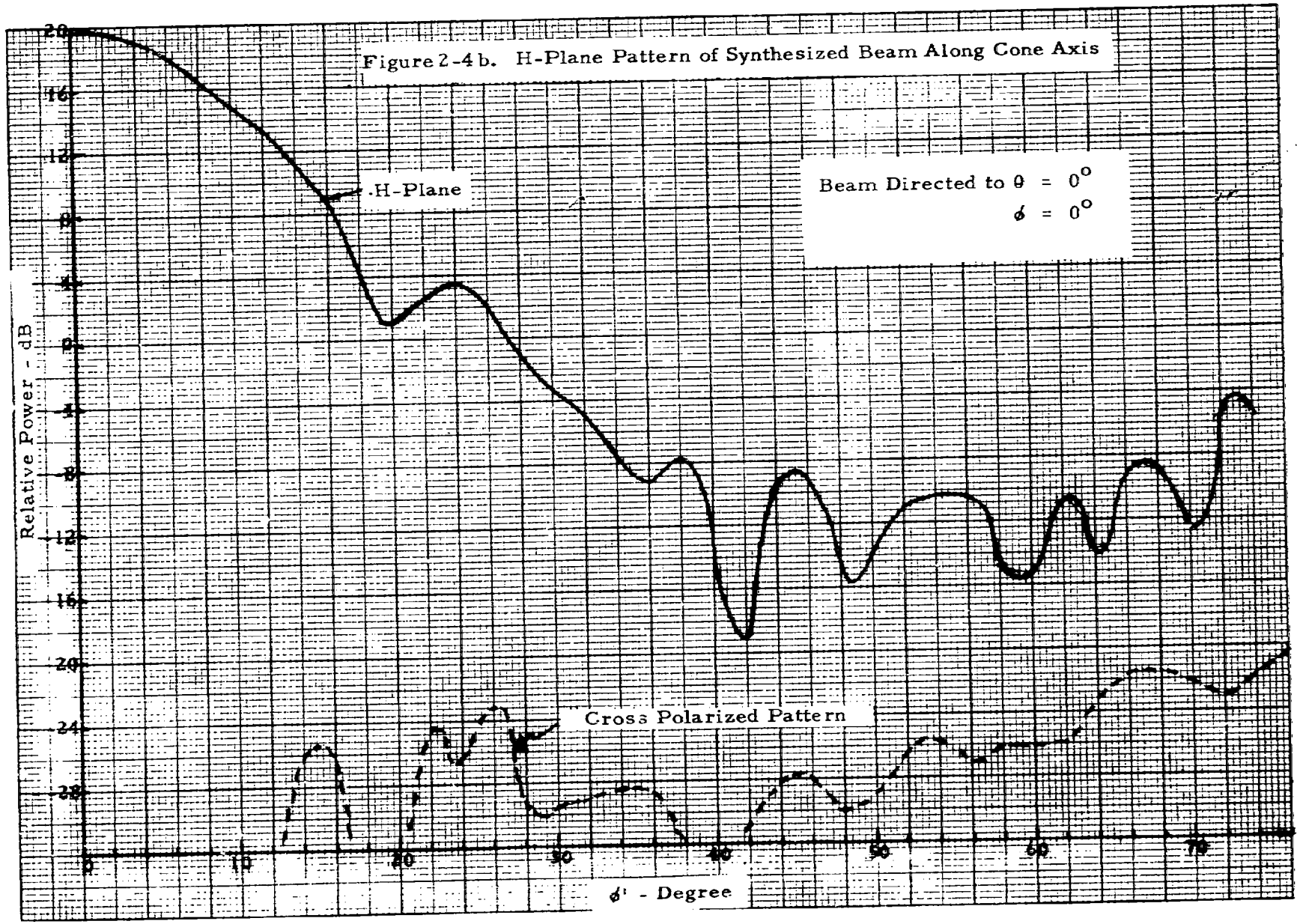

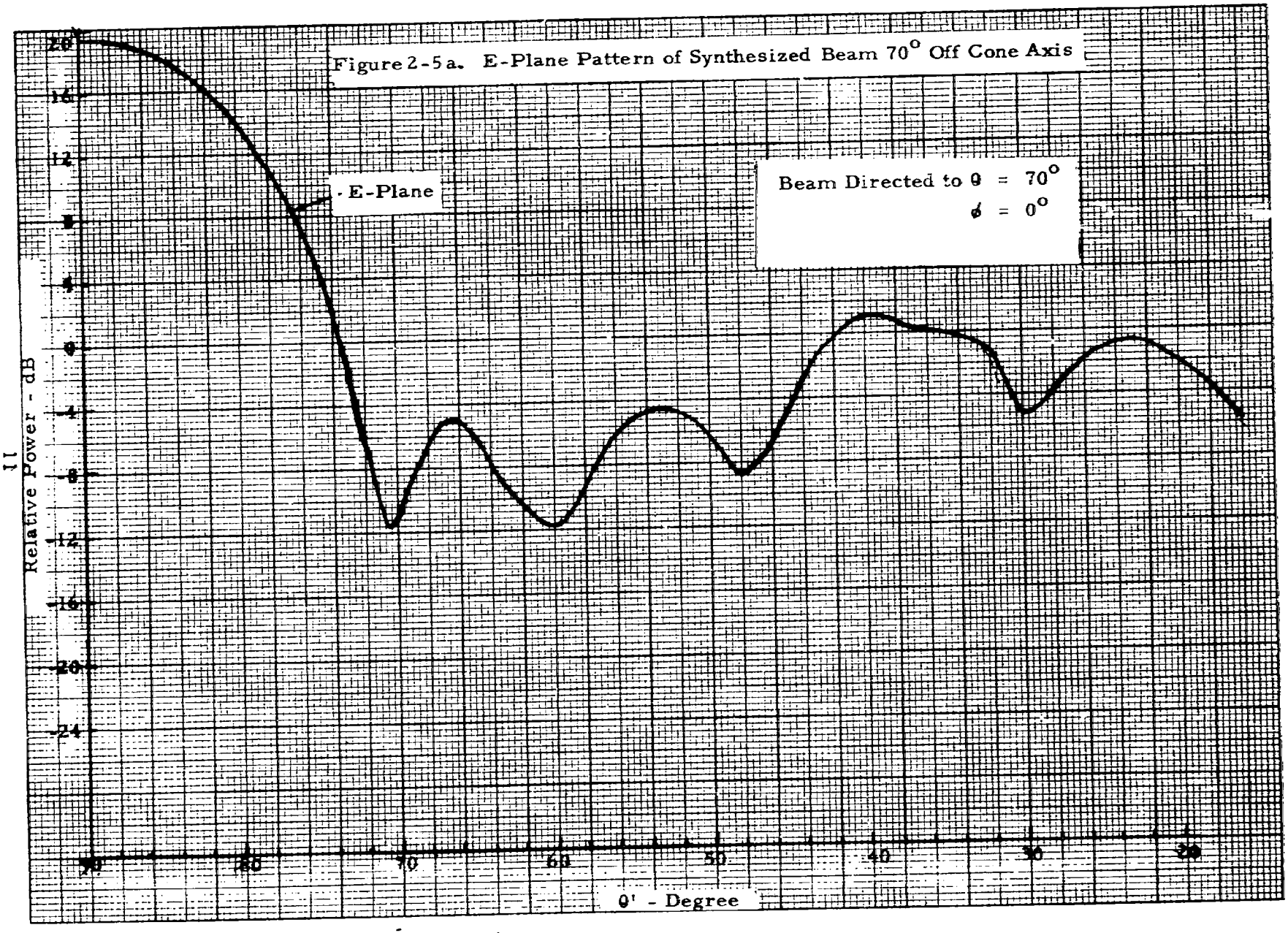

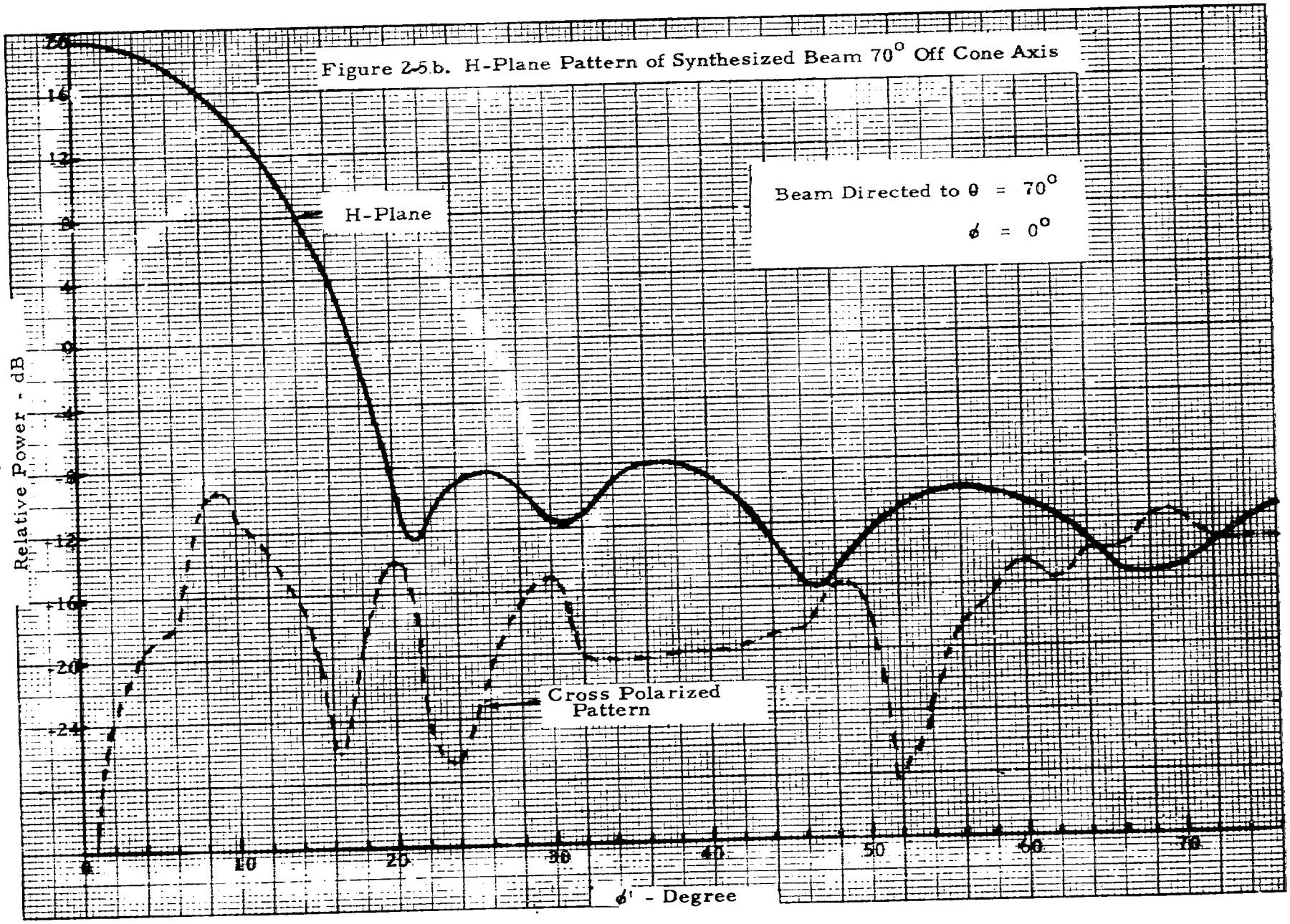

These calculations indicate that the equivalence principle can be a powerful tool when applied to the synthesis of antenna patterns from general conformal arrays.

3.0 HEURISTIC METHODS OF BEAM SYNTHESIS

This section summarizes the results of pattern computations made for several different slot configurations. The placement of the elements for these configurations was based to a large extent on extrapolations from linear and cylindrical array theory and experience. To a lesser extent considerations of the practical problems of actually building such an array influenced the slot configurations chosen for study.

3.1 288 ELEMENT CONFIGURATION

In this particular part of the program a 288 element array was examined. The arrangement of elements for the filled cone was as shown in Table I. The abrupt steps from 16 to 8, and from 8 to 4 were necessitated by the physical size of the crossed waveguide elements assumed for the cone and the interlaced arrangement used for closest packing (see Figure 3.1-1). The locations of the centers of phase of the elements are shown to scale in Figure 3.1-2 in an "unrolled" view of the cone.

Table I
Distribution of Elements on Full Cone

Location On Cone	Number of Rings	Elements per Rings	Number of Elements
Base of cone	9	16	144
Center portion	12	8	96
Upper portion	8	4	32
Near tip (loaded elements)	4	4	16
		Total	288

The center portion of the cone was assumed to contain the same crossed-waveguide elements as those near the base of the cone. The upper portion contained a crossed-waveguide element similar to the others but of a shorter length. The difference in length would make matching more difficult and tolerances would have to be tighter, but the short length

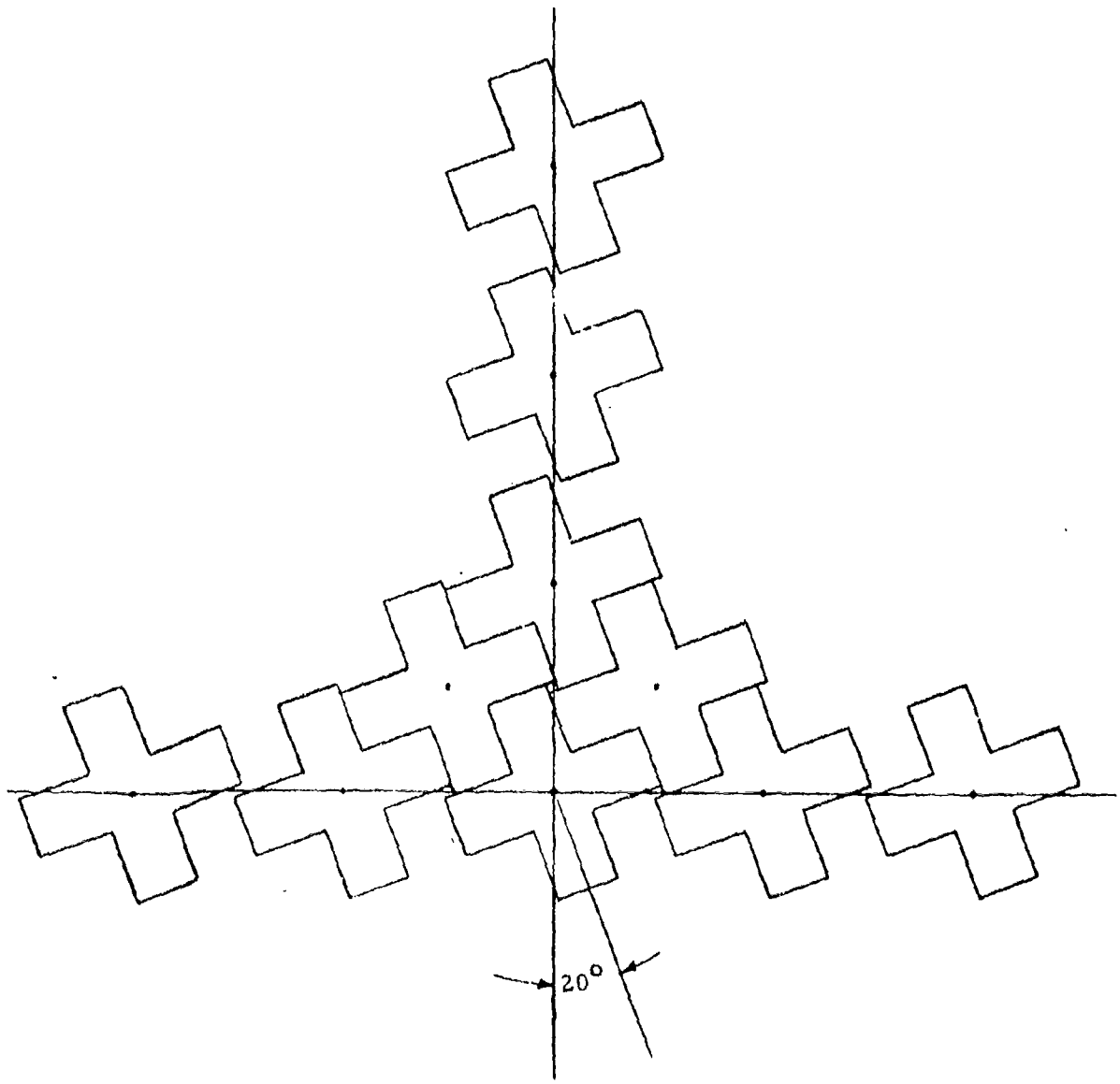

Figure 3.1-1. Closest Packing of Crossed Waveguide Elements Occurs When They are Tilted at an Angle of Approximately 20^{o} in Staggered Arrangement.

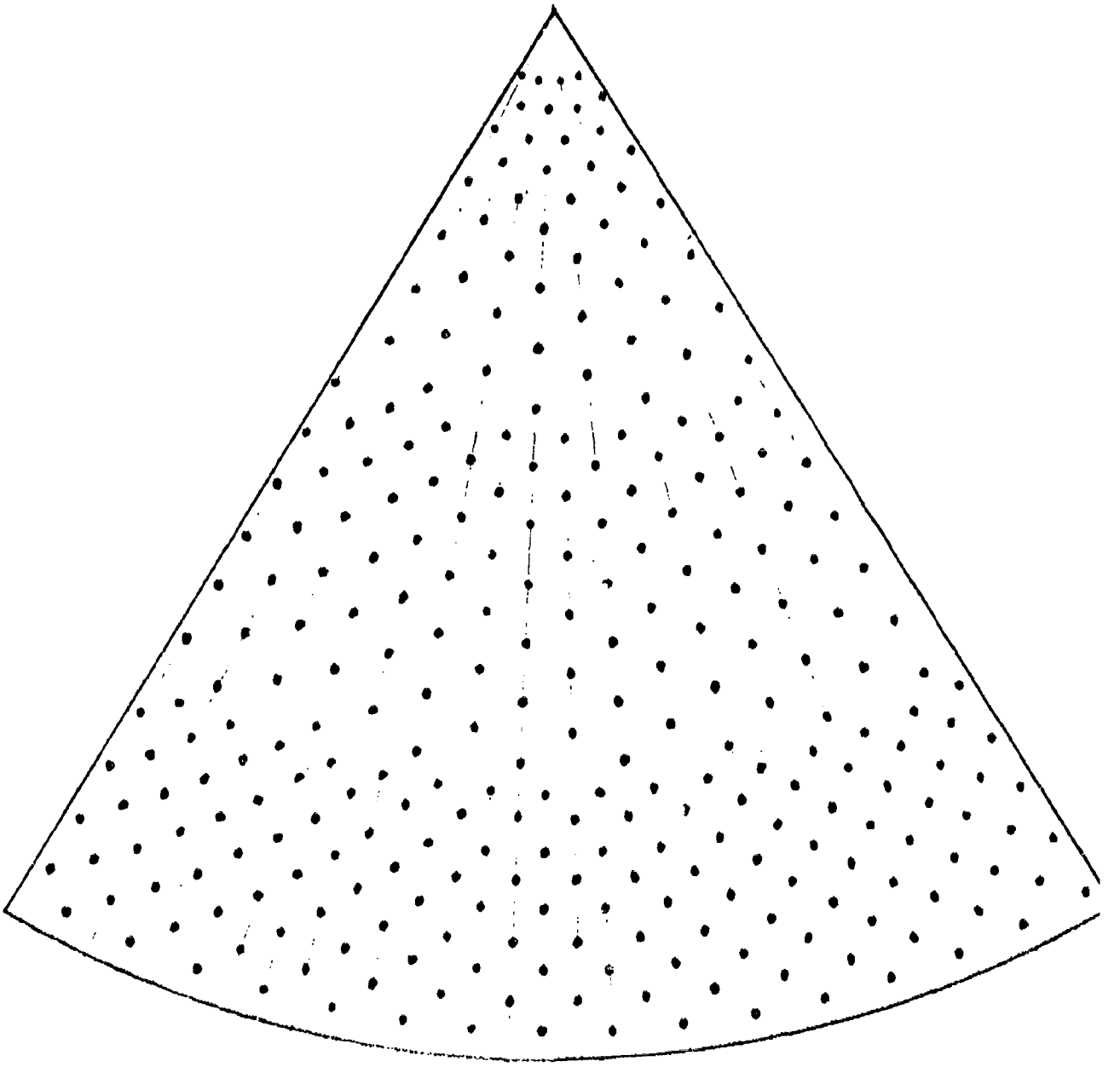

Figure 3.1-2
Scale Drawing of Centers of Phase of the Elements on the Cone
in an "Unrolled" View for 288 Element Configuration

is necessary to permit the location of as many rings as possible in the narrow region of the cone. Near the tip, the upper four rings would have to use loaded elements to make packaging feasible. Even with loaded elements, the first ring is theoretically 3 inches from the tip of the cone. The projected distance between two diametrically opposite elements in this first ring was 1.04 inch or 0.79 λ_o, so that a small "hole" still remained in the center of the aperture.

Computed patterns for this element arrangement with optimum weighting showed a marked difference in beamwidths between the θ and ϕ-polarized beams, and high sharp peaks close to the main beam in the θ-polarized pattern (Seaton, et al, Oct. 1972, pp. 4 and 5). Optimum weighting is defined as that weighting of a conformal array that yields the greatest signal-to-noise ratio when the array is used as a receiving antenna (Kummer, et al, 1970, Appendix B). Computed patterns for this arrangement with no weighting show a significant reduction in the inequality in beamwidths, and the sharp spikes in the θ-polarized pattern are much reduced in amplitude. Hence, all nose-fire patterns in this report are not weighted while all the rest of the patterns are optimally weighted.

It should be pointed out that the crossed waveguide element is not the only one that should be considered for conical arrays. Circular elements would be easier to load with a high temperature dielectric, for example. Also, they would be smaller than the waveguide elements, hence there would be more freedom in placing them on the cone. Although in general it is desirable to keep the number of elements as low as possible and to have some degree of symmetry in the geometry of the slot arrangement, these considerations should not predominate over the attainment of reasonably high efficiency from the available aperture. Hence, it may be necessary to investigate element arrangements where the interelement spacing is so small as to preclude the use of the unloaded crossed waveguide elements.

3.2 APPROXIMATE EXPRESSIONS FOR THE ELEMENT PATTERNS

Some of the first patterns computed for cuts around the cone showed step functions in the grating lobe and far-out sidelobe structure. The cause of this was traced to the element pattern that had been assumed for the ϕ-polarized slots (Seaton, et al, July, 1972).

Some approximate expressions for the patterns of slots on cylindrical surfaces had been previously derived. These expressions fit the published data for such slots quite well; therefore, the following expressions were incorporated into the computer program for the radial slots.

$$E_\phi(\theta, \phi) \simeq \frac{E_\phi(\theta, 0)}{1 + \left|\frac{\phi}{\phi_o}\right|^\nu}$$

where

$$\phi_o = 90 + 24.8 \exp(-0.0179\, k\, a \sin\theta) \text{ degrees}$$

$$\nu = \frac{5}{64}\, k\, a \sin\theta + 3.375$$

a = radius of cylinder approximately equal to cone in size.

$k = 2\pi/\lambda$

$E_\phi(\theta, 0)$ = peak of element pattern at point directly above slot in ϕ plane.

The assumed element pattern for the circumferential slots was left as that of a short slot in an infinite groundplane. This was done because that pattern extends principally along the length of the cone, and in that direction, the cone more nearly resembles a planar surface than a cylindrical surface.

3.3 SUCCESSIVE ELEMENT CONFIGURATIONS

The far-field patterns for the 28Q element configuration were unsatisfactory because of high grating lobes in some of the cuts and relatively high backlobes in other cuts. Hence, several other element configurations were devised.

In a first effort to improve the patterns the number of elements was increased by a factor of 1/2 by increasing the number of generatrices around the cone from 32 to 48. The distance between circles of elements along the generatrices was left unchanged. The same staggered element arrangement was used as for the 288 element case. The only difference between the two arrangements is that the elements are closer together in the ϕ plane. This new arrangement requires 432 elements to cover the cone, and would represent a considerable increase in complexity in practice.

Since the 432 element configuration reduced the element spacing only in the ϕ direction, it was decided to try a different modification of the original 288 element configuration that might improve the patterns of both principal planes. This scheme consisted essentially of extending the break points where the number of elements per ring drops from 16 to 8, and 8 to 4, to points further up toward the tip of the cone. This results in filling in those areas of the cone that were rather sparsely filled in the 288 element configuration. The new element configuration is shown in Figure 3.3-1 in an "unrolled" view. It can be compared to Figure 3.1-2 to visualize the difference in element density. The net result of these changes is to add 72 elements to the layout for a total of 360 elements on the cone.

None of the element configurations discussed so far produced excellent patterns at all beam pointing directions and for all cuts through the beams. Therefore, a more nearly equal distribution of elements over the whole surface of the cone was used. At the same time the interelement spacing was reduced to no greater than $.4\lambda_o$ in the circumferential direction. The inter-ring spacing was left at $.45\lambda_o$, but with the staggered arrangement no longer forced on the elements, the average distance between an element in one ring and its closest neighbors in adjoining rings has been much reduced. These changes resulted in 918 elements on the cone in 36 rings that varied from 4 elements in the ring nearest the tip, to 47 in the bottom ring. The element layout would be similar to that shown in Figure 3.3-2 with the exception that the interelement spacing would be reduced to approximately 1/2 that shown in the Figure in both principal planes.

The 918 elements may be an excessive number to consider for a practical array of this size, however, it should produce nearly ideal patterns and thus show approximately the ultimate in performance that can be expected from a conical array with a half-angle of 10^o.

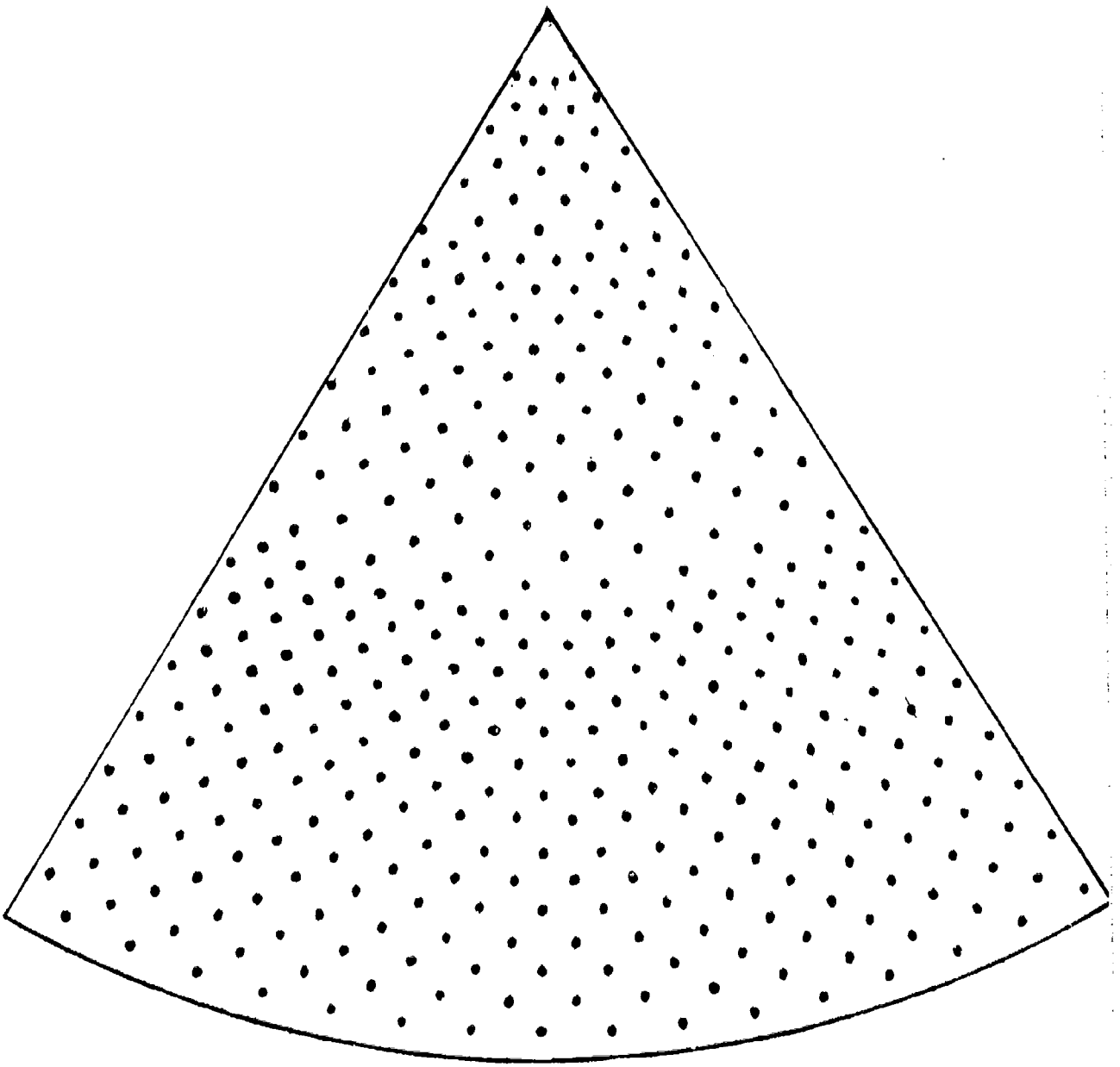

Figure 3.3-1
Scale Drawing of Centers of Phase of the Elements on the Cone
for the 360 Element Configuration

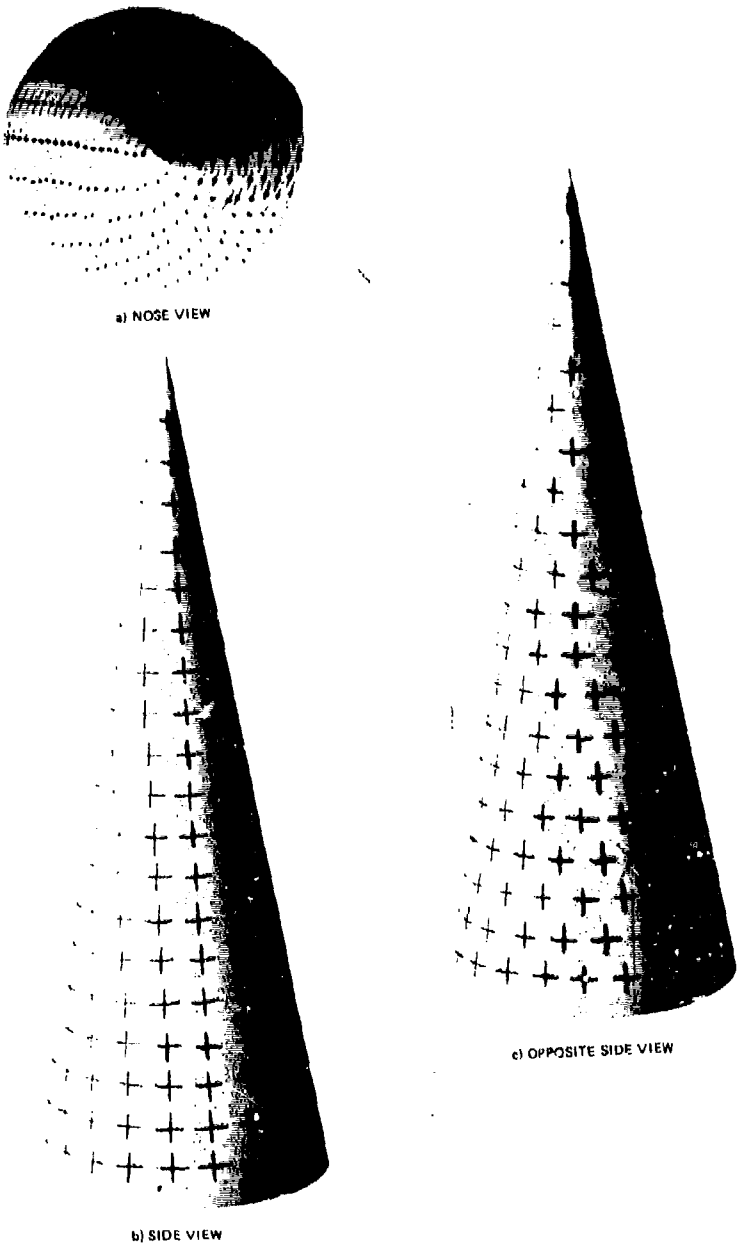

Figure 3.3-2. Cone with elements on rings

3.4 ANALYSIS OF COMPUTED PATTERNS

A selected sample of patterns for the 288, 432 and 360 element configurations (Seaton, et al, July, 1972 and Oct., 1972) are presented here. Patterns for the 918 element configuration are given for comparison. In the format selected the patterns for a particular beam pointing direction and a particular cut for all of the element configurations will be presented together. The 288 element patterns (θ-polarized and ϕ-polarized) will be given first, followed by the 432, 360, and 918 element patterns in that order.

These patterns are all computed in conformity with the IRIG Standard (Ref. No. 8), and Figure 3.4-1 is a simplified version of the IRIG coordinate system to assist in visualizing the beam positions and pattern cuts.

In the discussion of the patterns, a qualitative judgment will be made as to their acceptability or unacceptability. Acceptability depends to a great extent on the use to which an array is to be put. In many cases any grating lobe that causes the gain of the main beam to decrease by several dB would make the performance of the array unacceptable; a grating lobe -20 dB in height, and large in angular extent could subtract that much energy from the main beam. A clean pattern will be defined as one where the rating lobes are no higher than -30 to 35 dB.

A detailed discussion and analysis of the patterns follows in Sections 3.4.1 through 3.4.3.3 below. This will be followed in Section 4.0 by a summary of the results of the pattern study.

3.4.1 Beam Steered to $\theta_1 = 0^\circ$, $\phi_1 = 0^\circ$

Since the aperture is symmetrical in this beam position, only one cut is made for each element configuration. This was arbitrarily chosen to be along $\phi = 0^\circ$. The "nose-fire" patterns all use uniform weighting since it was found that optimum weighting aggravates the interferometer effect as mentioned in 3.1.

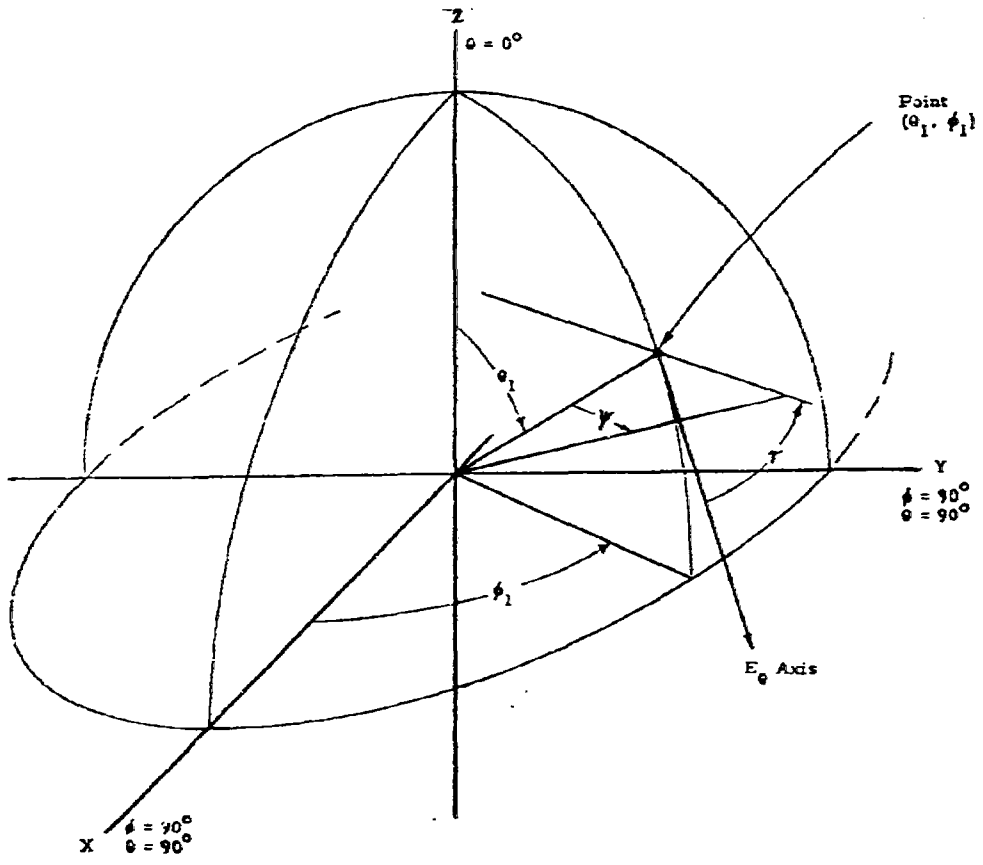

Figure 3.4-1. .Geometry for Pattern Cuts

3.4.1.1 $\phi = 0^\circ$ Cut Through Beam at θ_1, $\phi_1 = 0^\circ, 0^\circ$

The patterns for this cut for four element configurations are given in the series from Figure 3.4-2 through Figure 3.4-9.

The θ and ϕ patterns for the 288 element configuration are given in Figures 3.4-2 and -3, respectively. Although uniform weighting is necessary to improve the main beam performance, the grating lobes appearing, at $\theta = 90^\circ$ are somewhat degraded when compared to the case using optimum weighting and are not satisfactory. The backlobes in both patterns are reasonably low.

The nose-fire patterns for the 432 element configuration are given in Figure 3.4-4 and 3.4-5 for the θ-polarized and ϕ-polarized cases, respectively. All conditions are identical between these two patterns and the previous set except for the closer packing of the elements in the ϕ plane on the cone. As can be seen in Figure 3.4-4 (the θ-polarized pattern) the grating lobe at ψ = 90 to 100 degrees is considerably reduced compared to that in Figure 3.4-2. At most other points there is very little difference in the two patterns. In particular, the main beam and the backlobe areas are almost identical for the two cases.

The ϕ-polarized patterns also show similar characteristics. The grating lobe in Figure 3.4-5 is reduced in magnitude and considerably narrower than it was for the 288 element configuration shown in Figure 3.4-3. The main beams in the two patterns are nearly identical; and the backlobes are similar with some improvement noted in the 432 element case.

The 360 element configuration is considered next. The θ-polarized pattern for the 360 element case is given in Figure 3.4-6. It compares to Figure 3.4-4 for the 432 element case and to Figure 3.4-2 for the 288 element case. The cross-polarized grating lobe in Figure 3.4-6 is quite high and is very little improved over the 288 element case. The grating lobe for the preferred polarization, however, is considerably lower. The 432 element case gives the best suppression of both components of grating lobes of the three configurations considered. The main beam of the 360 element case is somewhat cleaner than either of the other two cases. The backlobe region is different from the other two cases, and it appears to be slightly degraded over a region covering about three backlobes, rather than improved.

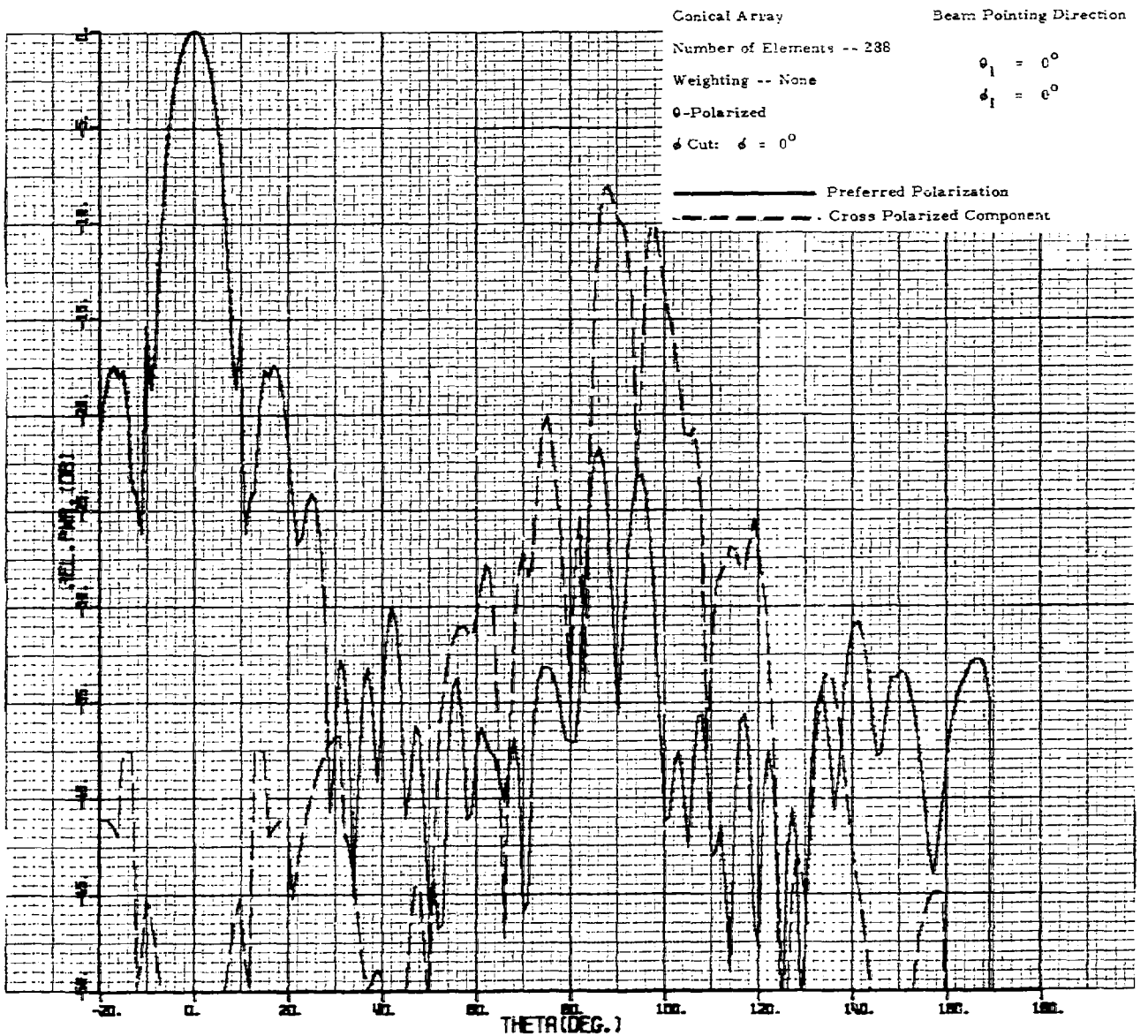

Figure 3.4-2. θ-Polarized Pattern of Nose-Fire Beam for 288 Element Configuration

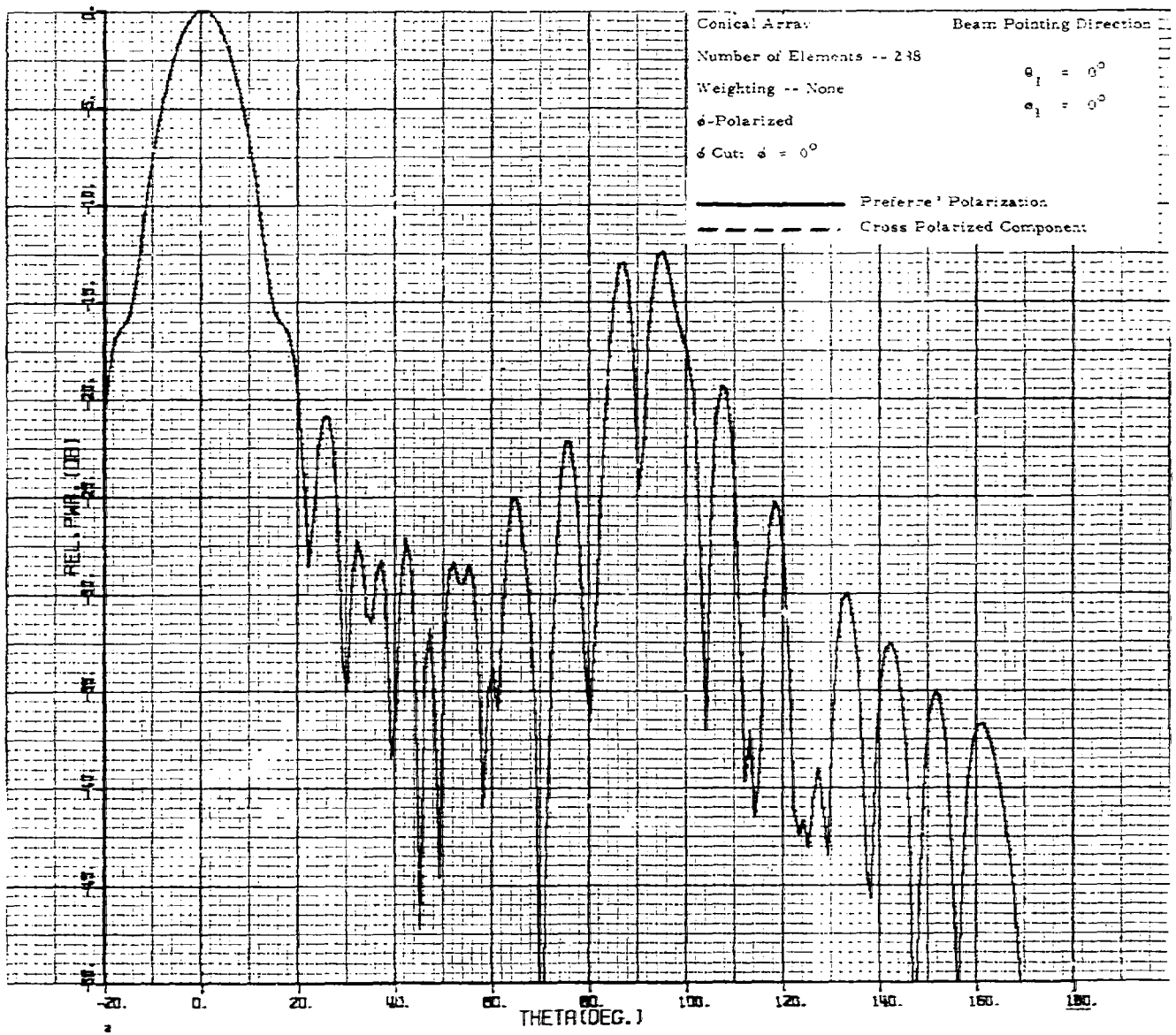

Figure 3.4-3. ϕ-Polarized Pattern of Nose-Fire Beam for 288 Element Configuration

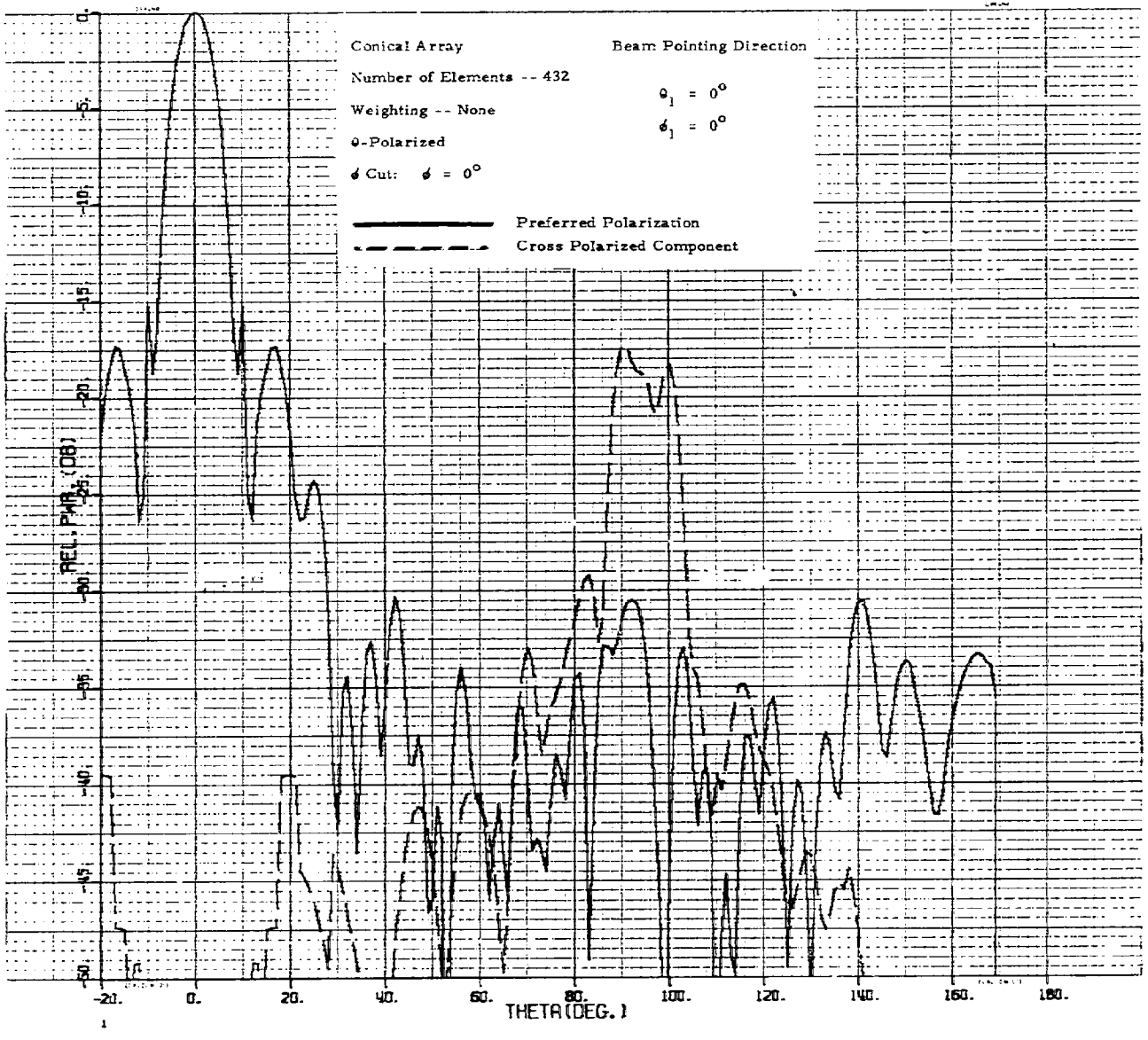

Figure 3.4-4. θ-Polarized Pattern for Principal Plane Cut Through Nose-Fire Beam for 432 Element Configuration

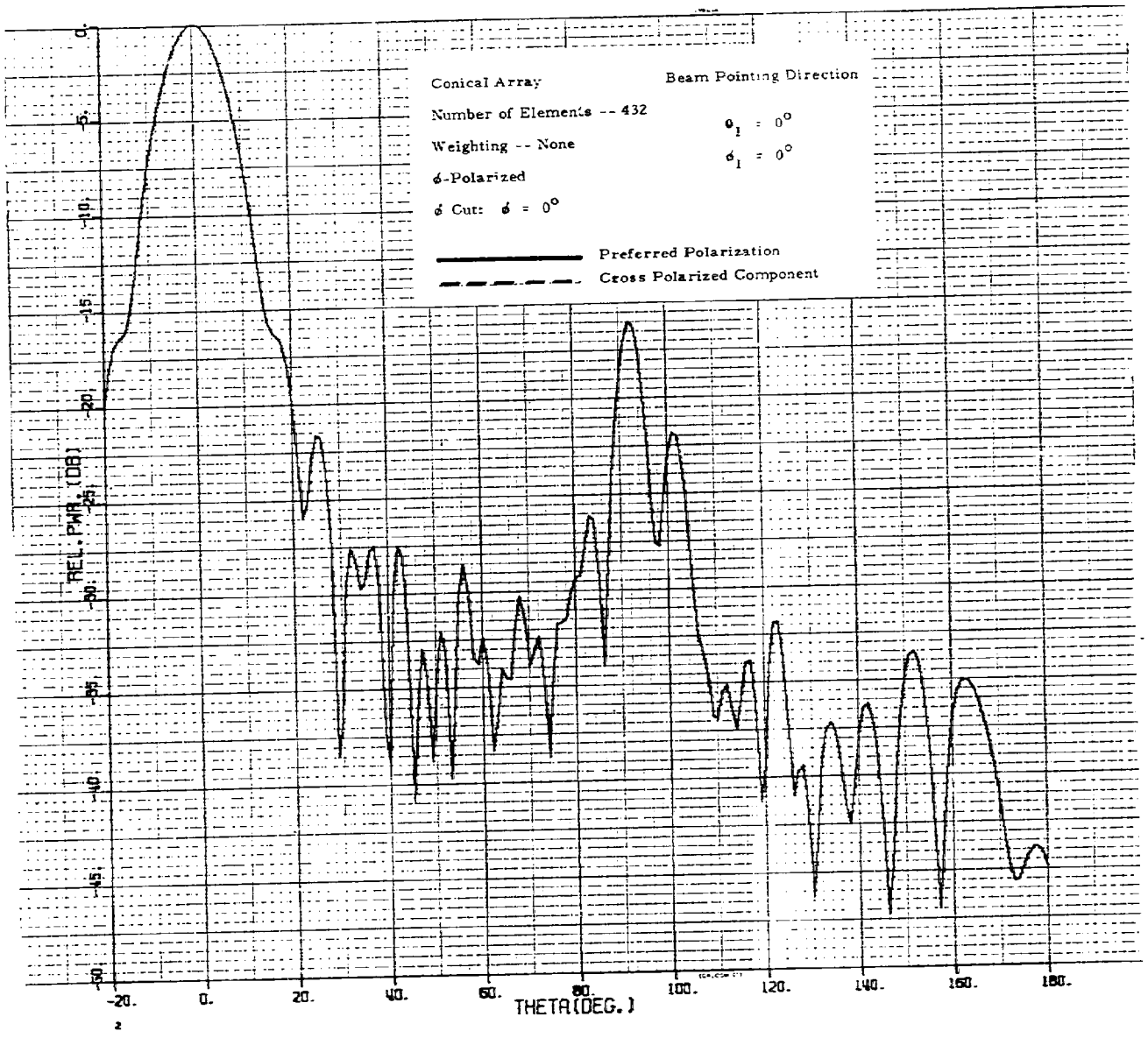

Figure 3.4-5. ϕ-Polarized Pattern of Principal Plane Cut Through Nose-Fire Beam for 432 Element Configuration

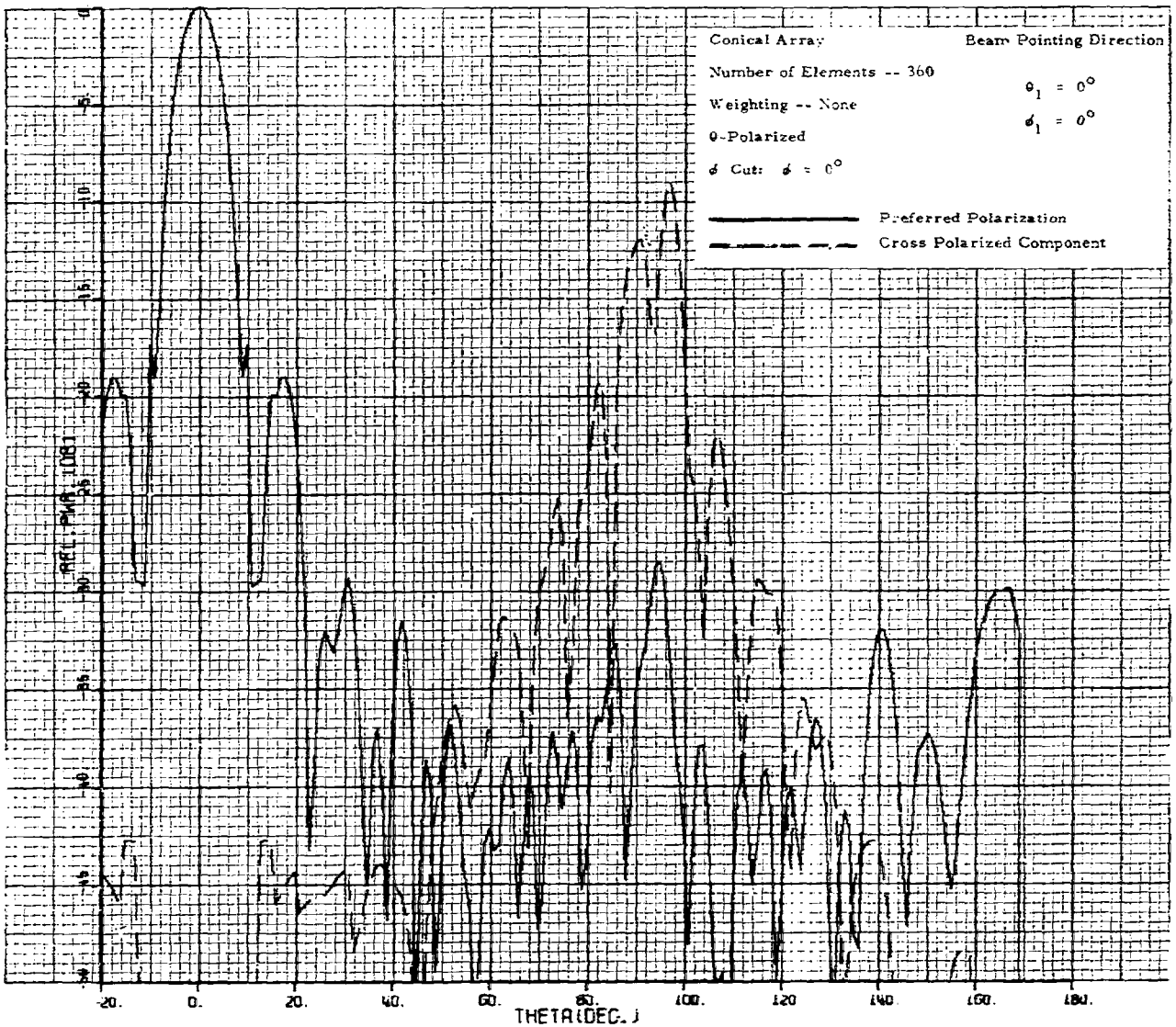

Figure 3.4-6. θ-Polarized Pattern of a Nose-Fire Beam for a 360 Element Configuration

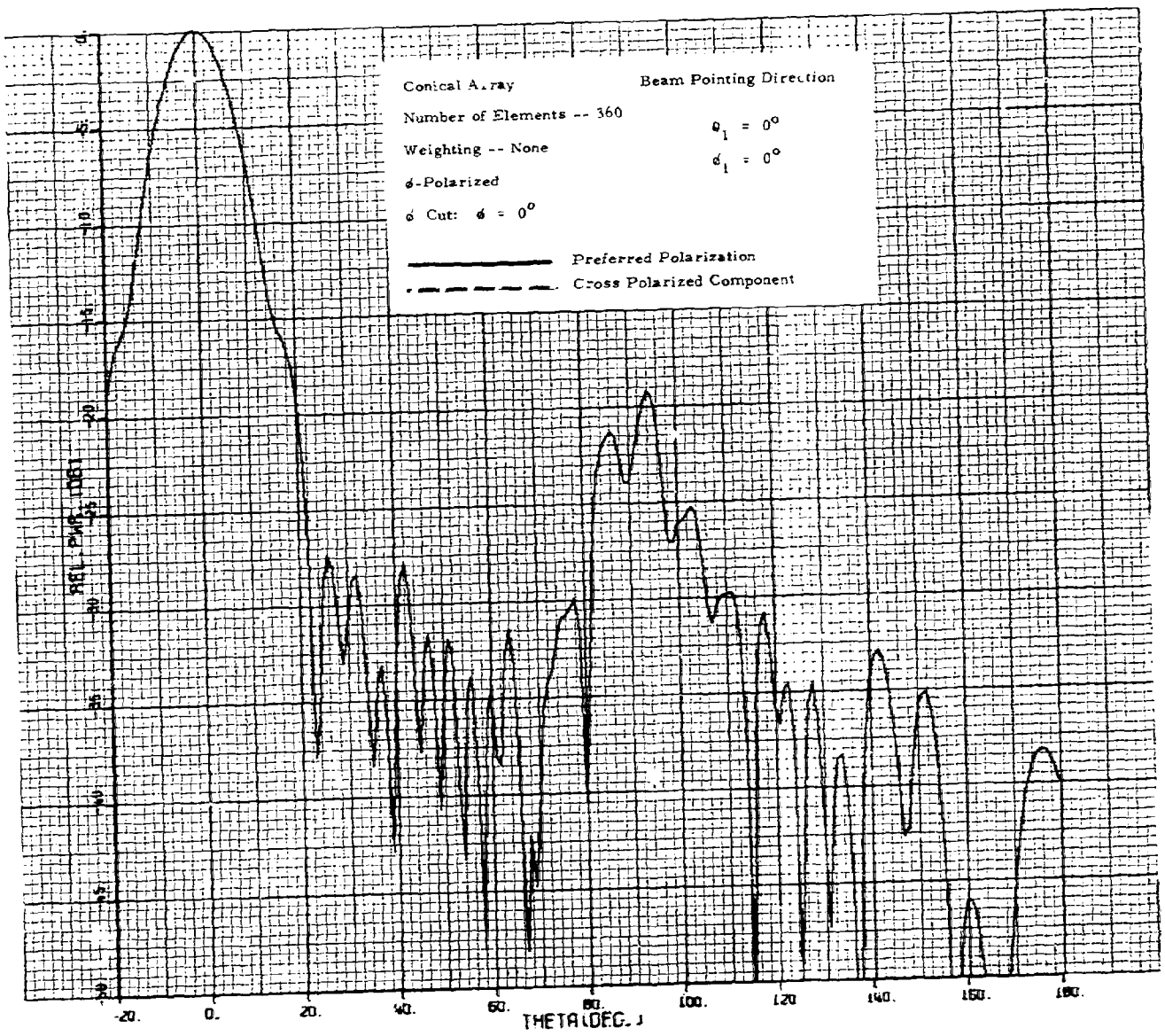

Figure 3.4-7. ϕ-Polarized Pattern of a Nose-Fire Beam for a 360 Element Configuration

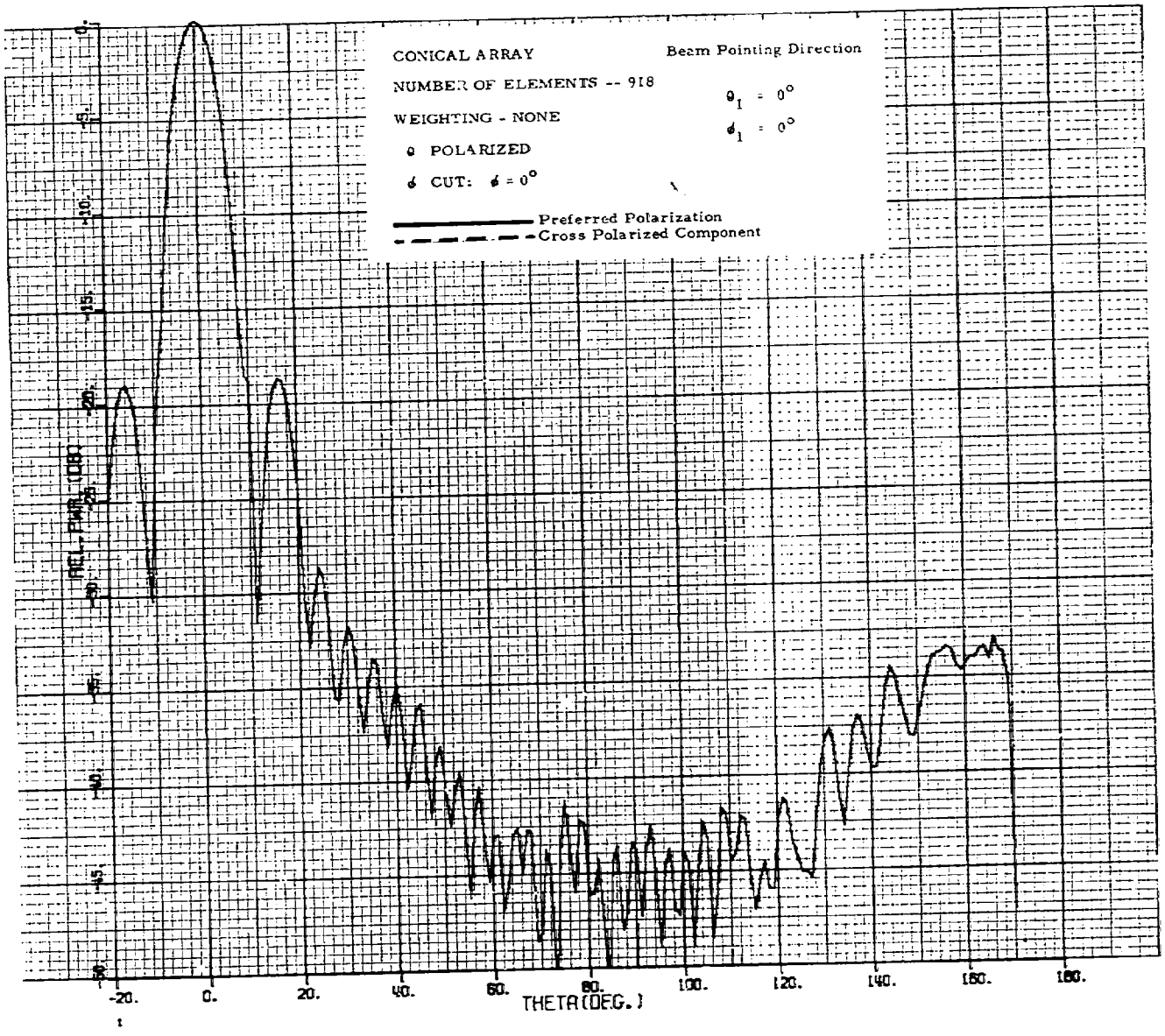

Figure 3.4-8. θ-Polarized Pattern of a Principal Plane Cut for a Nose-Fire Beam -- 918 Elements

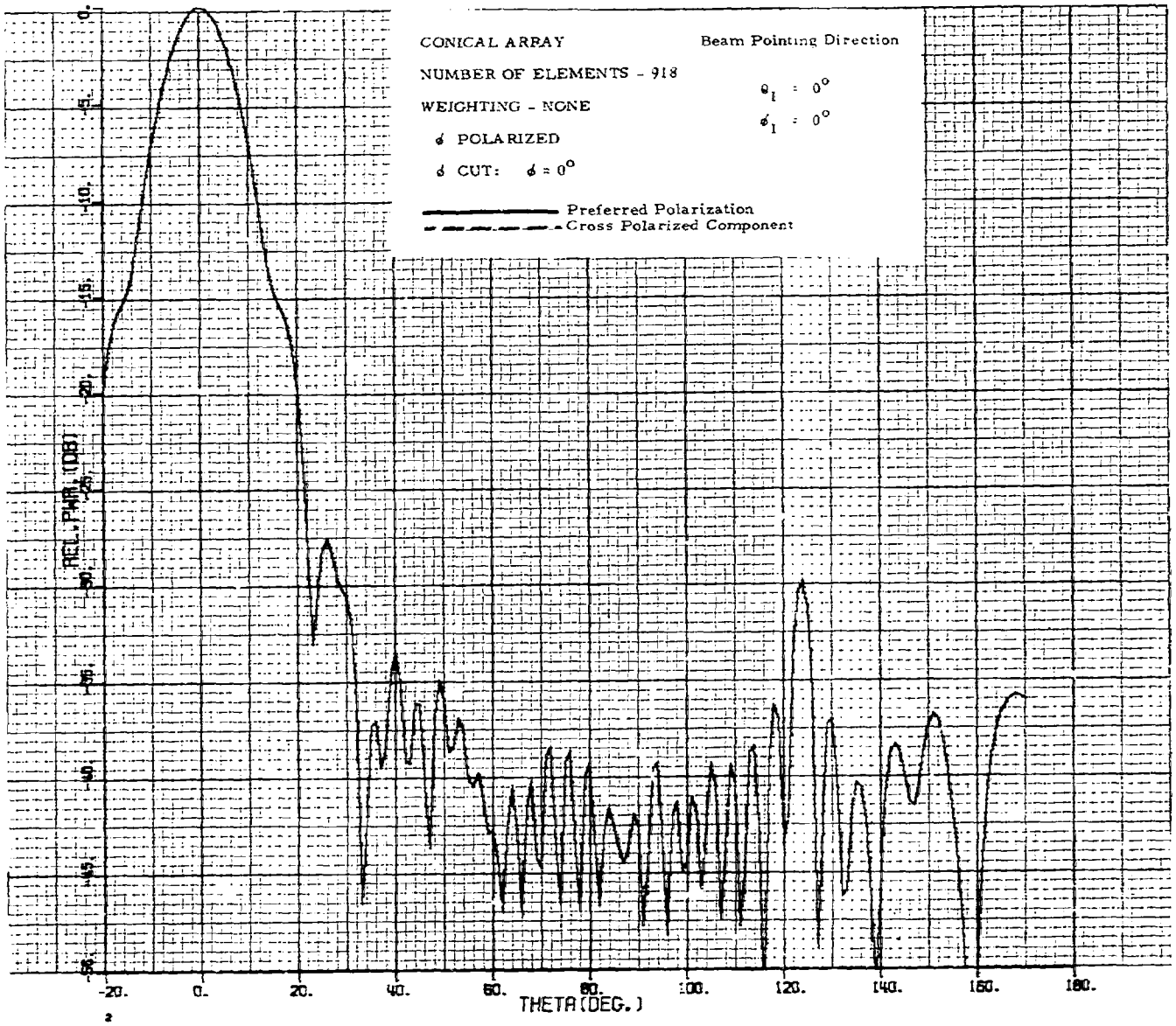

Figure 3.4-9. ϕ-Polarized Pattern of a Principal Plane Cut for a Nose-Fire Beam -- 918 Elements

The ϕ-polarized pattern for this case is shown in Figure 3.4-7. It can be compared to Figures 3.4-5 and 3.4-3 for the other two element configurations. The grating lobe region for the 360 element case (ψ = 80 to 100°) shows a large decrease over the 288 element case; and even shows a slight decrease over the 432 element case. The main beam region for the 360 element case is also slightly cleaner than the other two cases. In the backlobe region the 360 element case shows some lower lobes in comparison to the 288 element case and some increase in relation to the 432 element case.

The θ- and ϕ-polarized patterns for the 918 element configuration are given in Figures 3.4-8 and -9, respectively. As expected with such a large number of elements, these patterns represent a vast improvement over any of the other patterns for this cut. In the θ-polarized pattern (Fig. 3.4-8) the main beam is very clean with only one small shoulder on one side. The beam is slightly asymmetrical because the element layout on the cone is not quite symmetrical in this configuration. This results from one-half of the rings containing an odd number, and the other half containing an even number of elements. A slight step tends to occur in many of the nose-fire patterns at θ = 10° because, at that point, the back side of the cone starts to become shadowed. The computer simulates this shadowing by dropping out elements in the "geometrical shadow" of the far field point being computed. This results in 18 elements being dropped abruptly when θ reaches 10 degrees.

The ϕ-polarized pattern (Fig. 3.4-9) is not quite as smooth as the θ-polarized case, but it is nevertheless quite acceptable. Both of these patterns indicate that good results can be achieved from conical arrays for nose-fire beams when the interelement spacing is kept sufficiently small.

3.4.2 Beam Steered to $\theta_1 = 80°$, $\phi_1 = 90°$

The next 16 patterns are for various element configurations and two different cuts through a beam steered off to $\theta_1 = 80°$, $\phi_1 = 90°$. They will be presented by cuts (eight patterns per cut) with the different element configurations discussed under each cut.

3.4.2.1 $\phi = 90^\circ$ Cut Through Beam at θ_1, $\phi_1 = 80^\circ$, 90°

This is a principal plane cut along the plane $\phi = 90^\circ$. The series of patterns generated by this cut for four different element configurations is given in Figures 3.4-10 through 3.4-17.

The 288 element configuration generated θ and ϕ patterns as seen in Figures 3.4-10 and -11. In the θ-polarized pattern (Figure 3.4-10) it appears that a grating lobe is starting to form at about $\theta = 160^\circ$ to 170°. However, it is not well formed and probably does not represent a serious loss of energy. The cross-polarized component is larger than the preferred component in some places near both extremes of the pattern, but very low around the main beam. These conditions result from the peculiar geometry of the cone and the effective polarization at each element when the slots are adjusted to give only the preferred component in the beam pointing direction.

In the ϕ-polarized pattern (Figure 3.4-11) the cross-polarized component goes to zero everywhere because of symmetry conditions. Also, since the element pattern in this situation goes to zero along the generatrix directly below the peak of the beam, and the other elements are rotated only slightly to cancel the cross-polarized component at the peak of the main beam, the grating lobes tend to be sharply reduced by the element pattern.

Figures 3.4-12 and -13 give the θ- and ϕ-polarized patterns of the 432 element configuration. They can be compared to Figures 3.4-10 and -11 where patterns of a similar cut for the 288 element configuration are given. Not much reduction in sidelobe level was achieved in this plane by using the new element arrangement, as is to be expected since the element spacing was not altered in this plane. Some reduction does take place, however, in what appears to be grating lobes starting to form at about $\theta = 20^\circ$ and $\theta = 160^\circ$.

A set of patterns was generated for the 360 element configuration at this scan angle that corresponds to the previous sets that were run for the 288 and 432 element configurations. Figures 3.4-14 and -15 show the principal plane cut through the peak of the beam along θ with $\phi = 90^\circ$,

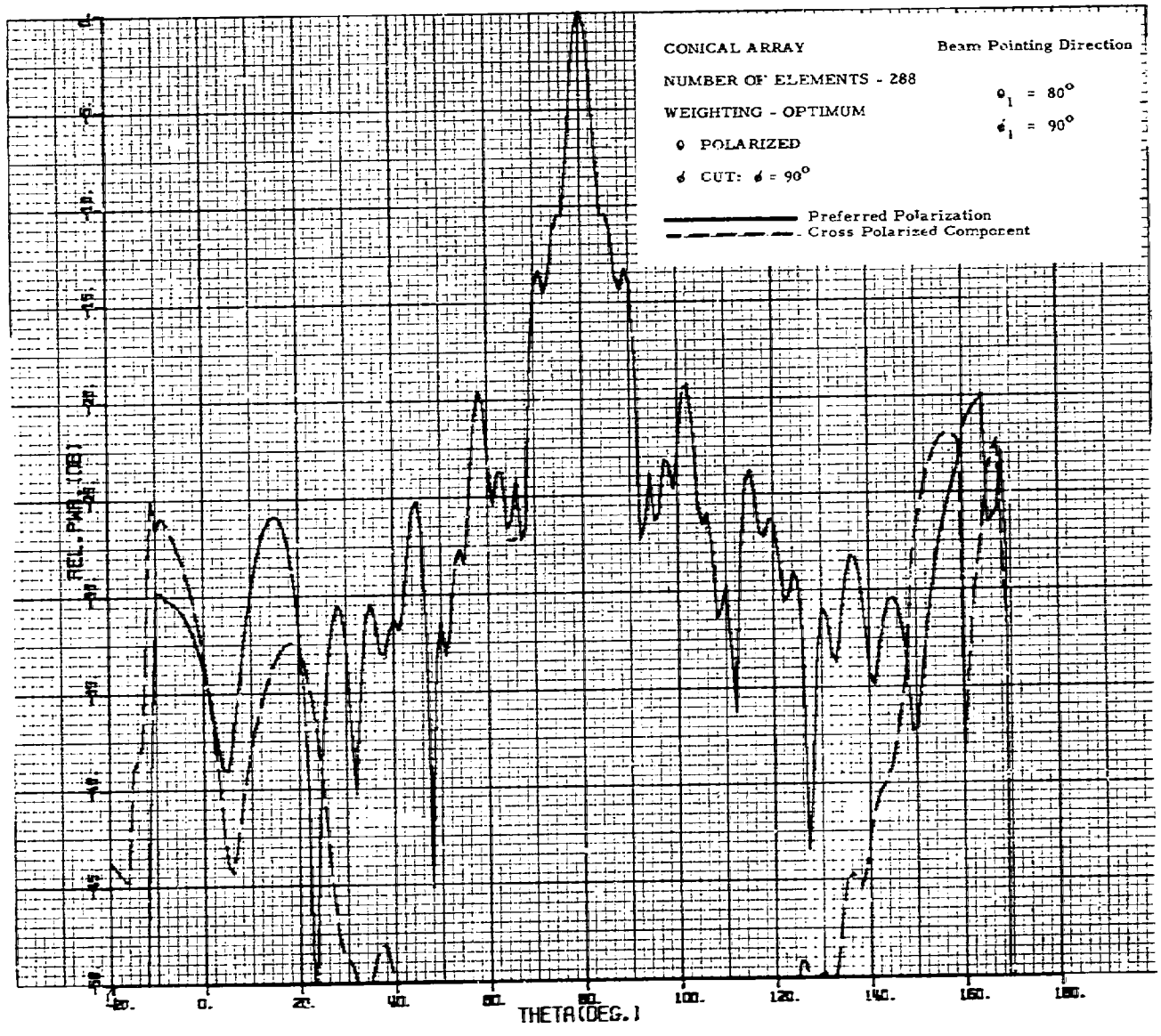

Figure 3.4-10. θ-Polarized Pattern of Principal Plane Cut for "Broadside" Beam -- 288 Elements

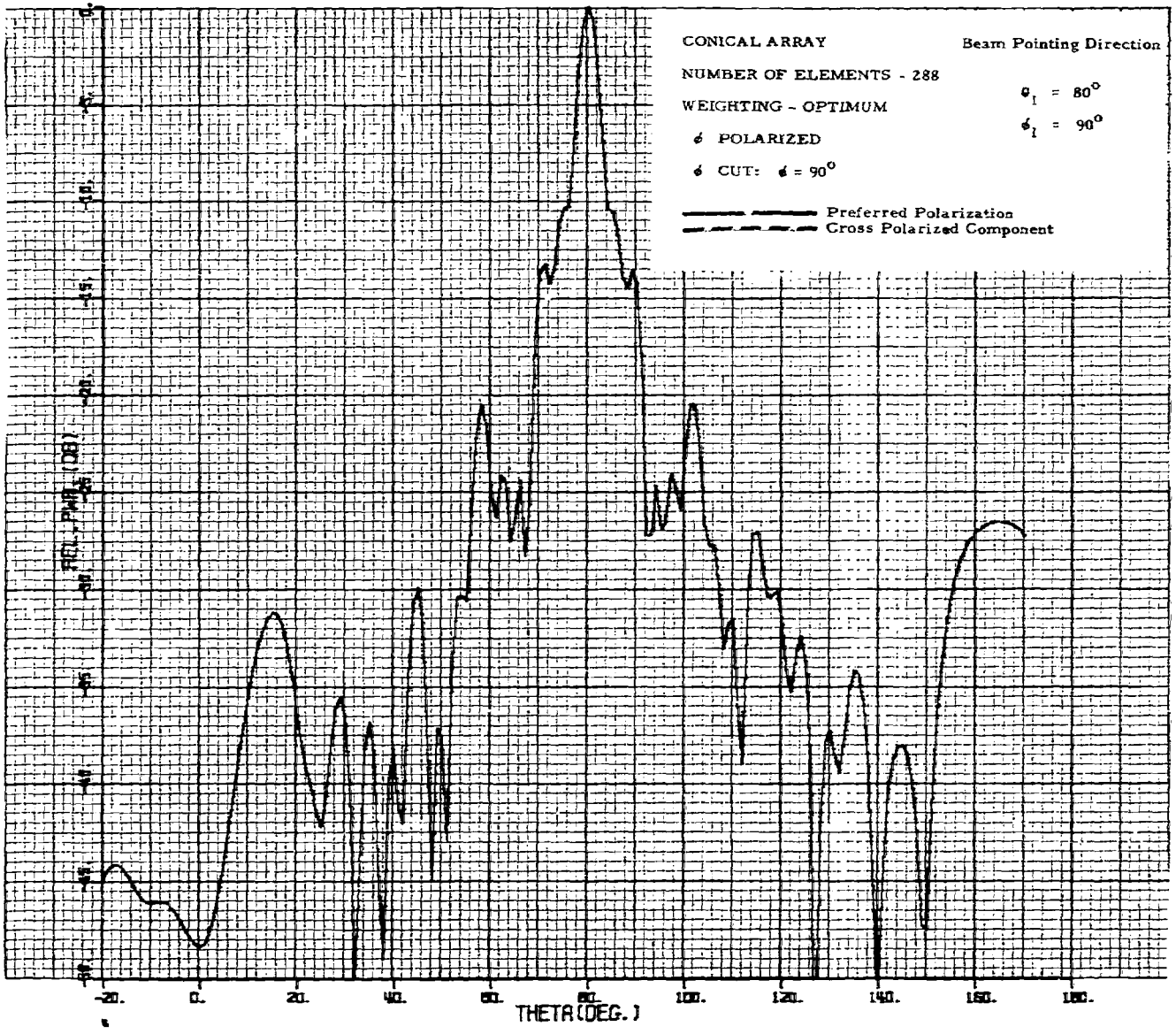

Figure 3.4-11. ϕ-Polarized Pattern of Principal Plane Cut For "Broadside" beam -- 288 Elements

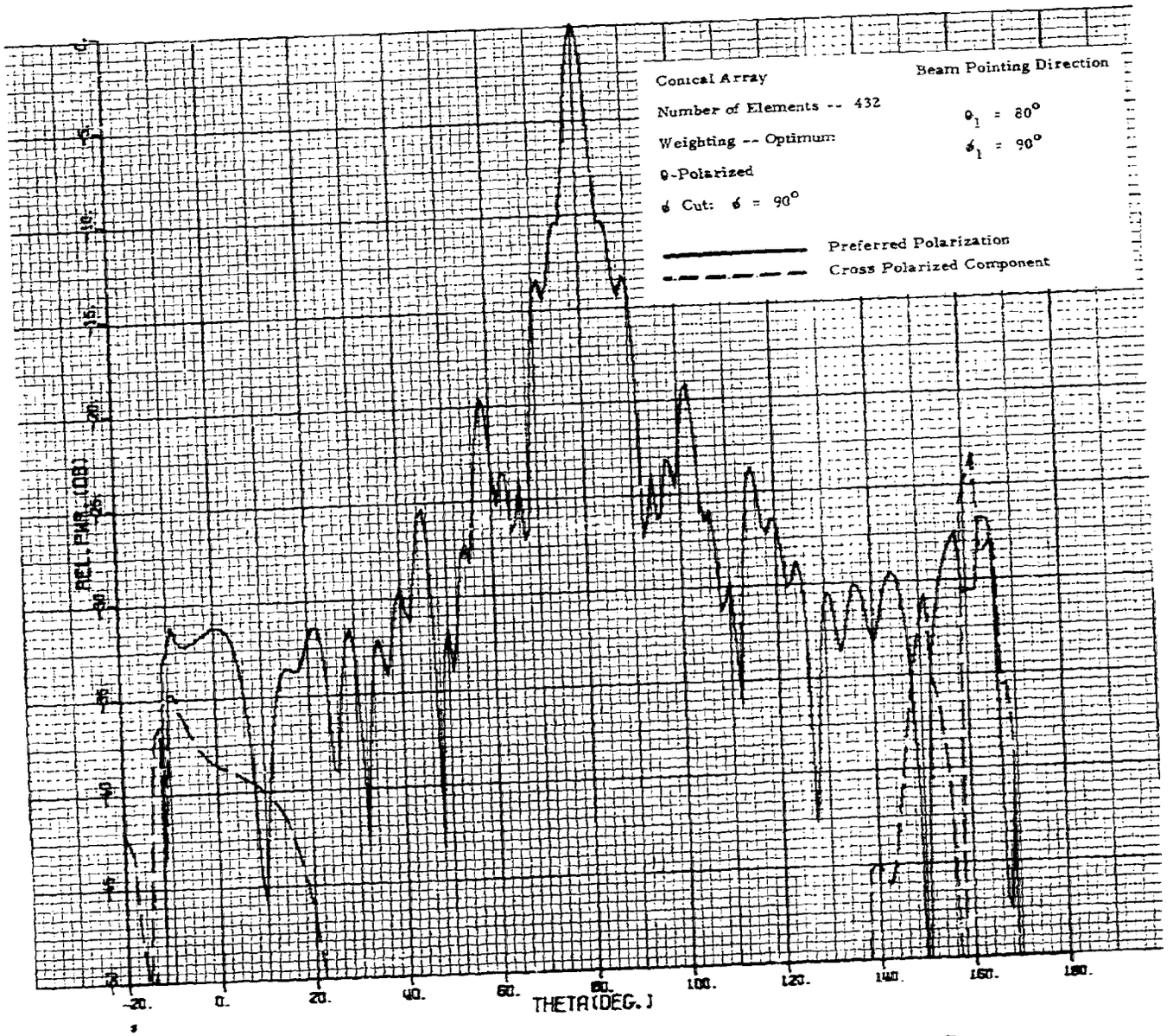

Figure 3.4-12. θ-Polarized Pattern of Principal Plane Cut For "Broadside" Beam -- 432 Elements

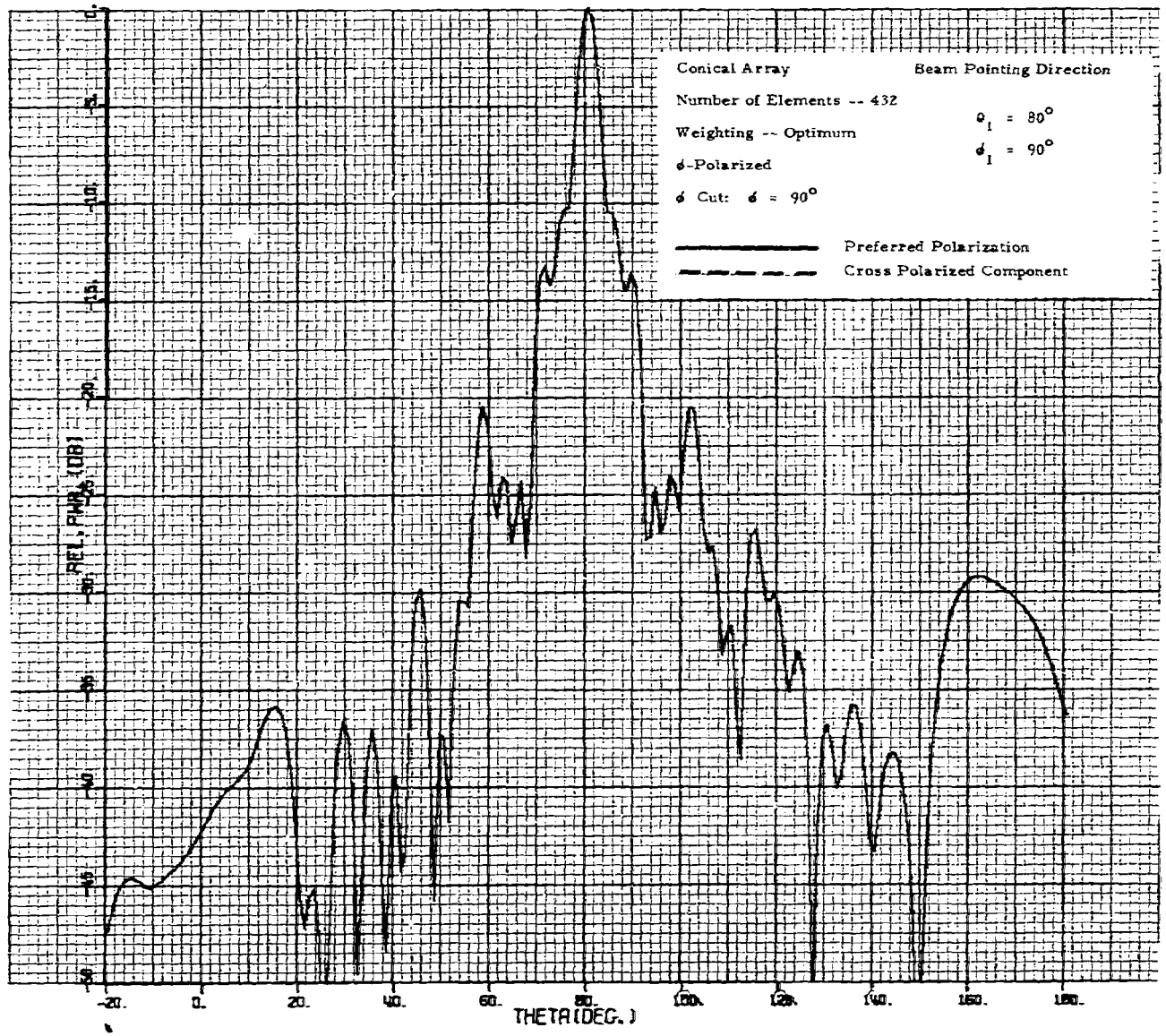

Figure 3.4-13. ϕ-Polarized Pattern of Principal Plane Cut For "Broadside" Beam -- 432 Elements

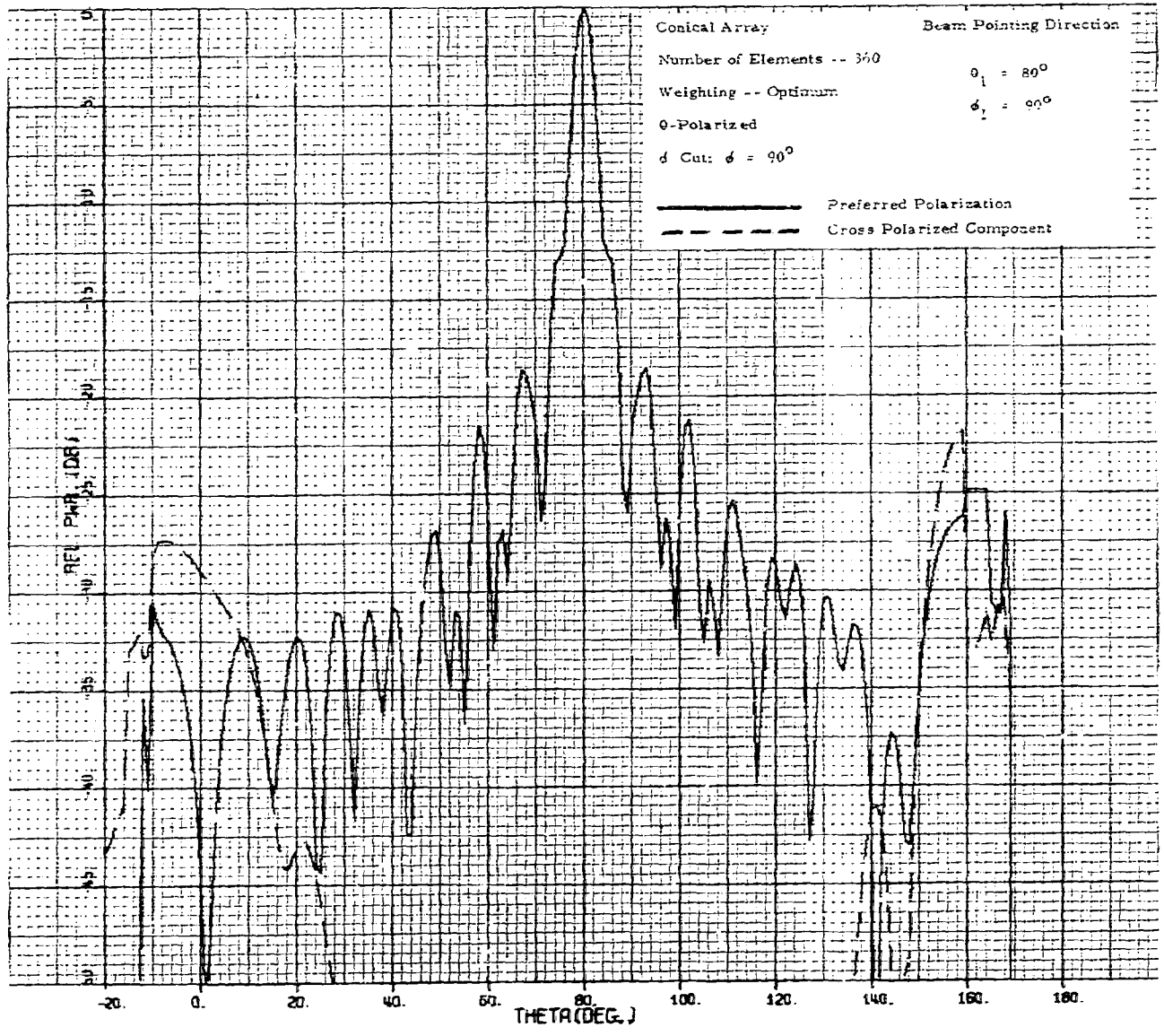

Figure 3.4-14. θ-Polarized Pattern of Principal Plane Cut Through a Broadside Beam -- 360 Elements

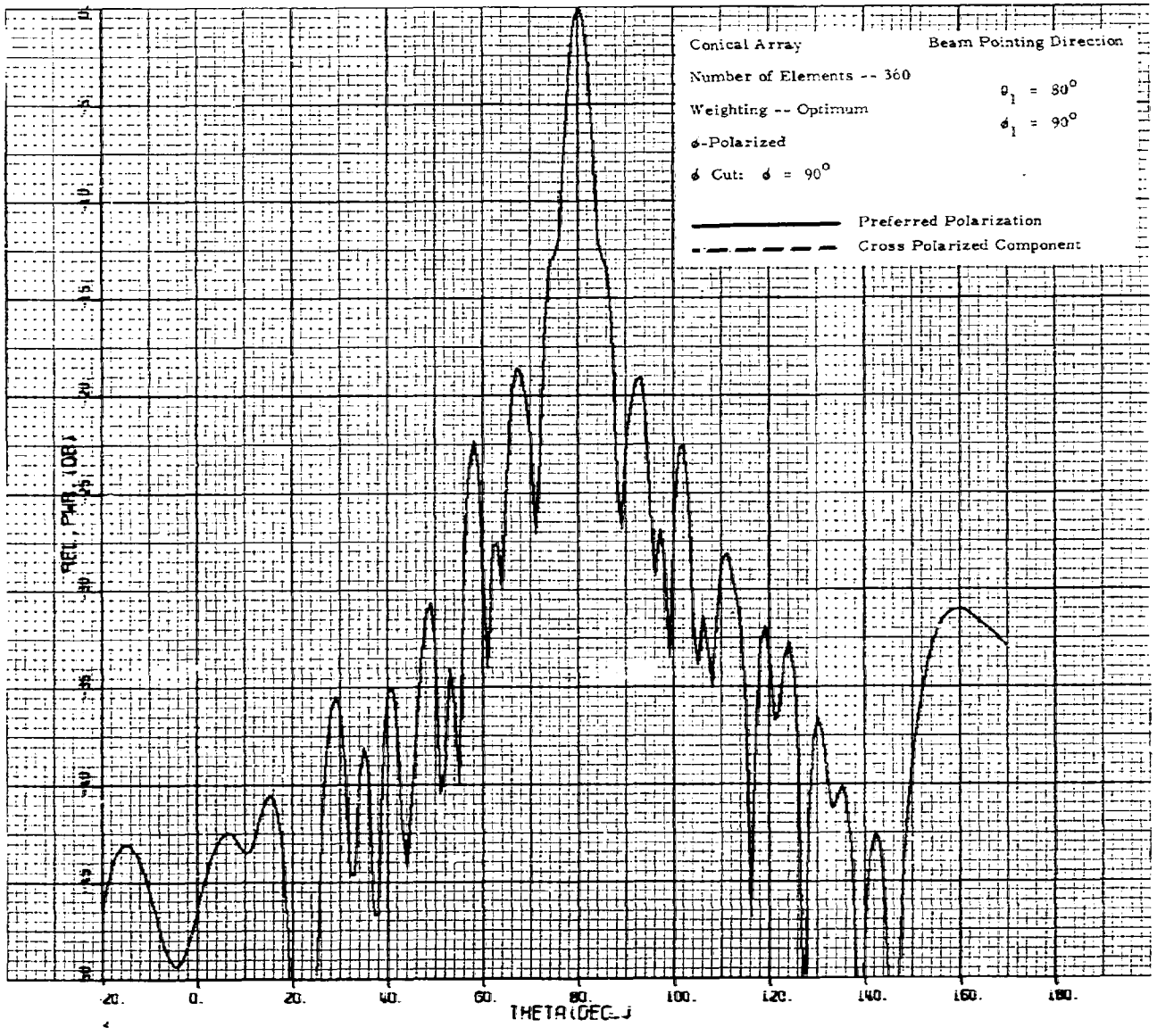

Figure 3.4-15. ϕ-Polarized Pattern of Principal Plane Cut Through a Broadside Beam -- 360 Elements

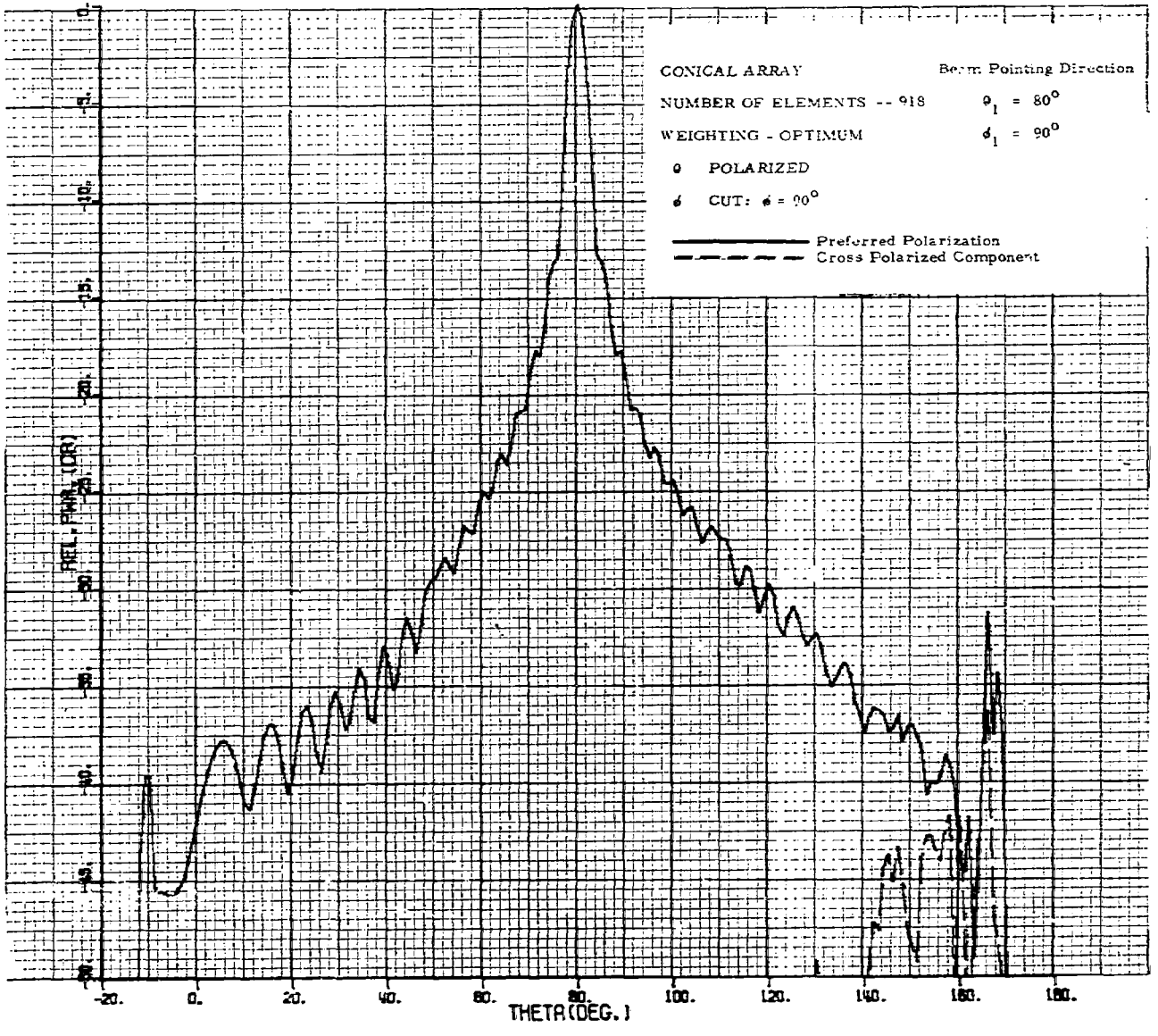

Figure 3.4-16. θ-Polarized Pattern of Principal Plane Cut Through "Broadside Beam" -- 918 Elements

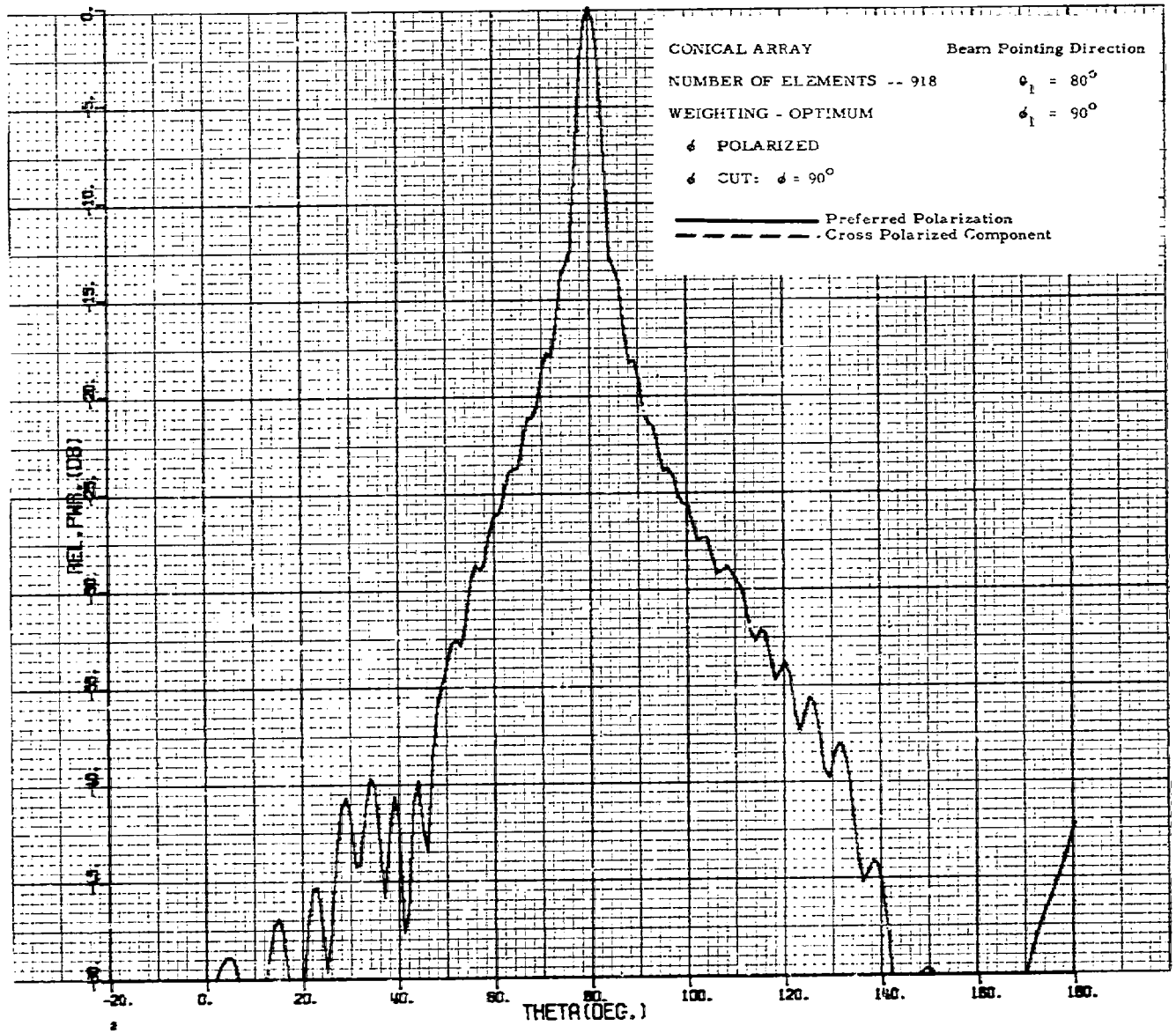

Figure 3.4-17. ϕ-Polarized Pattern of Principal Plane Cut Through a "Broadside" Beam -- 918 Elements

for the 360 element configuration. These patterns correspond to Figures 3.4-12 and -13 for the 432 element case, and to Figures 3.4-10 and -11 for the 288 element case. The main beam is considerably cleaner for the 360 element case than for either of the other two in both the θ-polarized and the ϕ-polarized patterns. The sidelobe structure is more systematic also. However, the grating lobes which tend to rise at extremely wide angles in this cut are reduced by only a few dB over the 288 element case, and are a few dB higher than for the 432 element case.

The nearly ideal patterns for this beam pointing direction are given in Figures 3.4-16 and -17 where the 918 element configuration patterns are presented. The θ-polarized pattern (Figure 3.4-16) shows an extremely symmetrical sidelobe structure and no grating lobes. A few sharp spikes appear near $\theta = 170^{\circ}$ and may be spurious lobes resulting from the approximations still remaining in the element pattern being used. This pattern is much better in all respects, except for the region near the main beam, than any of its counterparts for the other element configurations shown in Figures 3.4-10, -12, and -14.

The ϕ-polarized pattern for the 918 element case (Figure 3.4-17) has even lower sidelobes than the θ-polarized pattern; however, it is not as symmetrical. It compares with Figures 3.4-11, -13, and -15 and is considerably cleaner than any of these patterns for the other element configurations. None of the other patterns could be considered as really unacceptable though, because the element factor aids in keeping the far out sidelobes down for all of the element configurations in this polarization.

3.4.2.2 $\tau = 90^{\circ}$ Cut Through Beam at θ_1, $\phi_1 = 80^{\circ}$, 90°

This cut is the other principal plane cut for a beam pointing direction of $\theta_1 = 80^{\circ}$, $\phi_1 = 90^{\circ}$. It is perpendicular to the $\phi = 90^{\circ}$ cut discussed above. The next eight patterns (Figs. 3.4-18 through 3.4-25) are of this cut for four different element configurations.

Figures 3.4-18 and -19 show the θ- and ϕ-polarized patterns, respectively, of the 288 element configuration. The θ-polarized pattern has a grating lobe starting to form at $\psi \approx 75^{\circ}$, otherwise the pattern is quite good. The element pattern in this polarization has a null in the direction of the cut that contributes to cutting down far out sidelobes and backlobes.

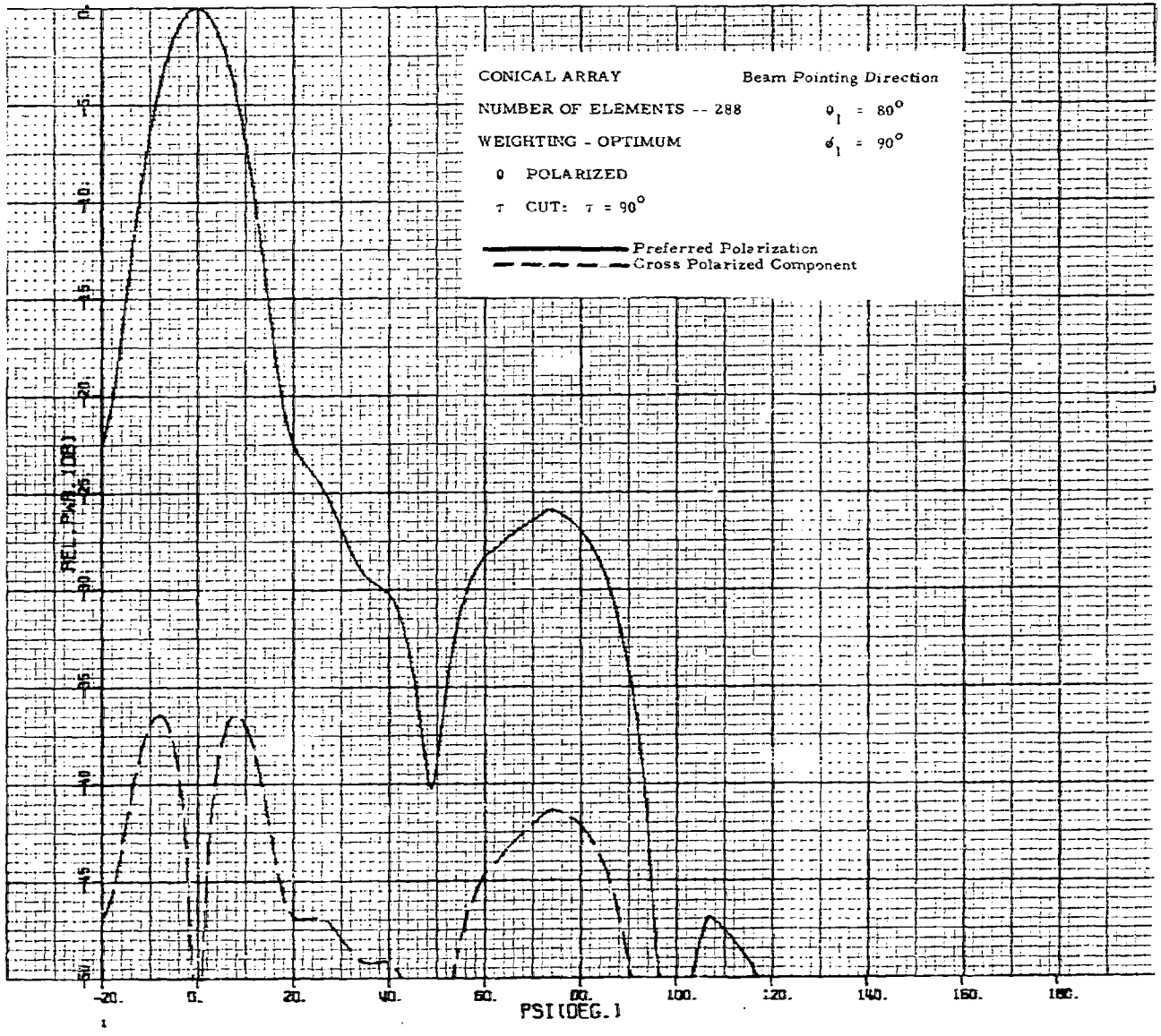

Figure 3.4-18. θ-Polarized Pattern of Principal Plane Cut ($\tau = 90^\circ$) Through Broadside Beam -- 283 Elements

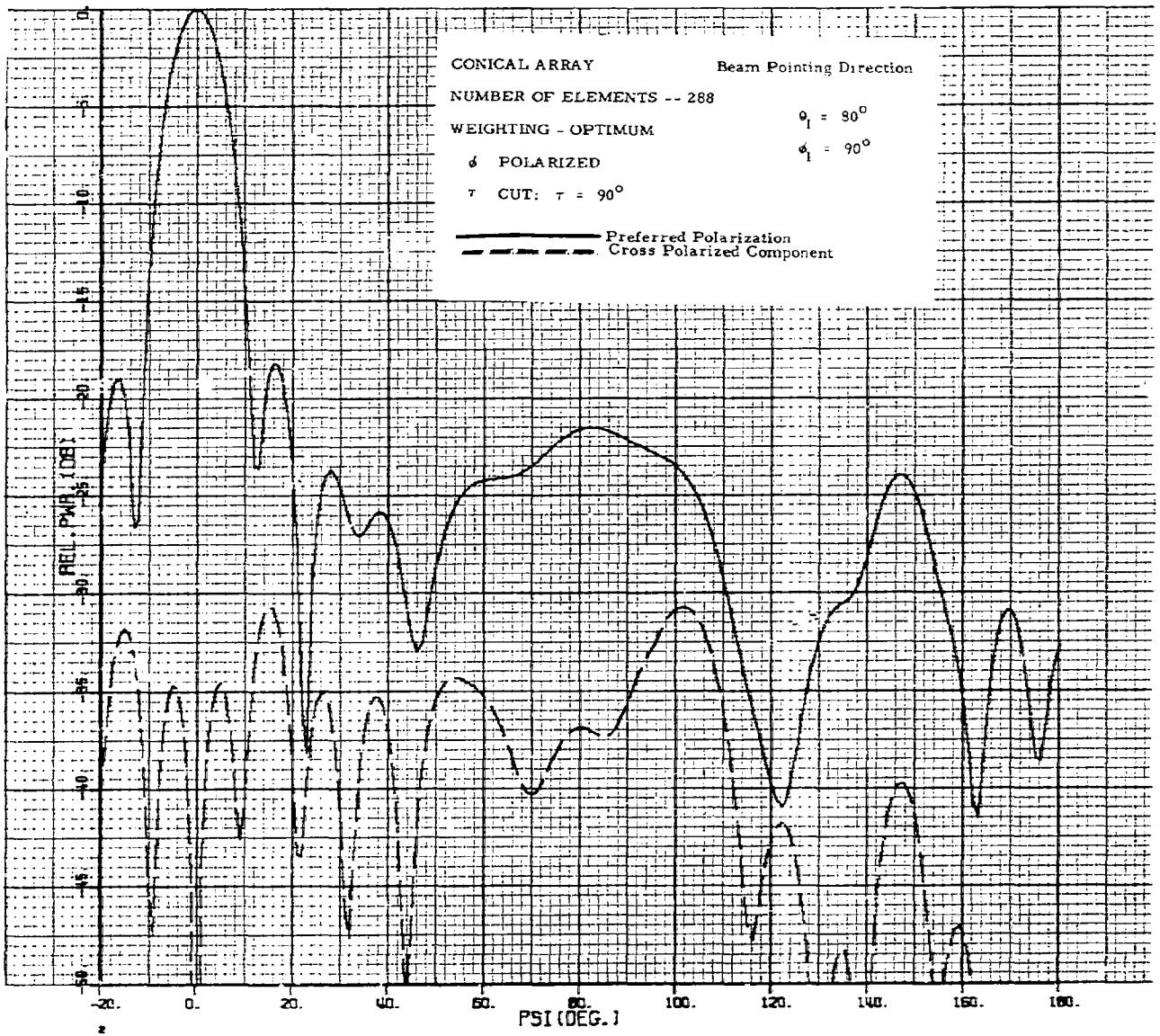

Figure 3.4-19. ϕ-Polarized Pattern of Principal Plane Cut ($\tau = 90^\circ$) Through Broadside Beam -- 288 Elements

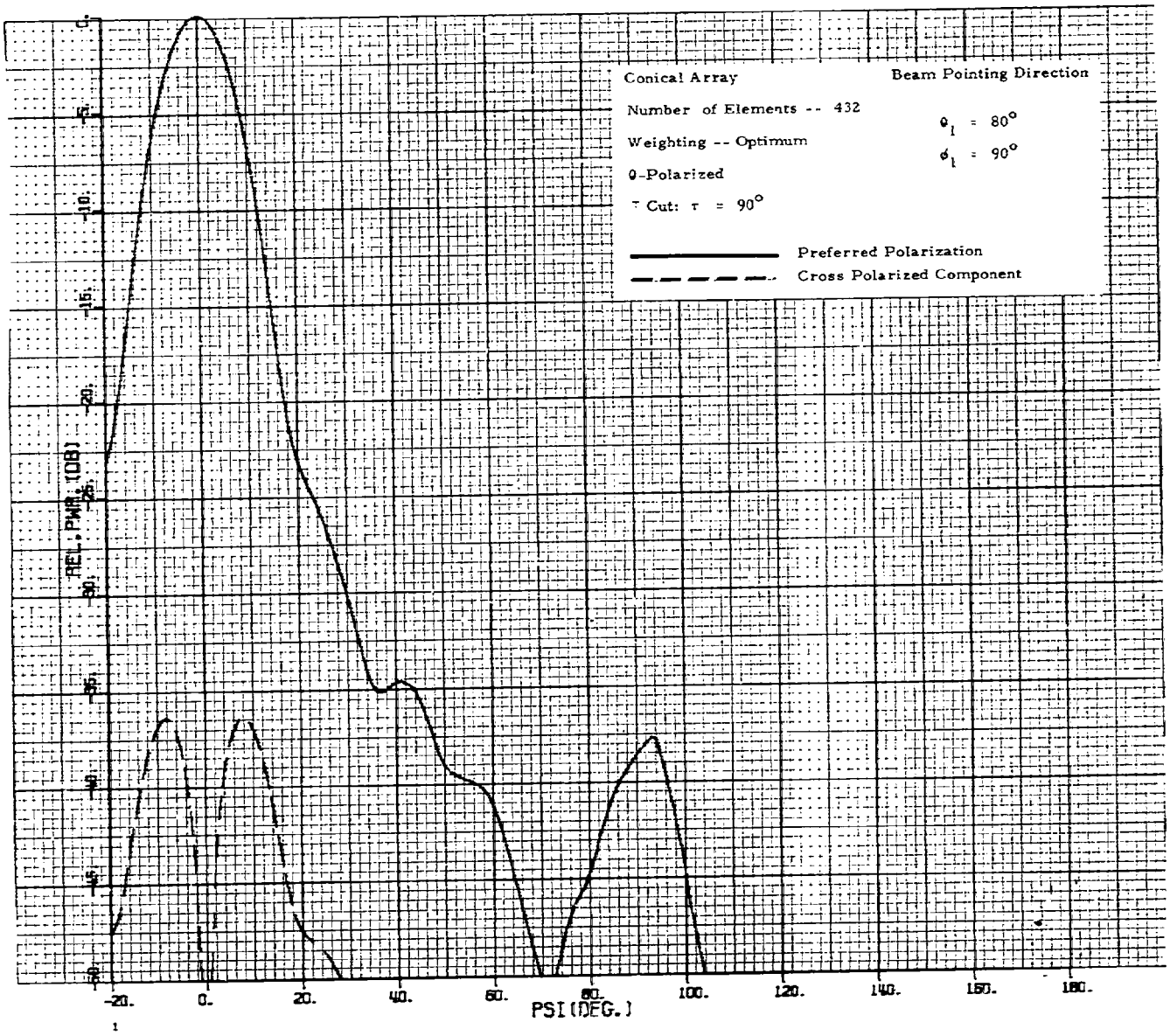

Figure 3.4-20. θ-Polarized Pattern of Principal Plane Cut ($\tau = 90^{\circ}$) Through Broadside Beam -- 432 Elements

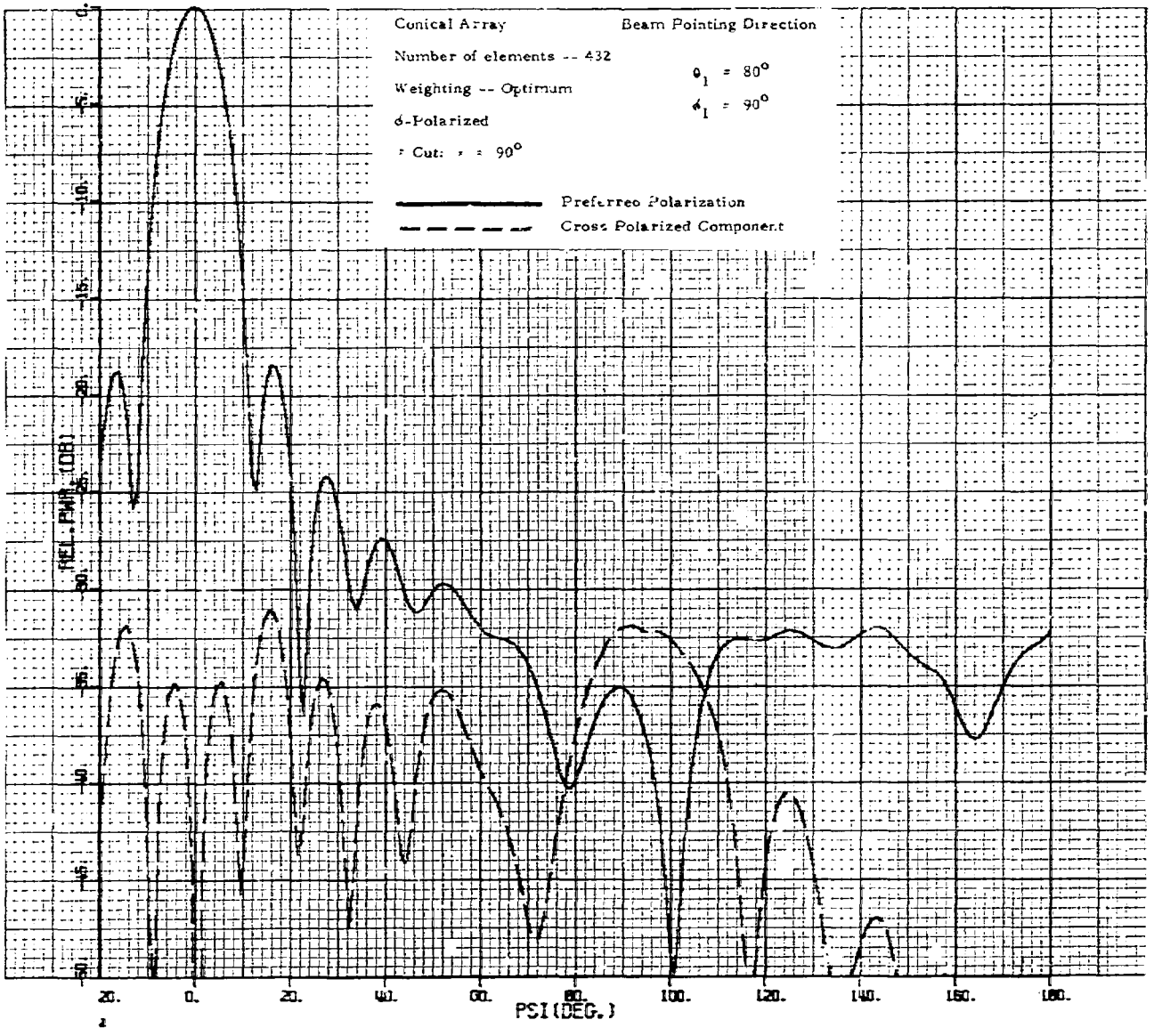

Figure 3.4-21. ϕ-Polarized Pattern of Principal Plane Cut ($\tau = 90^{\circ}$) Through Broadside Beam -- 432 Elements

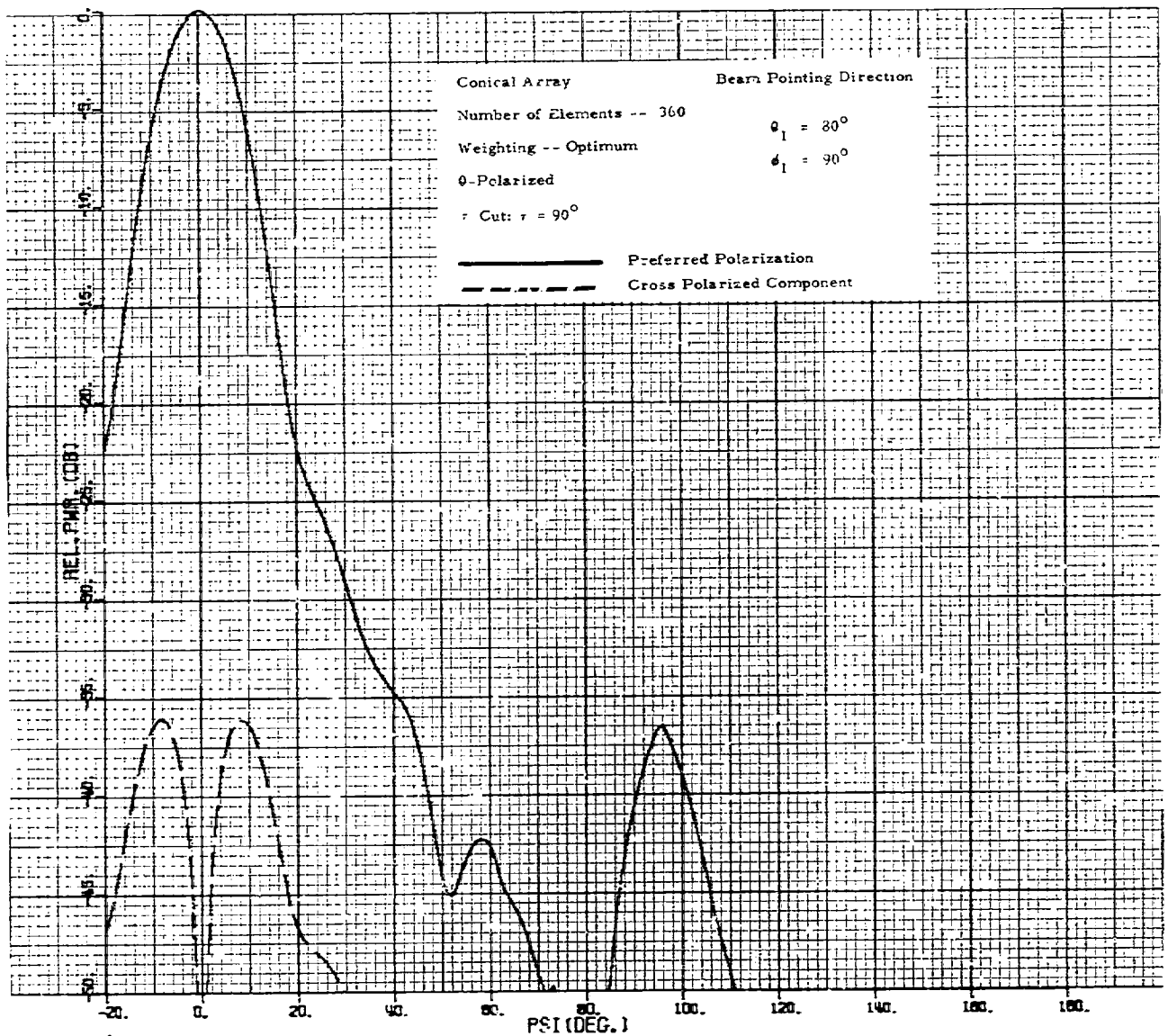

Figure 3.4-22. θ-Polarized Pattern of a Principal Plane Cut ($\tau = 90^{\circ}$) Through a Broadside Beam -- 360 Elements

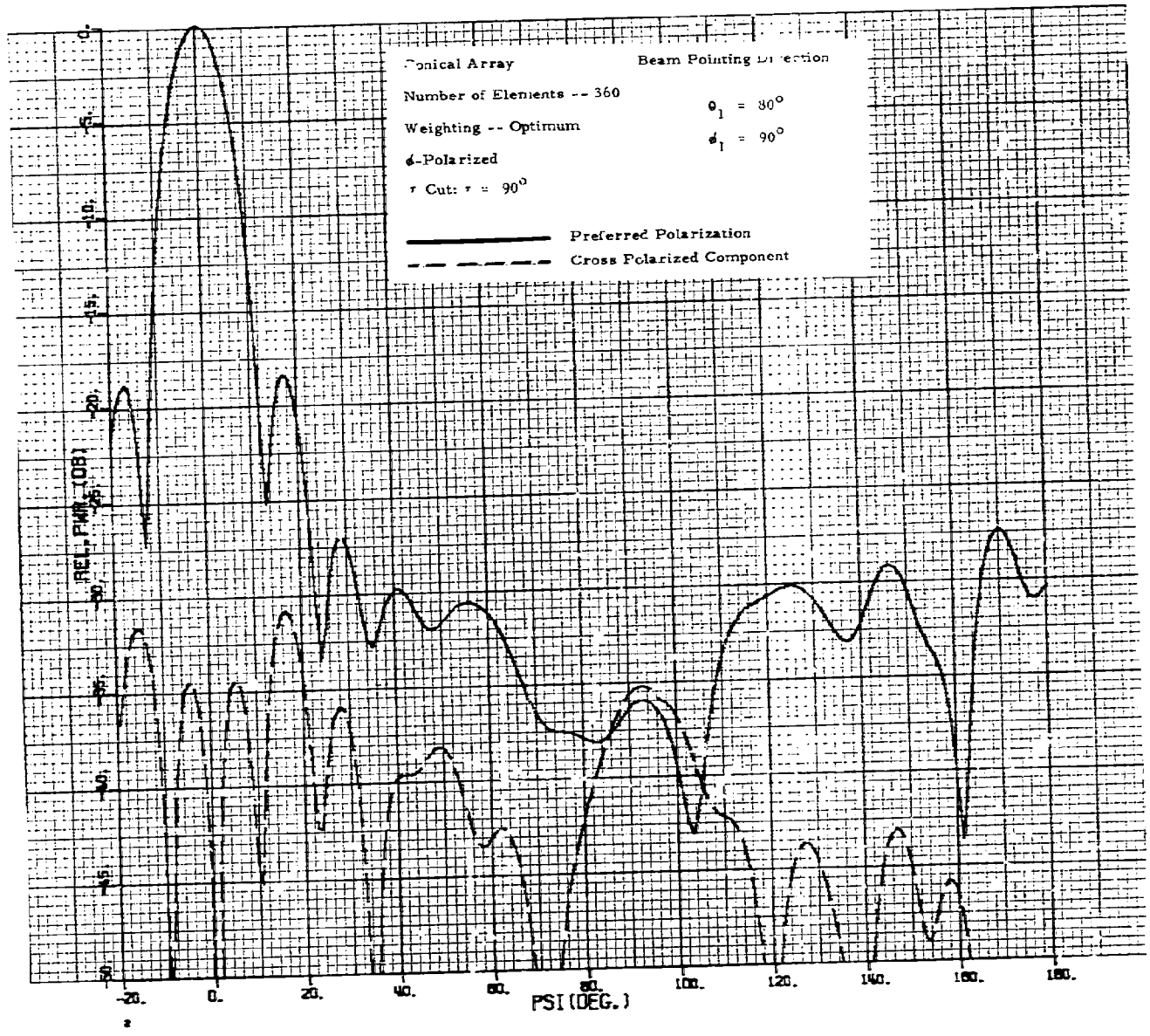

Figure 3.4-23. ϕ-Polarized Pattern of a Principal Plane Cut ($\tau = 90^{\circ}$) Through a Broadside Beam -- 360 Elements

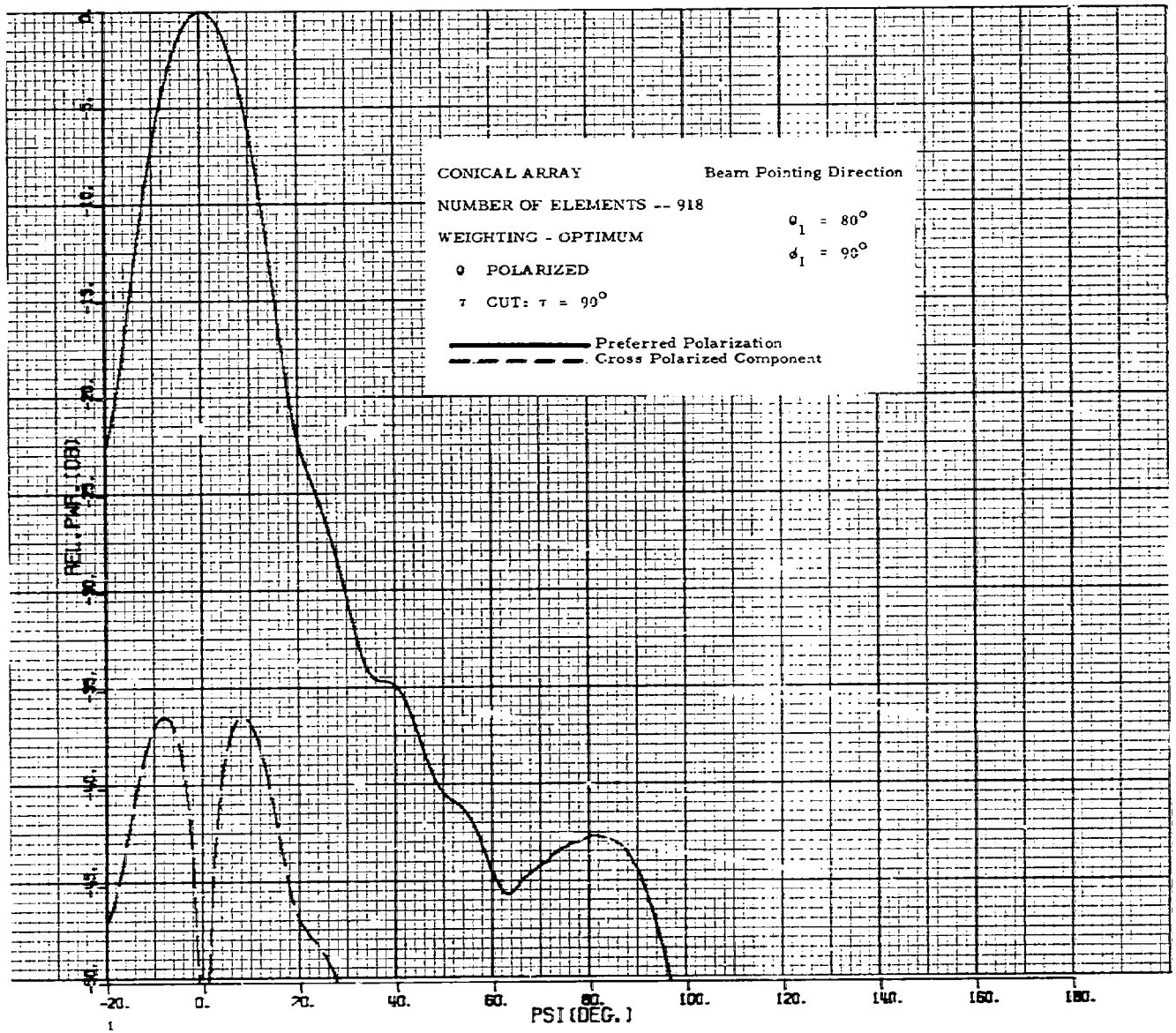

Figure 3.4-24. θ-Polarized Pattern of a Principal Plane Cut ($\tau = 90^{\circ}$) Through a Broadside Beam -- 918 Elements

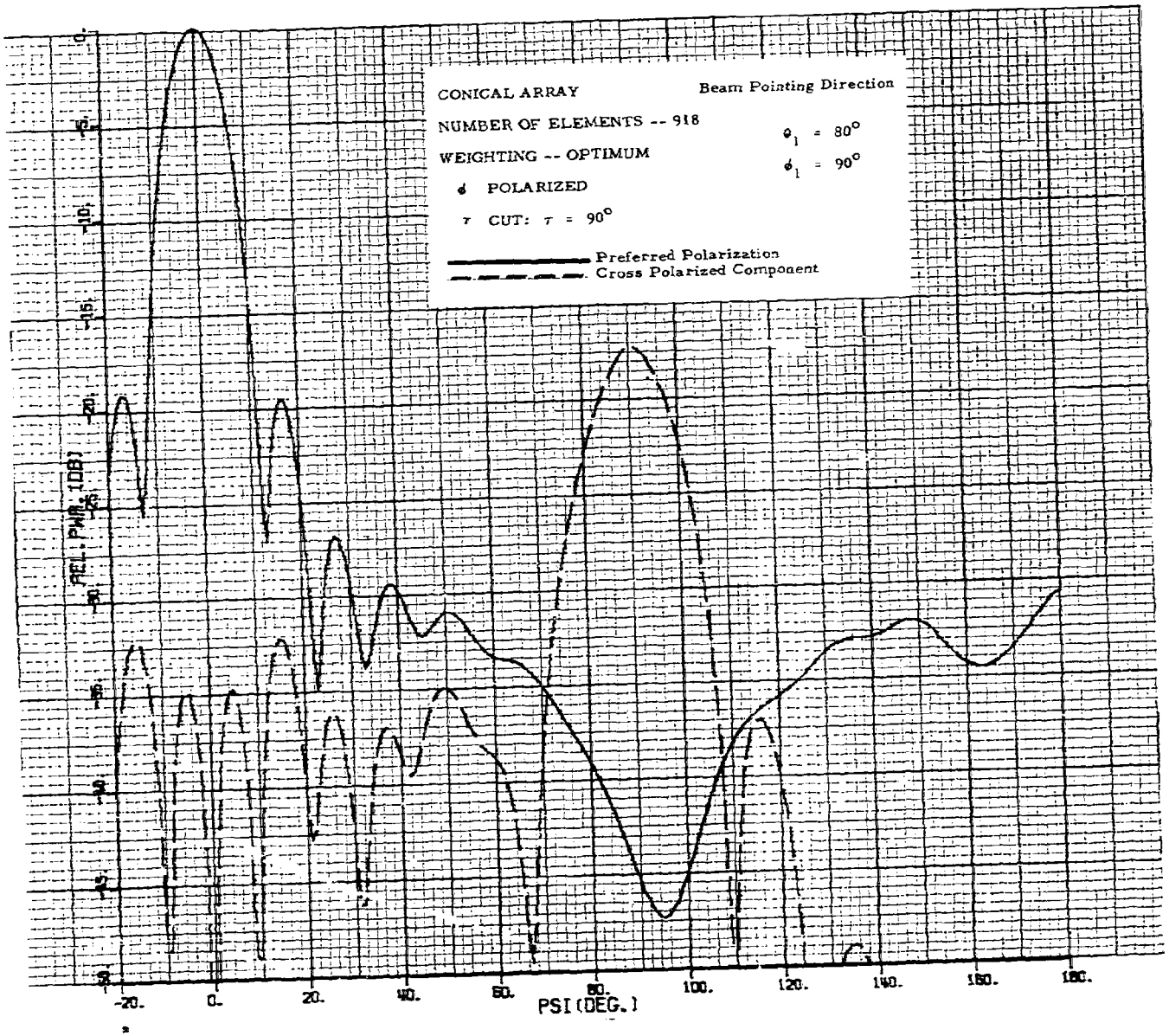

Figure 3.4-25. ϕ-Polarized Pattern of a Principal Plane Cut ($\tau = 90^{\circ}$) Through a Broadside Beam -- 918 Elements

The ϕ-polarized pattern is given in Fig. 3.4-19 and is not nearly as clean as the θ-polarized case. The grating lobe is higher and wider, and there are backlobes as well. Because of the large spread in ψ of the grating lobe it could absorb a lot of power unless it is very narrow in the θ direction.

For the 432 element configuration this cut produced the patterns shown in Figure 3.4-20 and -21. They correspond to Figures 3.4-18 and -19, respectively, for the 288 element case. A marked improvement is noted in these 432 element patterns. This was expected because the element spacing was reduced by a factor of 1/3 in this plane. In Figure 3.4-20 (the θ-polarized pattern) a grating lobe which formerly peaked at $\psi \approx 75^{\circ}$ with a magnitude of -26 dB has been pushed down and out to $\psi \approx 90^{\circ}$ and a magnitude of -37.6 dB. Figure 3.4-21 (the ϕ-polarized pattern) shows that a wide grating lobe has been moved from its former position of $\psi = 80^{\circ}$, a magnitude = -21.5 dB to a new position of $\psi = 130^{\circ}$, magnitude = -34 dB. Also a backlobe which formerly peaked at $\psi = 147^{\circ}$ has been moved all the way out into invisible space. In this cut the 432 element configuration is quite acceptable, whereas the 288 element configuration produced patterns that were of questionable use.

Patterns for this cut for the 360 element configuration are given in Figures 3.4-22 and -23. These patterns correspond to Figure 3.4-20 and -21 above for the 432 element case, and to Figures 3.4-18 and -19 for the 288 element case. The θ-polarized pattern (Figure 3.4-22) shows a considerable improvement over the 288 element case (Figure 3.4-18), and is only slightly degraded from the 432 element case (Figure 3.4-20). The ϕ-polarized pattern (Figure 3.4-23) is much improved over the 288 element case, (Figure 3.4-19), in that the main grating lobe has been moved out and down to $\psi = 130^{\circ}$, magnitude = -30 dB. However, it falls short of performing like the 432 element case (Figure 3.4-21) where the grating lobe is 5 dB lower and the backlobe is nearly completely missing.

The 918 element configuration patterns are given in Figures 3.4-24 and -25. The θ-polarized pattern (Fig. 3.4-24) compares with Figures 3.4-18, -20, and -22 for the other element configurations. It is much better than the 288 element case (Fig. 3.4-18), but not significantly better than the patterns for the other two cases. This indicates that for this cut and polarization, that more than 360 element is not needed. However, it must be kept

in mind that the element configuration in this case helps to suppress far-out lobes. The ϕ-polarized pattern for the 918 element configuration does not appear nearly as ideal as the other patterns seen so far for this configuration (See Fig. 3.4-25). In particular it has a large grating lobe in the cross-polarized component at $\psi = 90^{\circ}$. Comparing it to the other patterns for 288, 432, and 360 elements shows that the cross-polarized component for the 918 element configuration is higher than any of the others. The preferred component of polarization is considerably lower than for the 288 element configuration, but not significantly lower than the other two. What characteristic of the 918 element configuration caused this high lobe in the cross-polarized component is not clear. Since the element arrangement is somewhat random, it is likely that a beam pointed to the same angle in θ but a different angle in ϕ would have a different sidelobe structure. Other beam pointing directions should be investigated to see if this characteristic changes.

3.4.3 Beam Steered to $\theta_1 = 55^{\circ}$, $\phi_1 = 45^{\circ}$

All of the remaining patterns are for various cuts and various element configurations with the beam pointing in the direction of $\theta_1 = 55^{\circ}$, $\phi_1 = 45^{\circ}$. This is approximately midway in the first quadrant of the coordinate system.

3.4.3.1 $\tau = 90^{\circ}$ Cut Through Beam at θ_1, $\phi_1 = 55^{\circ}$, 45°

Figures 3.4-26 through -31 all represent patterns of this principal plane cut. Three different element configurations will be considered.

Figures 3.4-26 and -27 are the θ and ϕ-polarized patterns, respectively, of the 288 element configuration. There is a marked difference between the θ-polarized and the ϕ-polarized conditions here. The θ-polarized pattern (Fig. 3.4-26) has sidelobes that drop off very rapidly and then drop below -50 dB beyond 140 degrees. The ϕ-polarized pattern (Fig. 3.4-27), on the other hand, has high sidelobes near the main beam, and some lobes that are higher than desired around on the back side of the cone. These lobes are too far from the main beam to be considered as grating lobes, but probably exist because such "back-lobes" have been observed experimentally on cylindrical arrays.

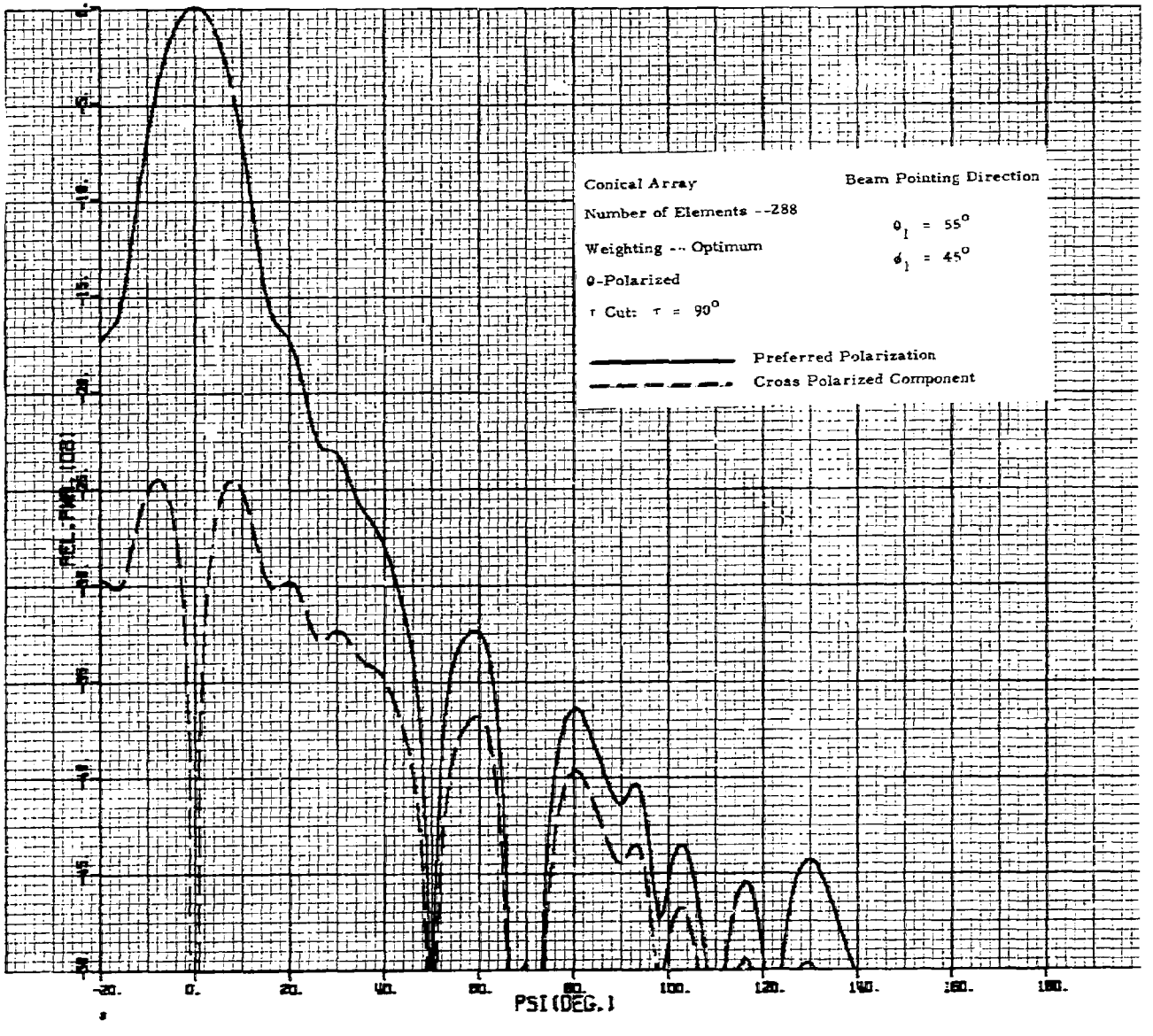

Figure 3.4-26. θ-Polarized Pattern of Principal Plane Cut ($\tau = 90^{\circ}$) for Beam in First Quadrant -- 288 Elements

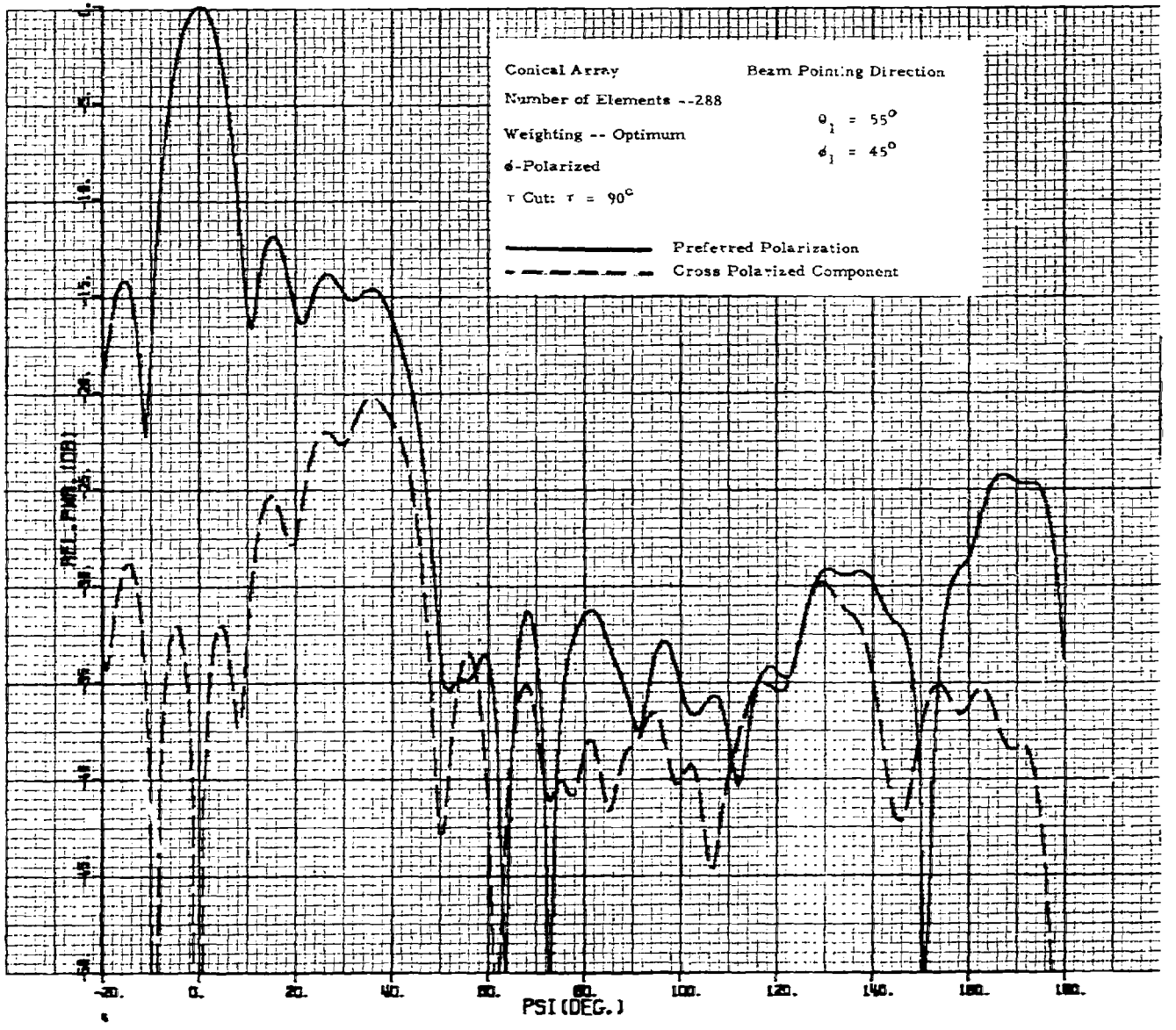

Figure 3.4-27. ϕ-Polarized Pattern of Principal Plane Cut ($\tau = 90^{\circ}$) for Beam in First Quadrant -- 288 Elements

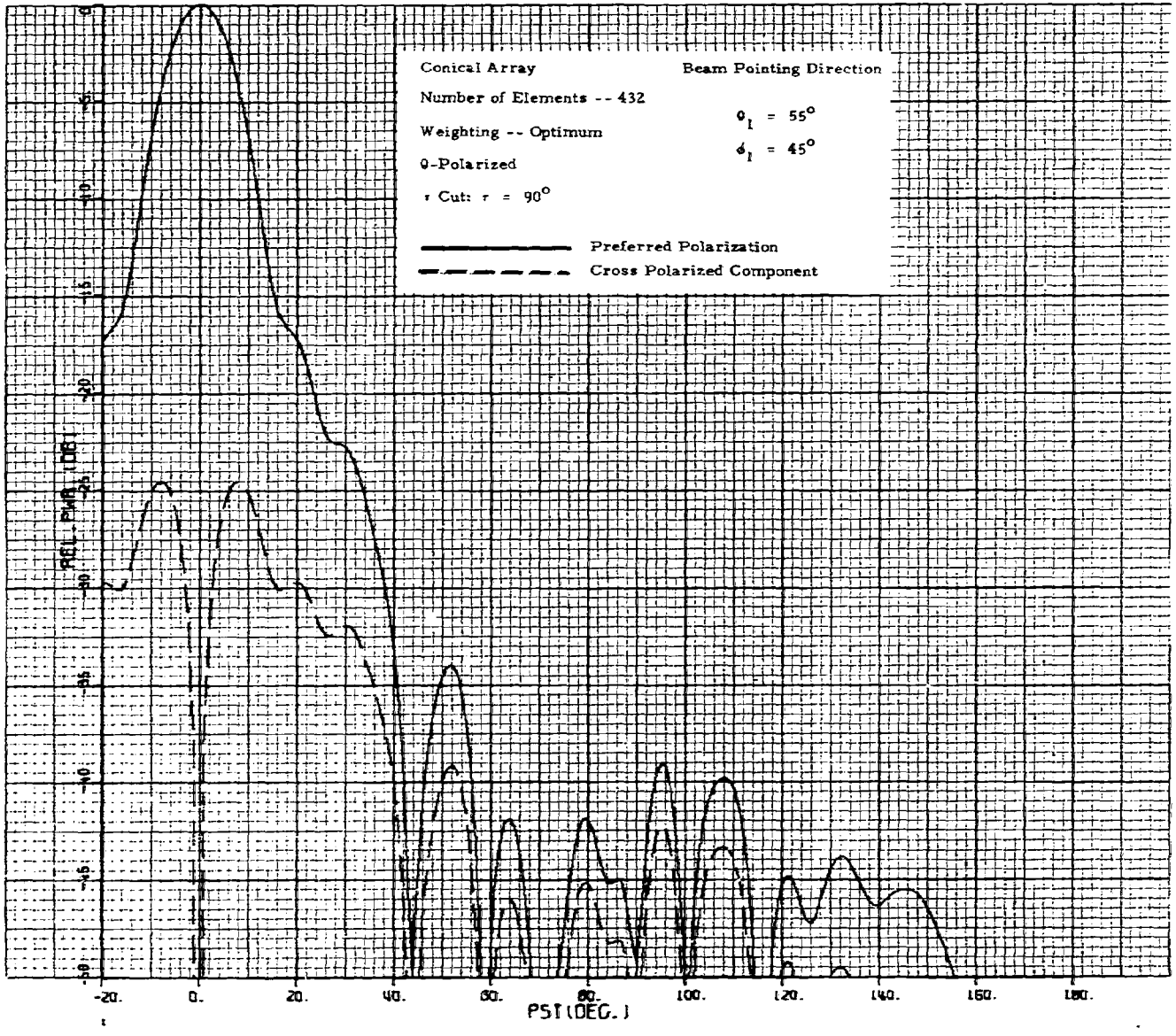

Figure 3.4-28. θ-Polarized Pattern of Principal Plane Cut ($\tau = 90^{\circ}$) Through Beam in First Quadrant--432 Elements

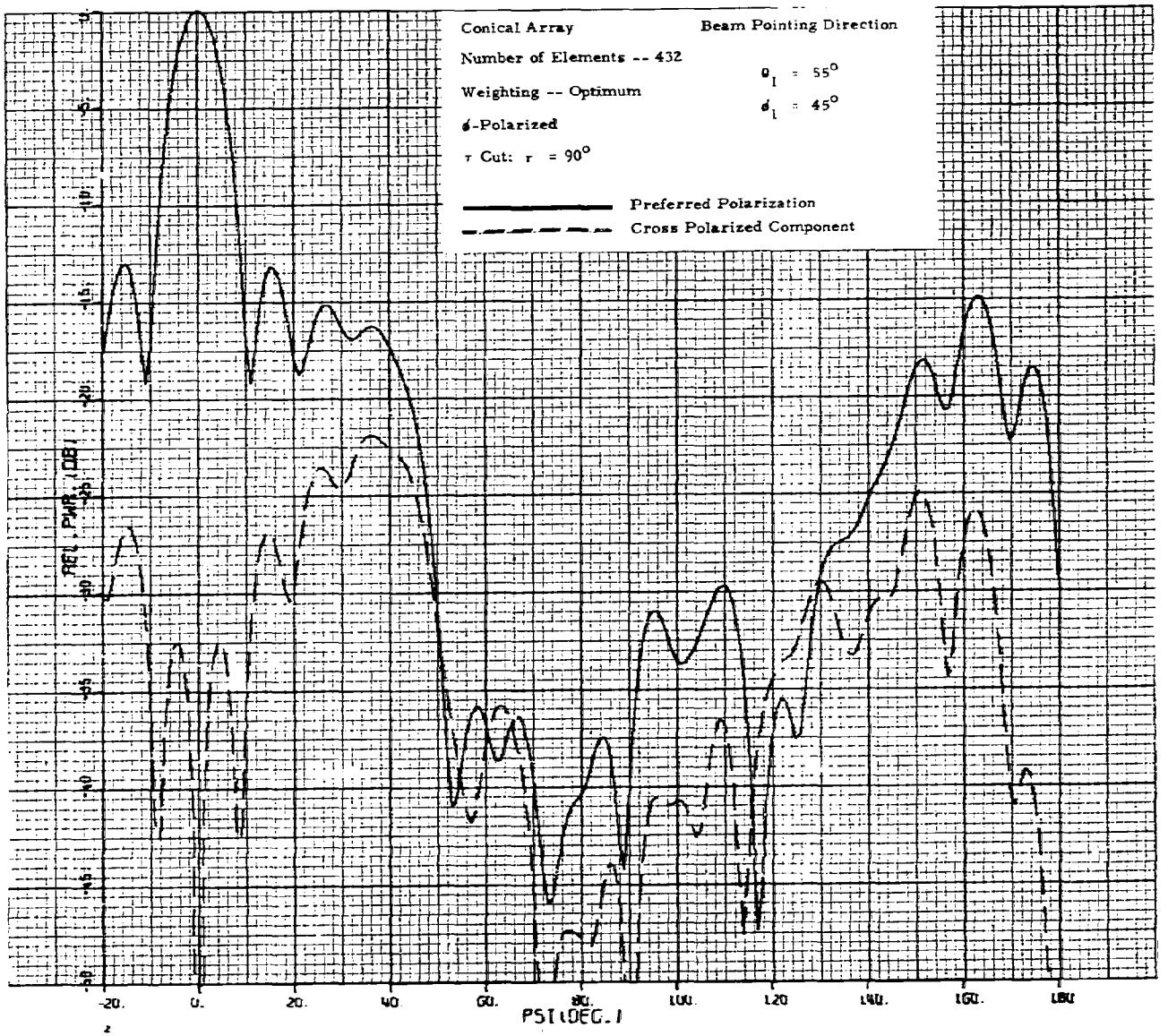

Figure 3.4-29. ϕ-Polarized Pattern of Principal Plane Cut ($\tau = 90^{\circ}$) Through Beam in First Quadrant -- 432 Elements

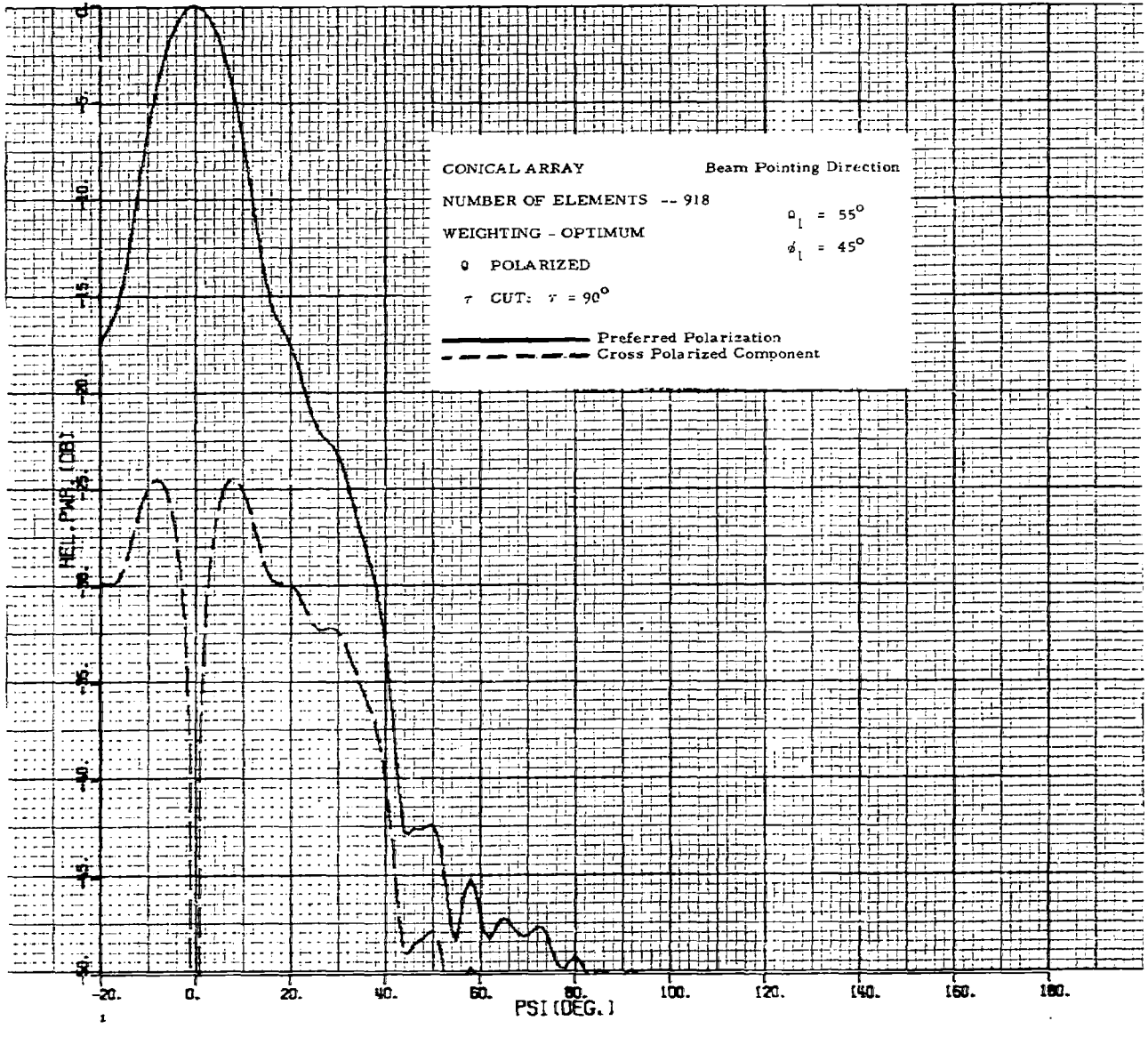

Figure 3.4-30. θ-Polarized Pattern of a Principal Plane Cut ($\tau = 90^{\circ}$) Through Beam in First Quadrant -- 918 Elements

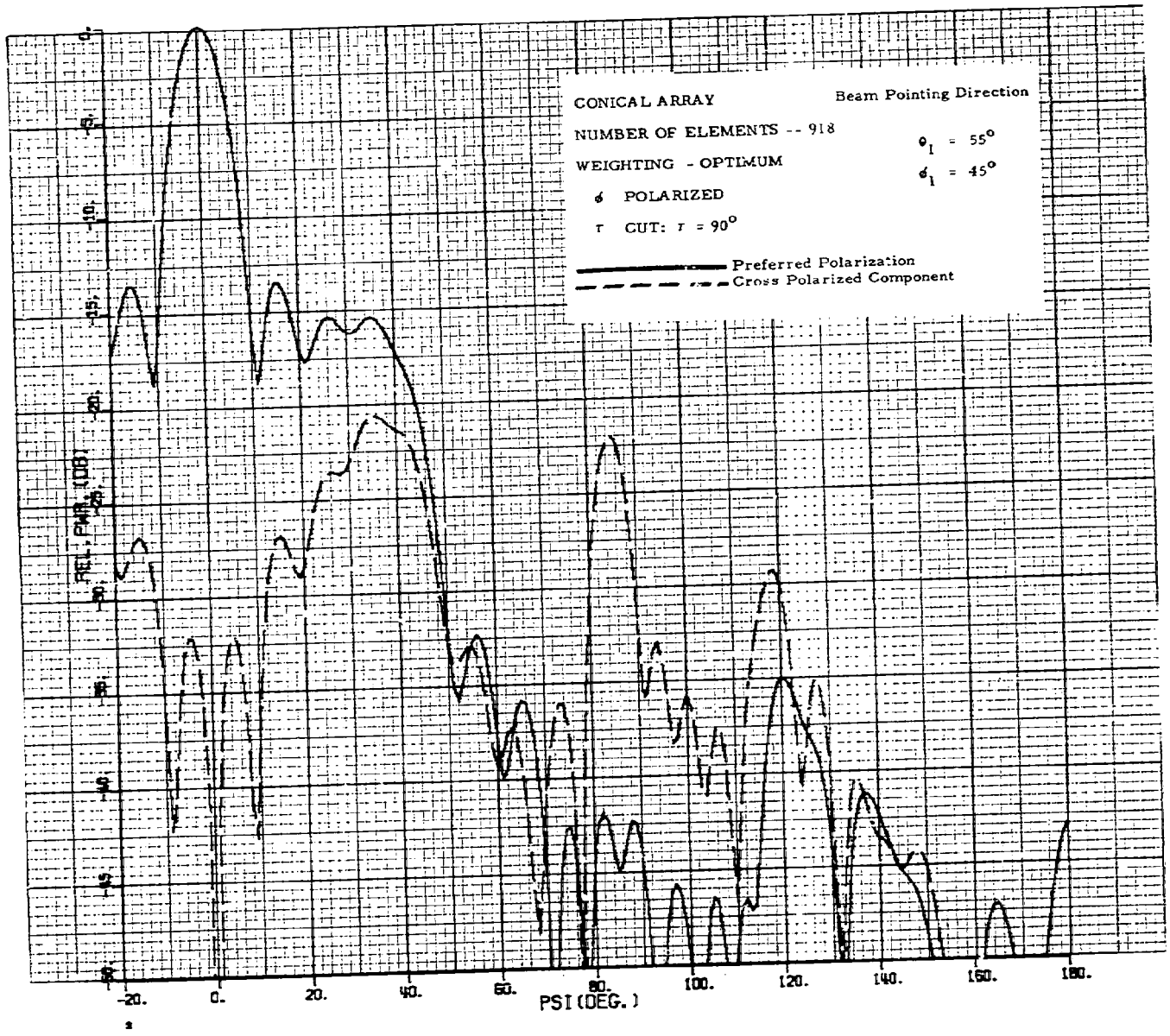

Figure 3.4-31. ϕ-Polarized Pattern of a Principal Plane Cut ($\tau = 90^\circ$) Through Beam in First Quadrant -- 918 Elements

The patterns for the 432 element configuration will be considered next. The θ- and ϕ-polarized patterns for this cut are given in Figures 3.4-28 and -29. The θ-polarized pattern (Fig. 3.4-28) represents a slight improvement over the corresponding pattern for 288 elements (Fig. 3.4-26). The pattern for 288 elements was already very good. The ϕ-polarized pattern, Figure 3.4-29, has a very high backlobe; in fact, it is considerably higher than the backlobe for the 288 element case. The increase of this lobe with an increase in the number of elements is not readily apparent. In general, a larger number of elements yields better patterns. This increase may be an anomaly that arises from the particular cone geometry being used and the particular scan angle of $\theta = 55^{\circ}$, $\phi = 45^{\circ}$. It could possibly arise from the less than perfect element pattern that is being used for computations. It should be investigated further. The corresponding pattern in Figure 3.4-27 for a 288 element array also has a high backlobe.

The patterns for the 918 element configuration are given in Figures 3.4-30 and -31. In this case the large number of elements produces a nearly ideal pattern for the θ-polarized beam but not for the ϕ-polarized beam. This is similar to the situation that existed for the $\tau = 90^{\circ}$ cut through the beam steered to $\theta_1 = 80^{\circ}$, $\phi_1 = 90^{\circ}$. The θ-polarized pattern (Fig. 3.4-30) has extremely low far-out sidelobes and no backlobes. It compares to Figure 3.4-26 for the 288 element case and to Figure 3.4-28 for the 432 element case, and is a considerable improvement over each. The ϕ-polarized pattern (Fig. 3.4-31) has high shoulders close in to the main beam. However, its grating lobe and backlobe structures are satisfactory. Comparing this pattern with Fig. 3.4-27 for 288 elements and Fig. 3.4-29 for 432 elements shows that both of those patterns had the same close-in shoulder structure that appears in the 918 element pattern. Therefore, it must be concluded that the shoulders are a result of the inherent geometry of the cone and the optimum taper being used to feed the elements. In regards to grating lobes and backlobes, the 918 element pattern is superior to each of the other two.

3.4.3.2 $\tau = 45^\circ$ Cut Through Beam at θ_1, $\phi_1 = 55^\circ$, 45°

This is a quadrant cut through the beam in the first quadrant. It is half-way between the two principal plane cuts. Figures 3.4-32 through -37 will give the patterns in this series.

Figures 3.4-32 and -33 show the θ- and ϕ-polarized patterns, respectively, for the 288 element configuration. The grating lobes in both these patterns are much worse than in the $\tau = 90^\circ$ cut. In the θ-polarized pattern the grating lobe rises to -14 dB at $\psi = 82^\circ$, and is fairly broad, but drops off sharply between 110° and 130°. The sharp drop off, and particularly the step functions, are unrealistic and are probably caused by the semi-circular nature of the element patterns used for the circumferential slots in the θ plane. The ϕ-polarized pattern shows the same high grating lobes starting at about 80°; however, these lobes stay up over quite a wide angle, and re-appear as a backlobe after a short drop off at about $\psi = 160$ degrees. These patterns are not satisfactory.

The patterns for the 432 element configuration are much improved over the 288 element case as can be seen in Figures 3.4-34 and -35. The main beams are almost identical for the two cases. The high grating lobe that showed up at $\psi \approx 90^\circ$ in the earlier θ-polarized pattern is still present in Figure 3.4-34 for the 432 element case. However, it has been reduced about 5 dB in peak magnitude, and its width in ψ is much reduced. Although the pattern in this Figure could not be called desirable, under certain circumstances it could be considered as usable.

The ϕ-polarized pattern for this cut, Figure 3.4-35, is considerably improved compared to its 288 element counterpart in Figure 3.4-33. Again the main beams are very similar, and the close-in sidelobe structure is not markedly different. The difference shows up in the grating lobes where a high, wide grating lobe in Figure 3.4-33 has been reduced to a much lower, narrower one limited to the region of $\psi = 90^\circ$ in Figure 3.4-35. Each of the patterns has a backlobe, and here it appears that the element arrangement with the larger number of elements is actually worse than the simpler arrangement. Overall, however, the 432 element pattern is better than the 288 element pattern.

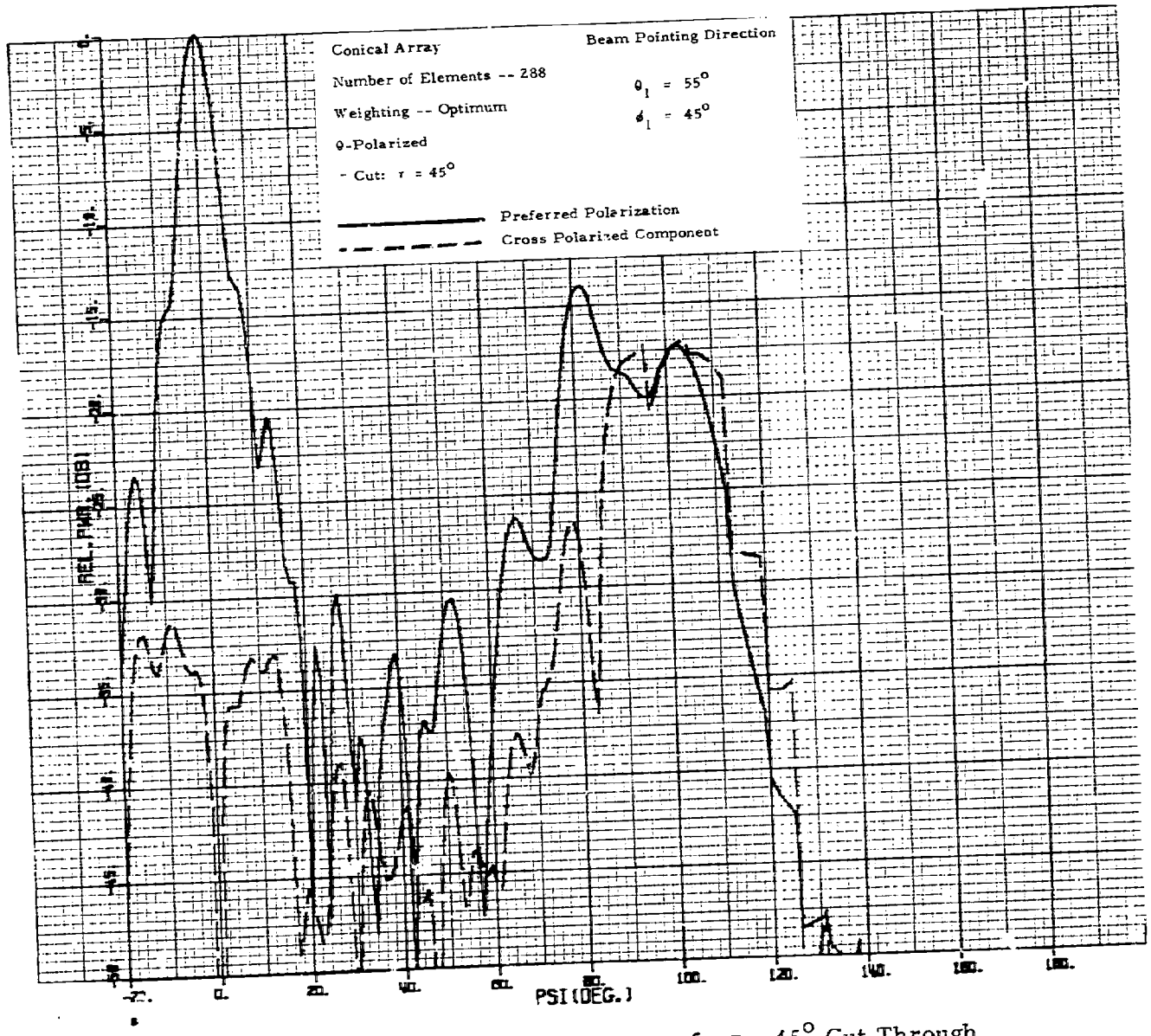

Figure 3.4-32. θ -Polarized Pattern of a $\tau = 45^{\circ}$ Cut Through a Beam in First Quadrant -- 288 Elements

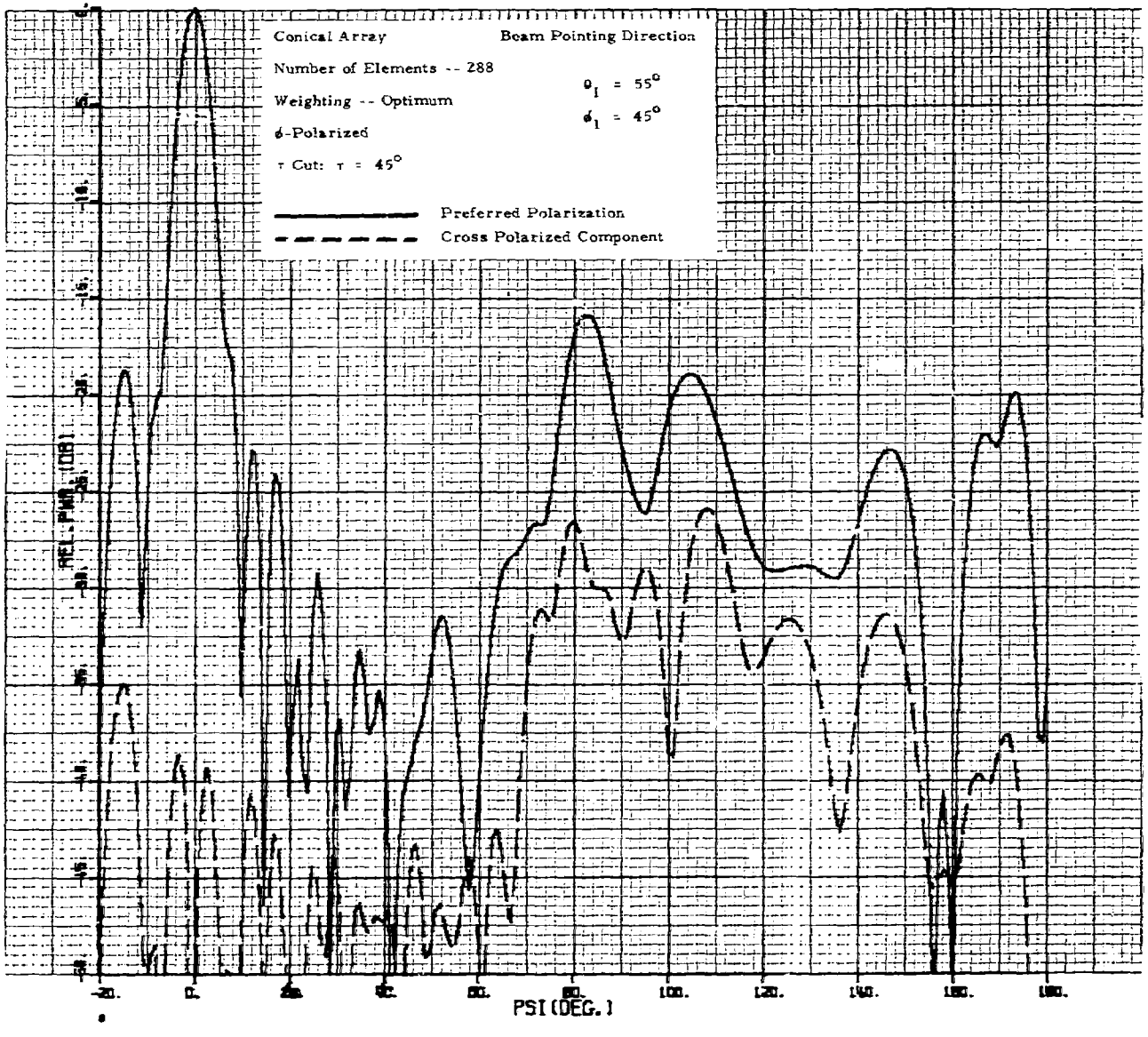

Figure 3.4-33. ϕ-Polarized Pattern of a $\tau = 45^\circ$ Cut Through a Beam in the First Quadrant -- 288 Elements

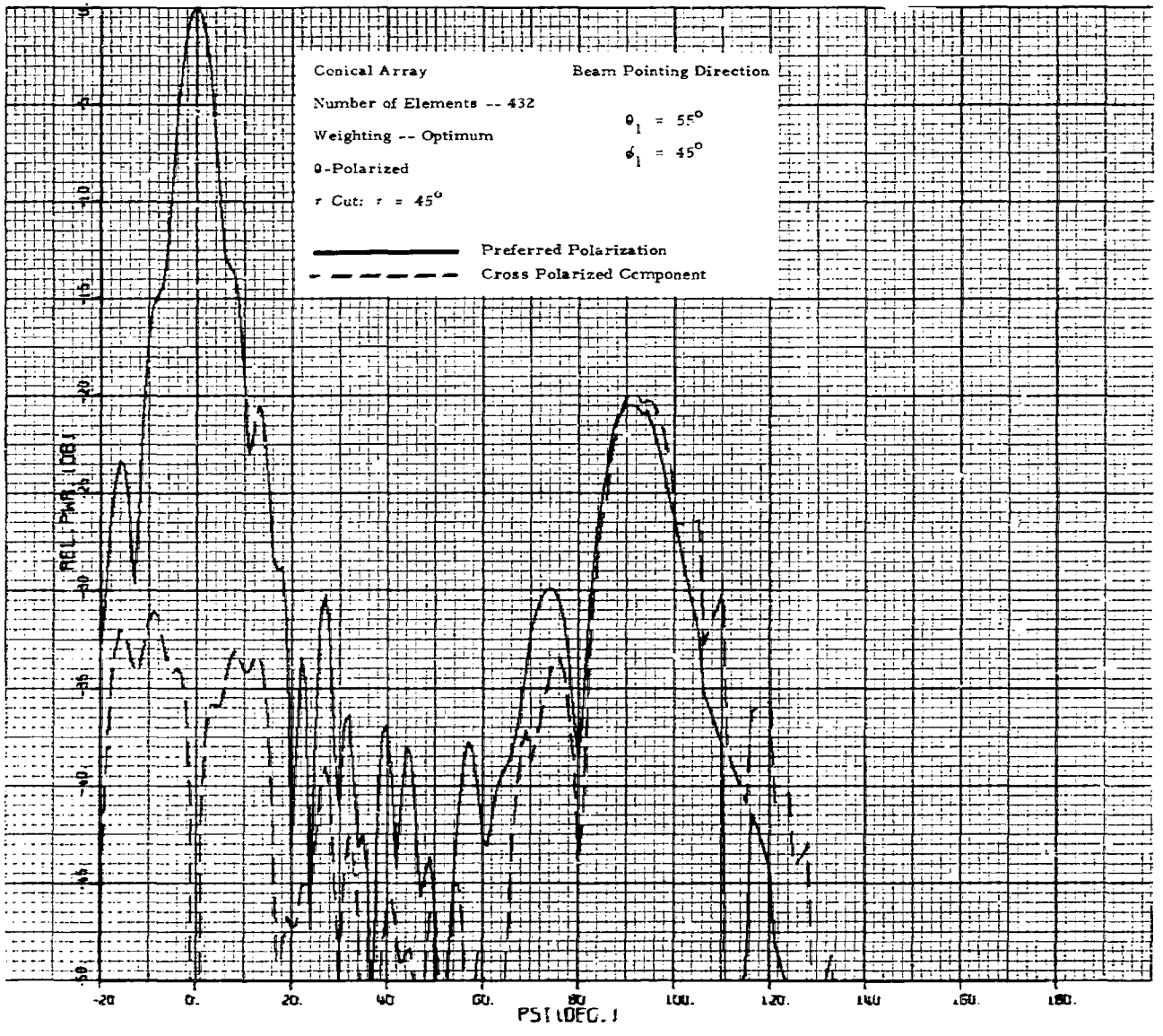

Figure 3.4-34. θ-Polarized Pattern of $\tau = 45^{\circ}$ Cut Through Beam in First Quadrant -- 432 Elements

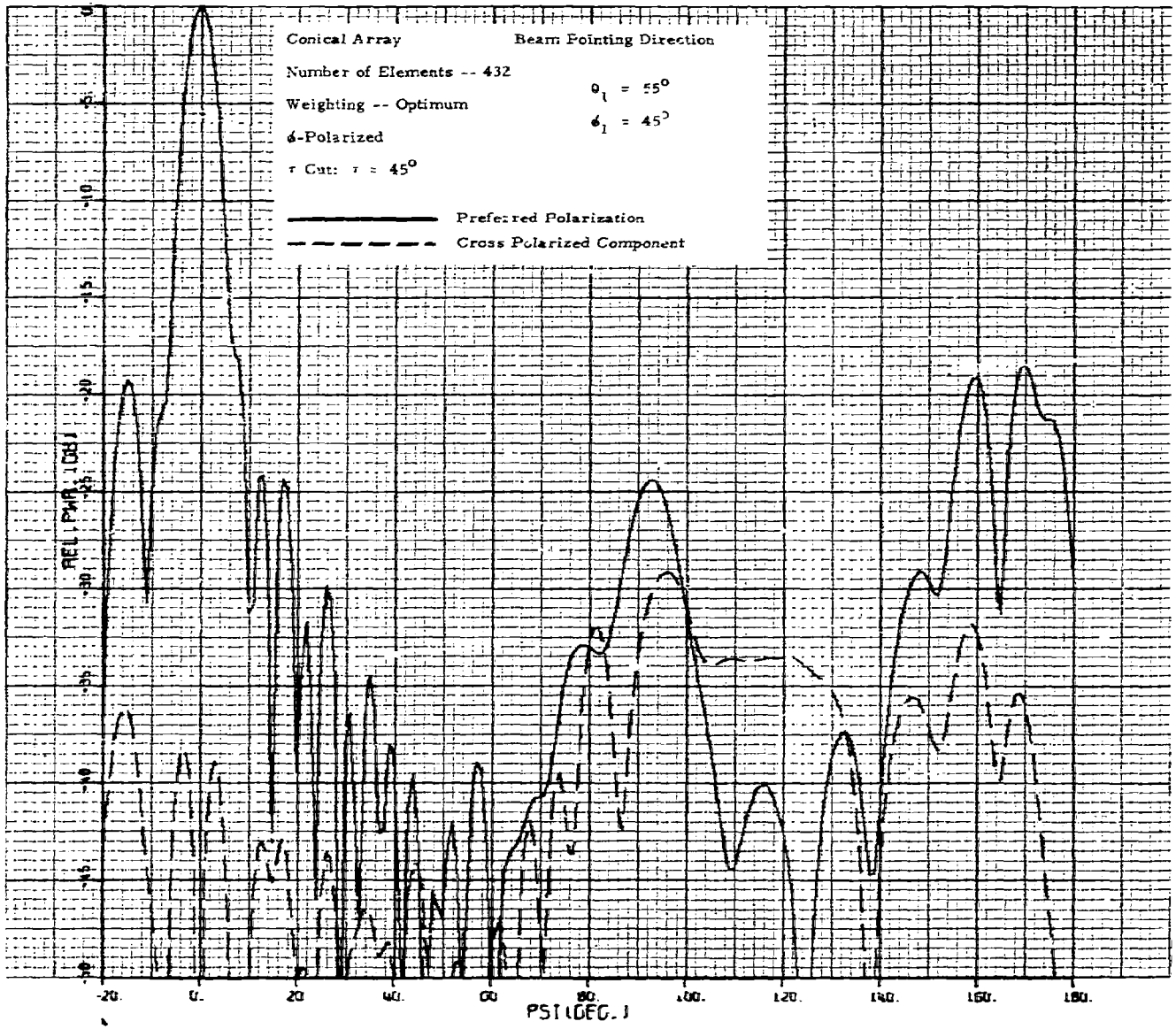

Figure 3.4-35 ϕ-Polarized Pattern of $\tau = 45^\circ$ Cut Through Beam in First Quadrant -- 432 Elements

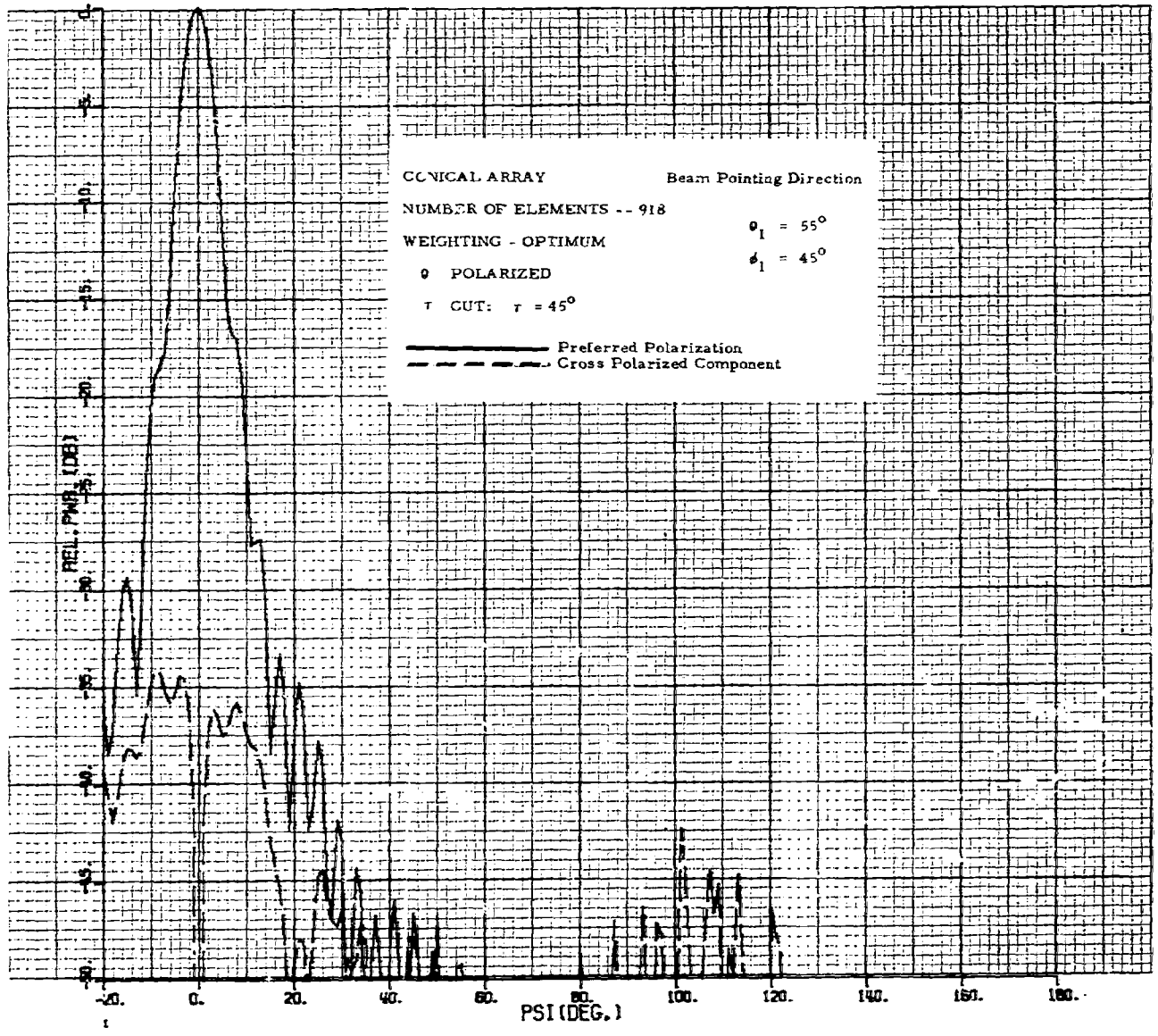

Figure 3.4-36. θ-Polarized Pattern of $\tau = 45^\circ$ Cut Through Beam in First Quadrant -- 918 Elements

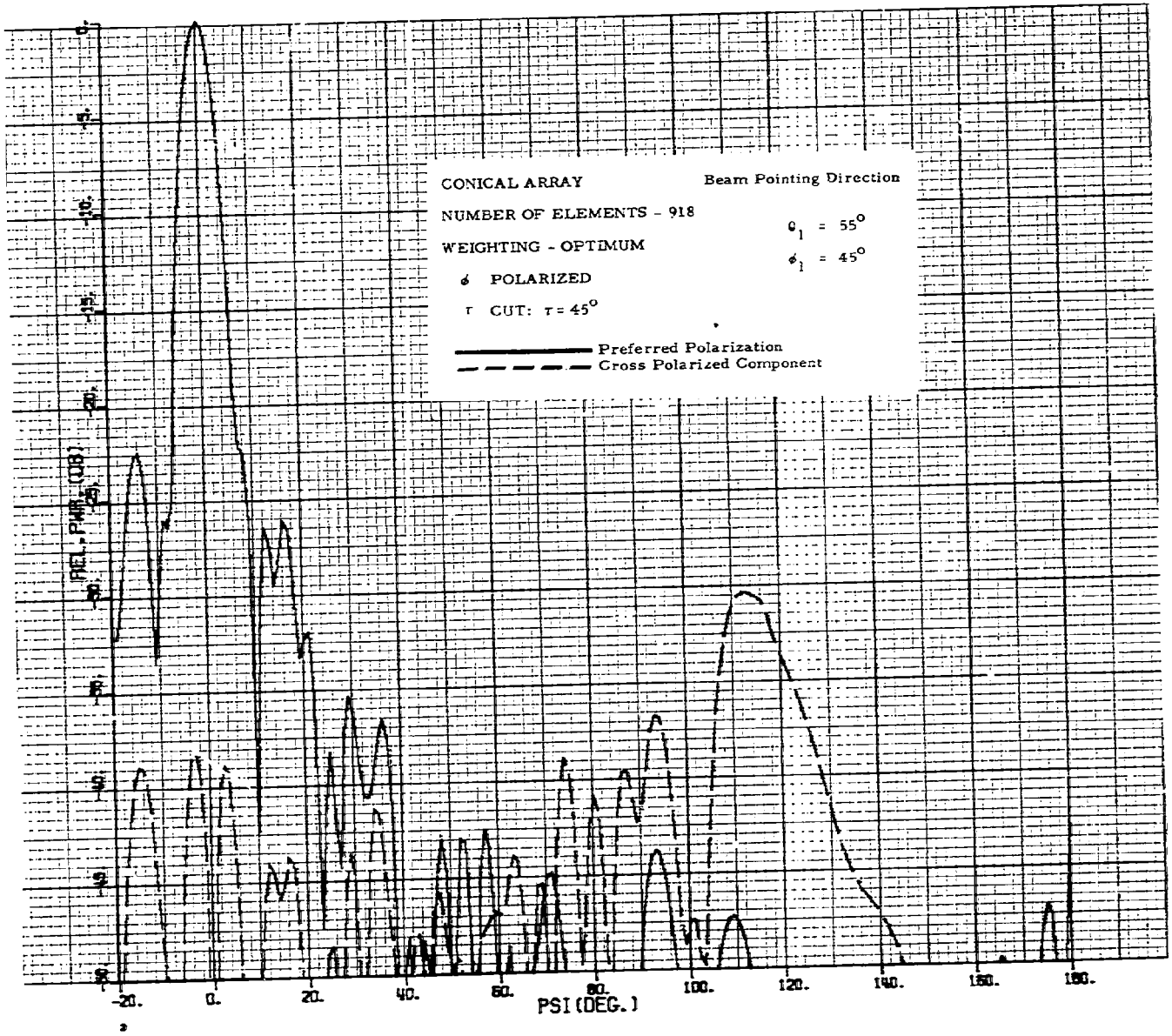

Figure 3.4-37. ϕ-Polarized Pattern of $\tau = 45^{\circ}$ Cut Through Beam in First Quadrant -- 918 Elements

The 918 element patterns, shown in Figures 3.4-36 and -37, are again close to ideal as would be expected with so many elements. The θ-polarized pattern (Fig. 3.4-36) has neither grating lobe nor backlobes. A comparison with the 288 element case (Fig. 3.4-32) shows a vast improvement; and a comparison with the 432 element case (Fig. 3.4-34) shows a large improvement.

The ϕ-polarized pattern for the 918 element case (Fig. 3.4-37) is not quite so ideal, but still very good. It is much better than either the 288 or 432 element cases (Figs. 3.4-33 and -35, respectively). The 918 element pattern has a somewhat large cross-polarized lobe at $\psi = 115^{\circ}$ at a point where there is virtually no preferred polarization component. This characteristic seems to be a dominant feature of the 918 element configuration.

3.4.3.3 $\tau = 135^{\circ}$ Cut Through a Beam at θ_1, $\phi_1 = 55^{\circ}$, 45°

This upper quadrant cut through the beam is at right angles to the $\tau = 45^{\circ}$ cut discussed above. The patterns for this series are given in Figures 3.4-38 through -43.

The 288 element configuration will be discussed first. Figures 3.4-38 and -39 show the θ- and ϕ-polarized patterns, respectively, of this cut. The main beams are much the same as for the 45° cut above (Fig. 3.4-32 and -33); however, the grating lobe structure is much less pronounced. In the θ-polarized case the preferred polarization component is quite low (around -35 to -40 dB); however, the cross-polarized component is still somewhat higher than desirable. The ϕ-polarized pattern, as before, shows lobe structure extending clear around to the backside of the cone at $\psi = 180$ degrees. The lobe region from $\psi = 70$ degrees to $\psi \approx 100$ degrees appears to be a grating lobe, while the peak at ≈ 175 degrees is probably a backlobe.

The patterns for the 432 element case are given in Figures 3.4-40 and -41, and their counterparts for 288 elements are given in Figures 3.4-38 and -39, respectively. In Figure 3.4-38 (the θ-polarized pattern) a grating lobe had started to form in the region of $\psi = 60$ to 100 degrees.

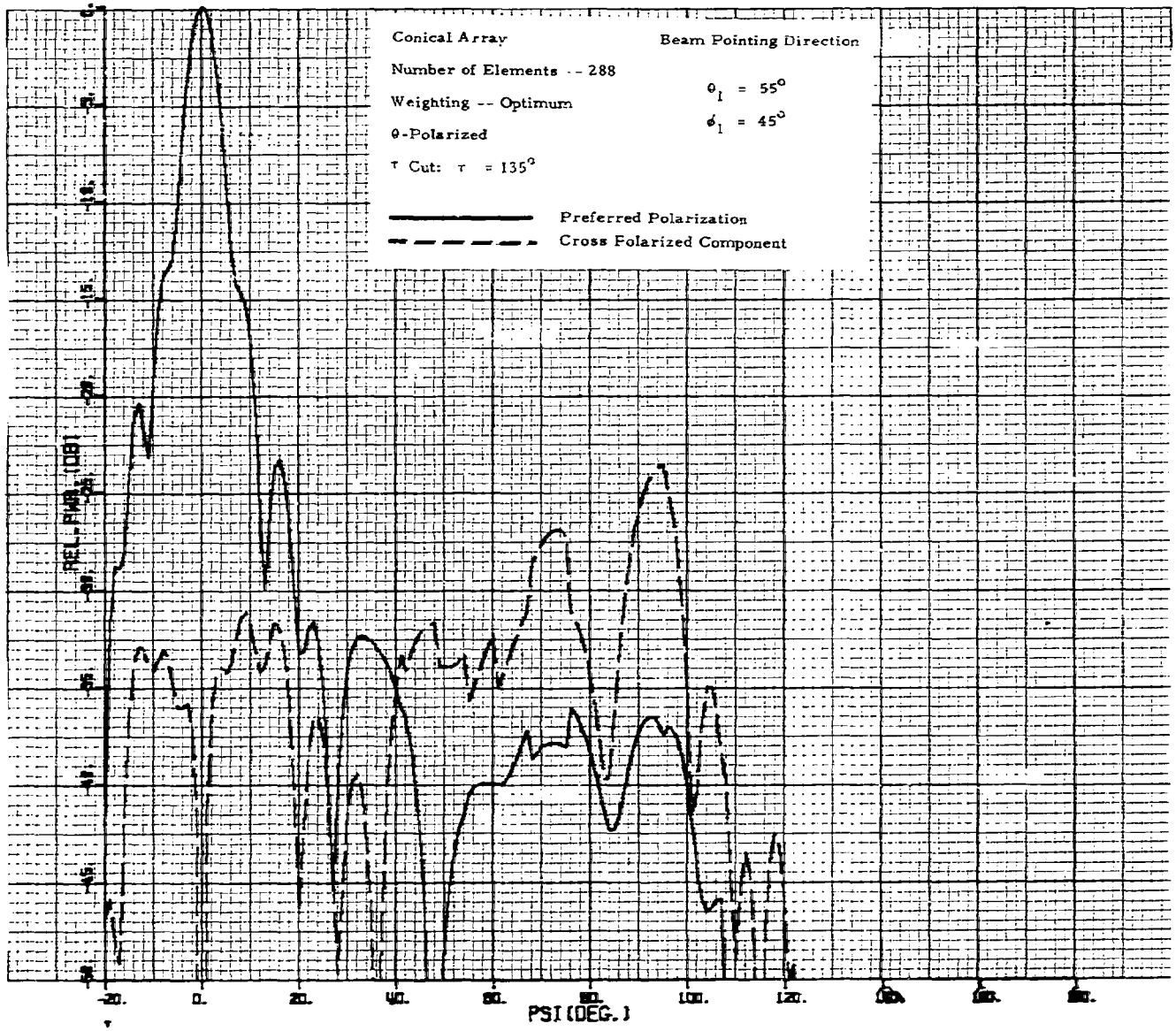

Figure 3.4-38. θ-Polarized Pattern for a $\tau = 135^{\circ}$ Cut Through a Beam in the First Quadrant -- 288 Elements

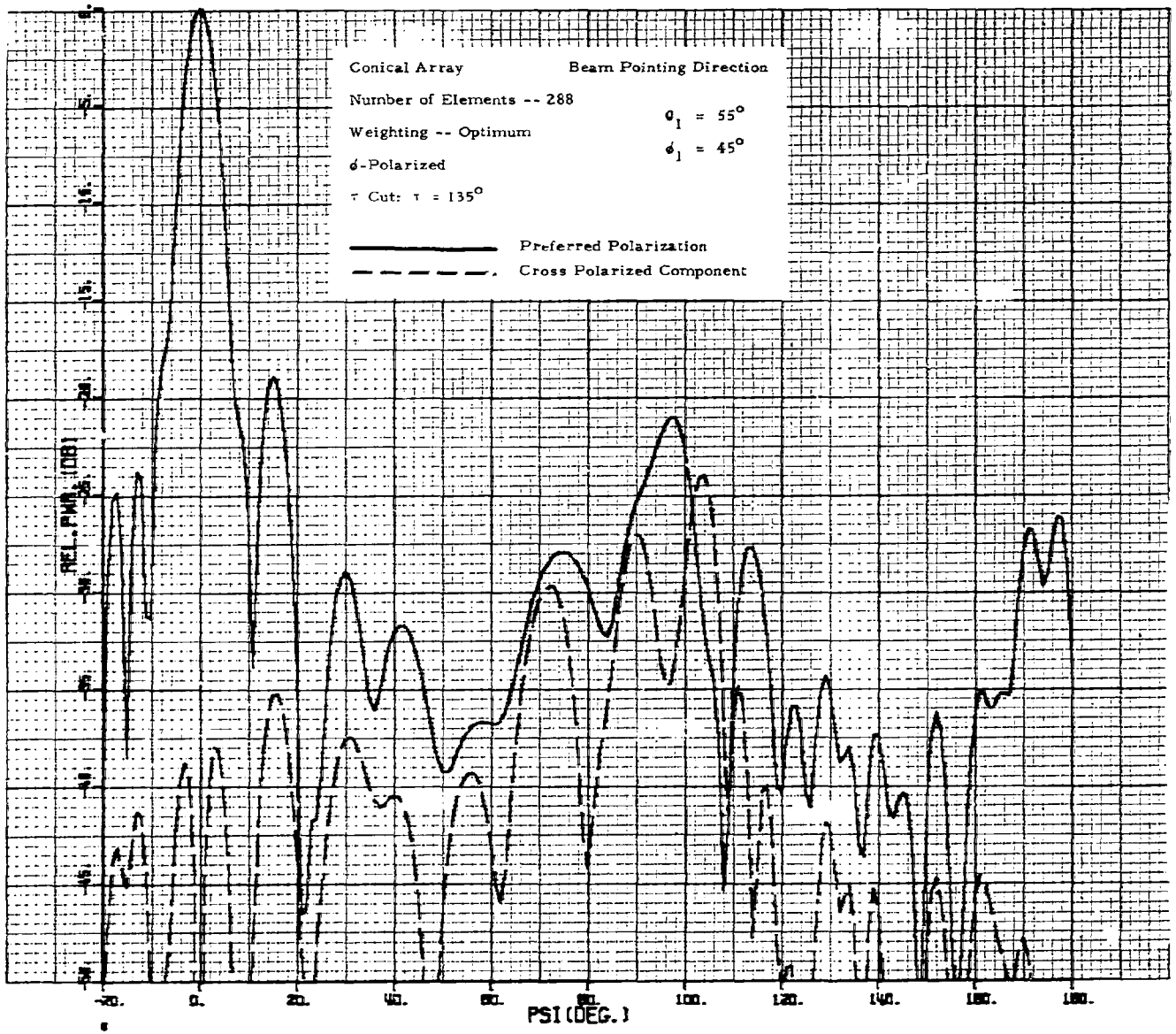

Figure 3.4-39. ϕ-Polarized Pattern for a $\tau = 135^{\circ}$ Cut Through a Beam in the First Quadrant -- 288 Elements

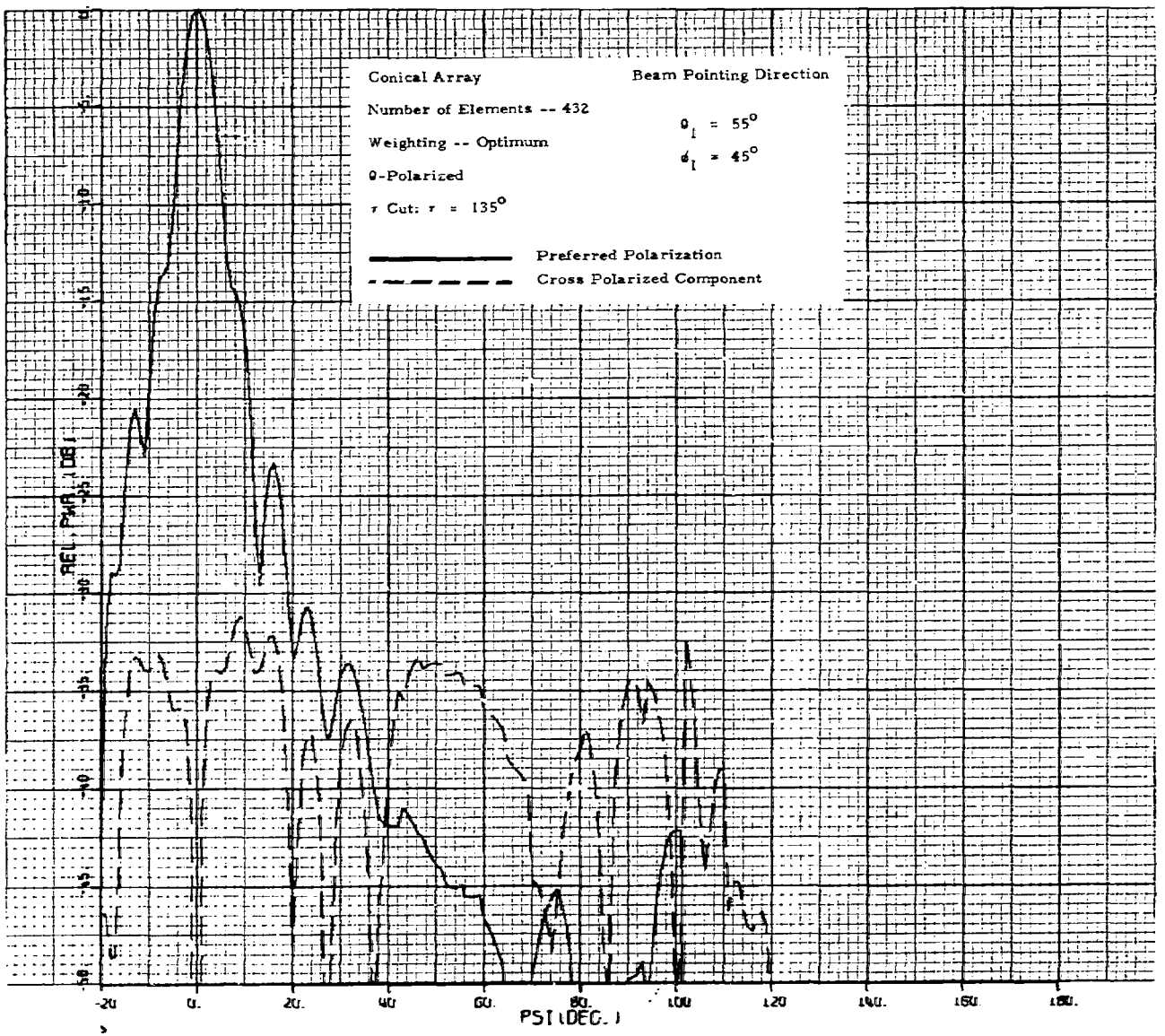

Figure 3.4-40. θ-Polarized Pattern of $\tau = 135^{\circ}$ Cut Through a Beam in First Quadrant -- 432 Elements

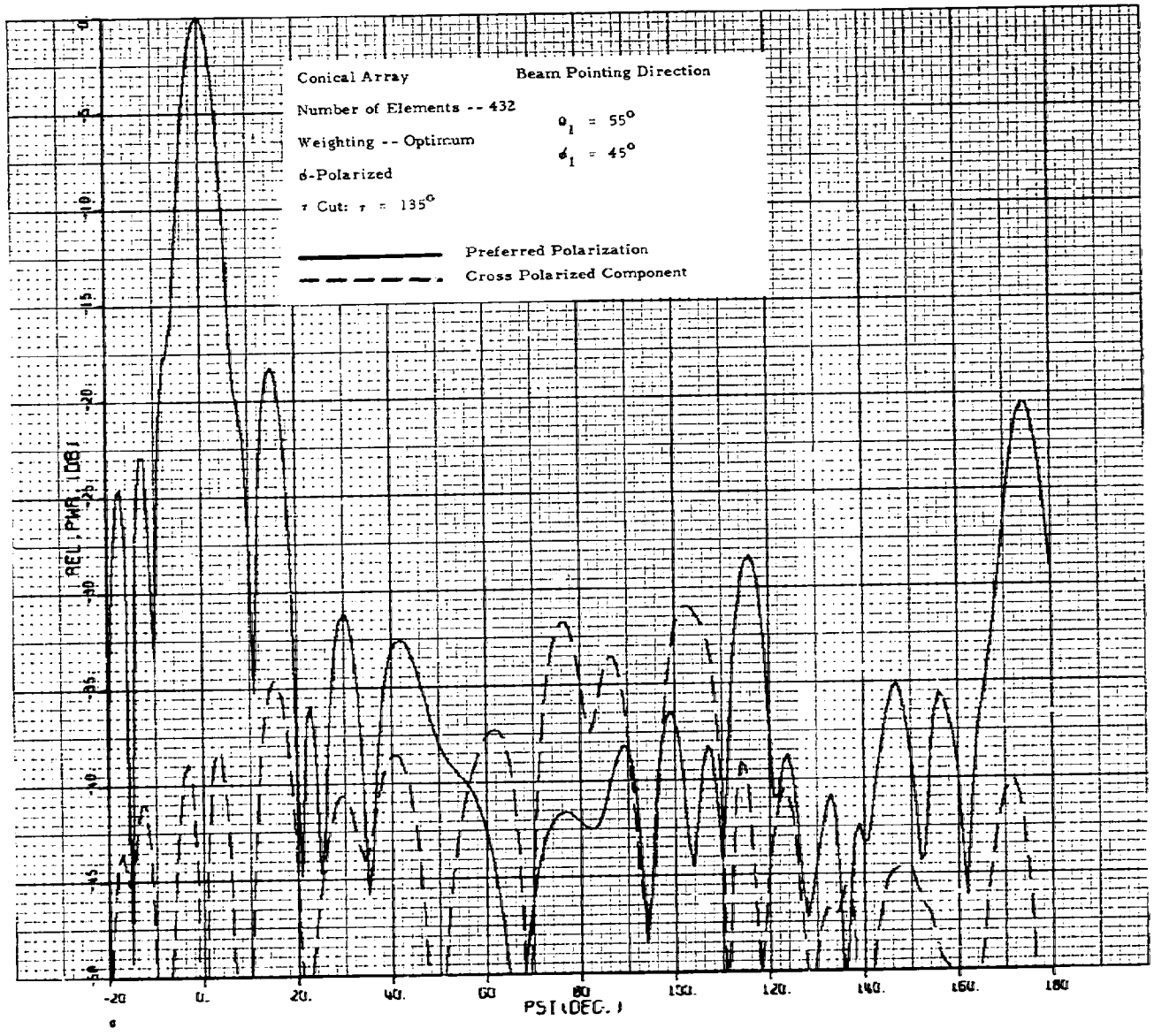

Figure 3.4-41. ϕ-Polarized Pattern of $\tau = 135^\circ$ Cut Through a Beam in First Quadrant -- 432 Elements

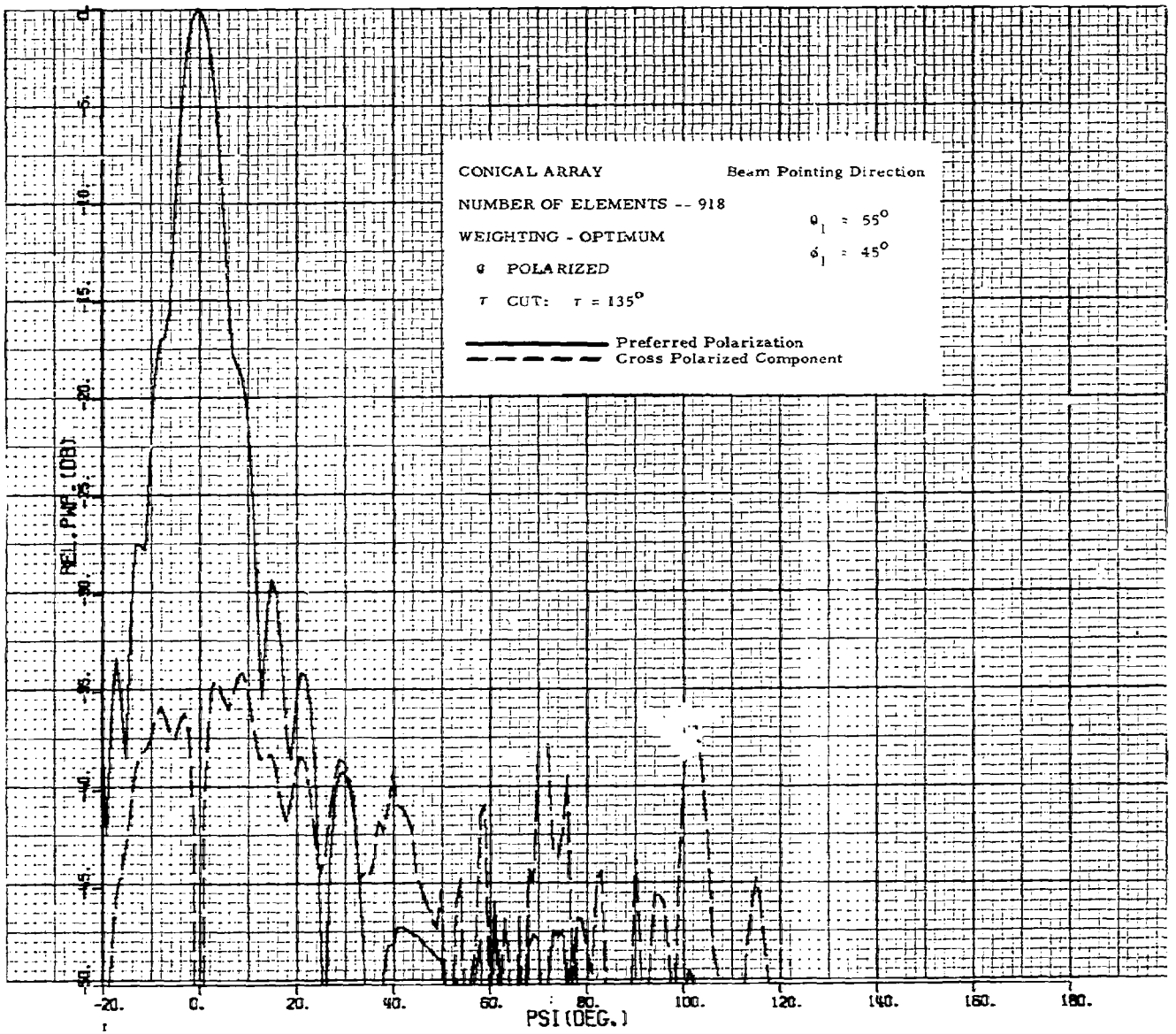

Figure 3.4-42. θ-Polarized Pattern of τ = 135° Cut Through a Beam in First Quadrant -- 918 Elements

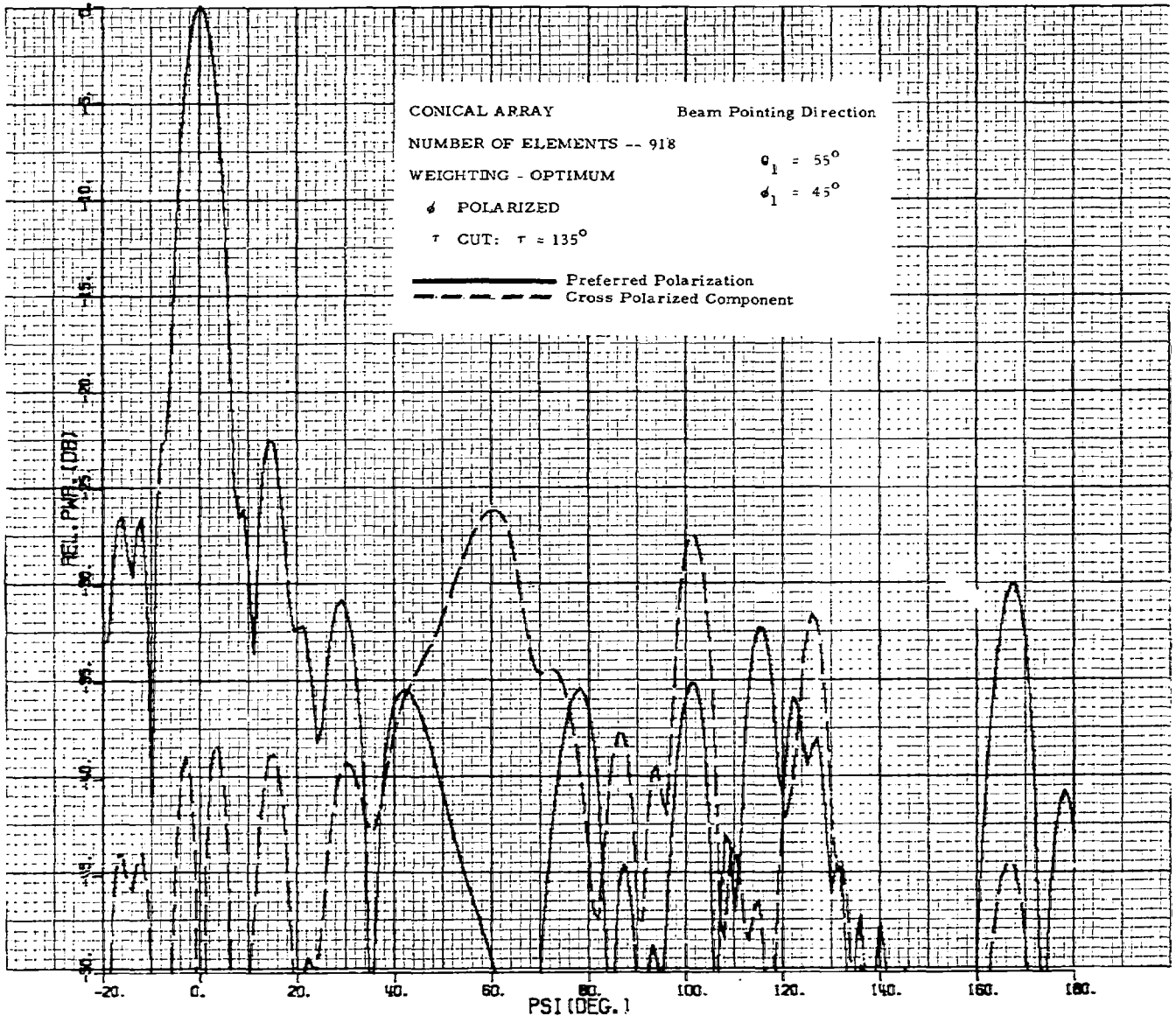

Figure 3.4-43. ϕ-Polarized Pattern of τ = 135° Cut Through a Beam in First Quadrant -- 918 Elements

In Figure 3.4-40 that lobe is much reduced, along with the cross-polarized component which is noticeably larger than the preferred polarization in that region. Figure 3.4-41 shows the ϕ-polarized pattern for the 432 element case. This pattern is an obvious improvement over the equivalent 288 element pattern shown in Figure 3.4-39. A large grating lobe shows up at about $\psi = 95^{\circ}$ in Figure 3.4-39 which has been much reduced in magnitude, and pushed out further in ψ, in Figure 3.4-41. However, the backlobe again is higher for the 432 element configuration as was the case for this beam pointing direction and element configuration in the $\tau = 90^{\circ}$ cut. (See Fig. 3.4-29) Thus, the backlobe seems to be consistently higher and suggests that the size of the backlobe is some type of cyclic function of the inter-element spacing. Hence, it may be possible to choose an optimum spacing rather than striving for the closest spacing possible.

The 918 element configuration for this cut produced a very good θ-polarized pattern (Fig. 3.4-42) and a reasonable good ϕ-polarized pattern (Fig. 3.4-43). The θ-polarized pattern for this configuration is much better than the comparable 288 pattern in Figure 3.4-38. The grating lobe that started to form at $\psi \approx 80^{\circ}$ in the 288 element case is almost completely suppressed in the 918 element case. Figure 3.4-42 also represents a considerable improvement over the 432 element case shown in Fig. 3.4-40. The cross-polarized component that had sizeable lobes at $\psi = 45^{\circ}$ and 90° in the 432 element case are also much reduced in the 918 element pattern.

The ϕ-polarized pattern for the 918 element case (Fig. 3.4-43) is not an ideal pattern by a considerable margin. None of the lobes are particularly high but there is a large number of small sharp lobes between $\psi = 70^{\circ}$ and $\psi = 170^{\circ}$. Also a cross-polarized lobe at $\psi = 60^{\circ}$ is rather wide as well as being higher than the preferred component. Despite these failings; however, the 918 element pattern is much improved over the 288 element case (Fig. 3.4-39), and somewhat improved over the 432 element case (Fig. 3.4-41). The relatively high graing lobe in the region of $\psi = 70^{\circ}$ to 120° in the 288 element case has been reduced to -35 dB. A backlobe in the 288 element pattern has been much reduced in width in the 918 element case.

Compared to the 432 element case the 918 element configuration is not so much of an improvement. The 432 element configuration (Fig. 3.4-41) has a reasonably good pattern with the exception of a rather high backlobe at $\psi = 175^{\circ}$. In the 918 element pattern that lobe has been reduced to -30 dB and the shoulders and sidelobes near the main beam have all been lowered by about 5 dB.

4.0 SUMMARY AND CONCLUSION OF COMPUTED PATTERNS OF HEURISTIC METHOD

The large number of patterns presented in Section 3.4 are summarized in the five graphs in this section. Several parameters are given as a function of the number of elements on the cone, the beam pointing direction, and the particular cut through the beam. The number of elements is treated as an independent variable; however, there are differences in the element arrangements so that there are changes between configurations not apparent from a study of these graphs.

The magnitudes of the grating lobes are given in Figure 4.0-1 and -2. From each pattern only the largest of the preferred or cross-polarized grating lobes was plotted. Figure 4.0-1 gives the results for the beam pointing directions of $\theta_1 = 0^\circ$, $\phi_1 = 0^\circ$ and $\theta_1 = 80^\circ$, $\phi_1 = 90^\circ$ while Figure 4.0-2 shows the lobes only for the direction $\theta_1 = 55^\circ$, $\phi_1 = 45^\circ$. It is apparent from studying these two figures that, in general, the configurations with the larger number of elements show lower grating lobes. This is to be expected from linear and circular array theory. However, some exceptions show up in the figures which may be due to the complex geometry of the conical array. They may also be due to the fact that some of the geometries of the element configurations are much different than the others. The beam pointing direction, the polarization of the beam, and the pattern cut all influence the magnitude of the grating lobe.

The backlobes of the patterns are given in Figure 4.0-3. In all cases, except the nose-fire beam pointing direction, the θ-polarization pattern did not have a backlobe. In the results that are plotted there is no clear trend that configurations with larger numbers of elements have lower backlobes except for the beam pointing direction of $\theta_1 = 55^\circ$, $\phi_1 = 45^\circ$. The $\phi = 90^\circ$ cut for the beam pointing direction of $\theta_1 = 80^\circ$, $\phi_1 = 90^\circ$ is not represented on this graph because its pattern was only taken over a range of approximately $\pm 90^\circ$ in relation to the main beam. Hence, any high lobe appearing at the edges of these patterns would be grating lobes rather than backlobes.

Figures 4.0-4 and -5 show the level of the highest shoulder appearing on the main beam of each pattern. In some cases there were no shoulders on the beams, or the first sidelobes were higher than the shoulders.

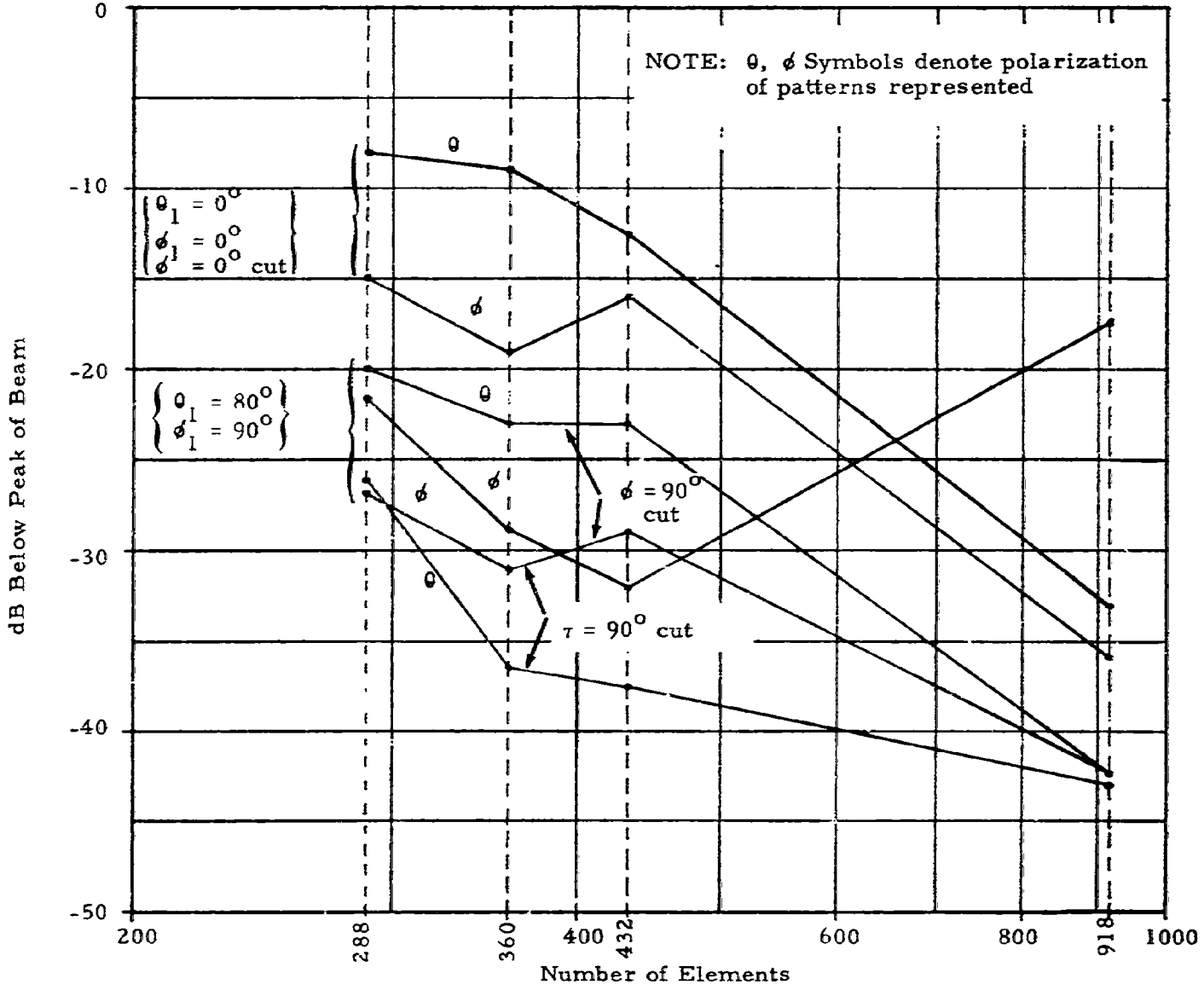

Figure 4.0-1. Grating Lobes vs. Number of Elements on Cone for Two Beam Pointing Directions

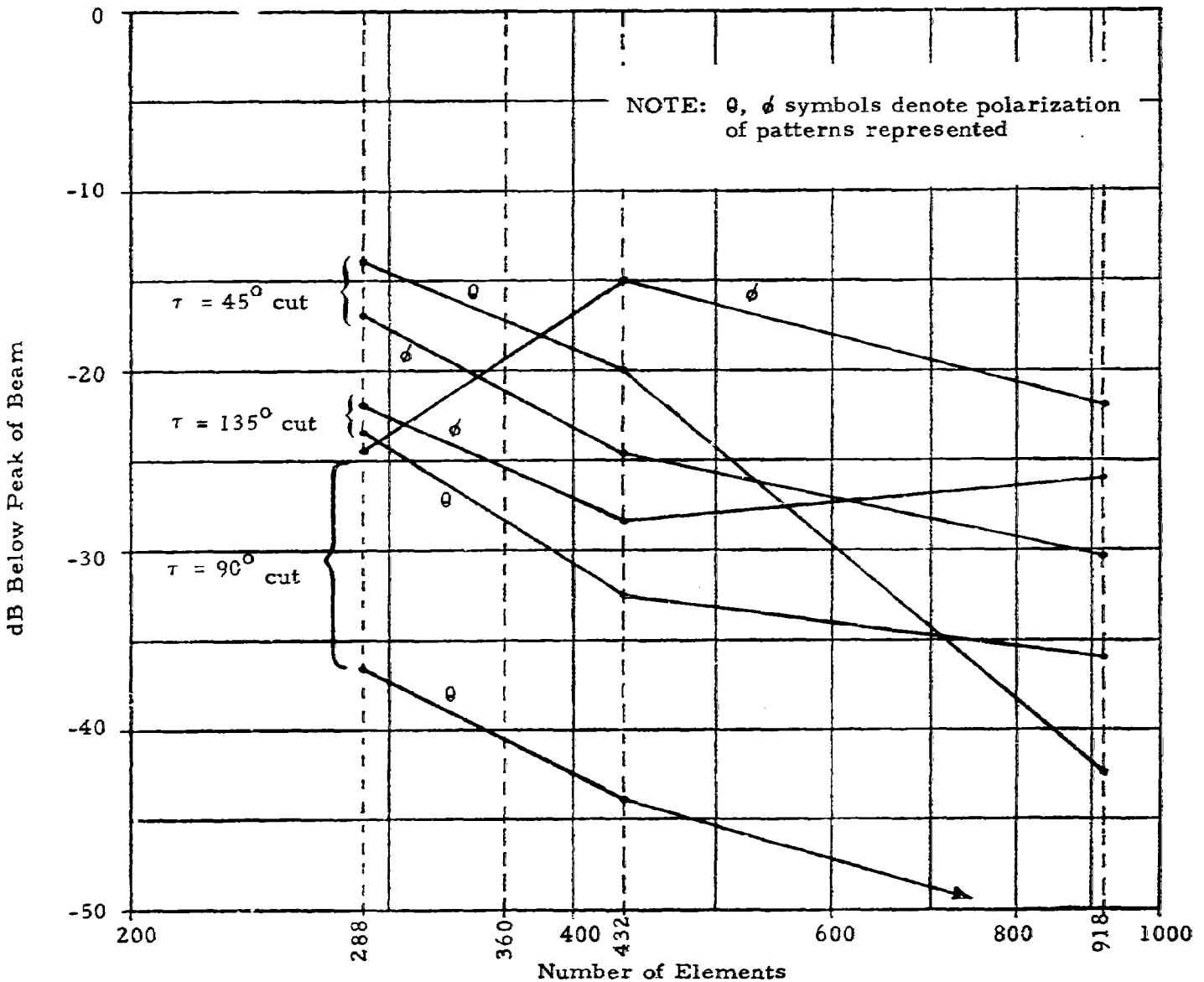

Figure 4.0-2. Grating Lobe Level vs. Number of Elements on Cone for Beam Pointing Direction of $\theta_1 = 55^\circ$, $\phi_1 = 45^\circ$

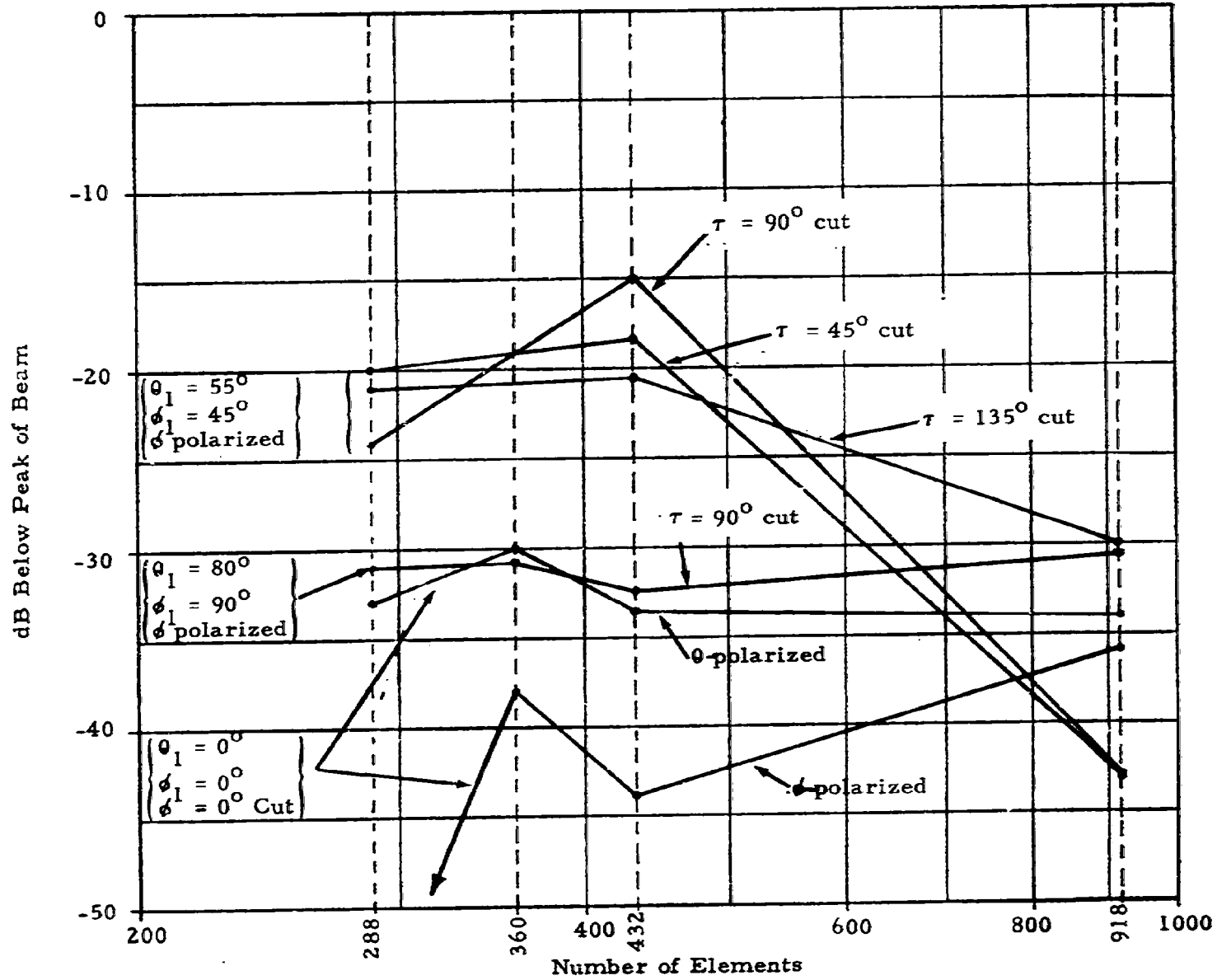

Figure 4.0-3. Backlobe Level vs. Number of Elements on Cone

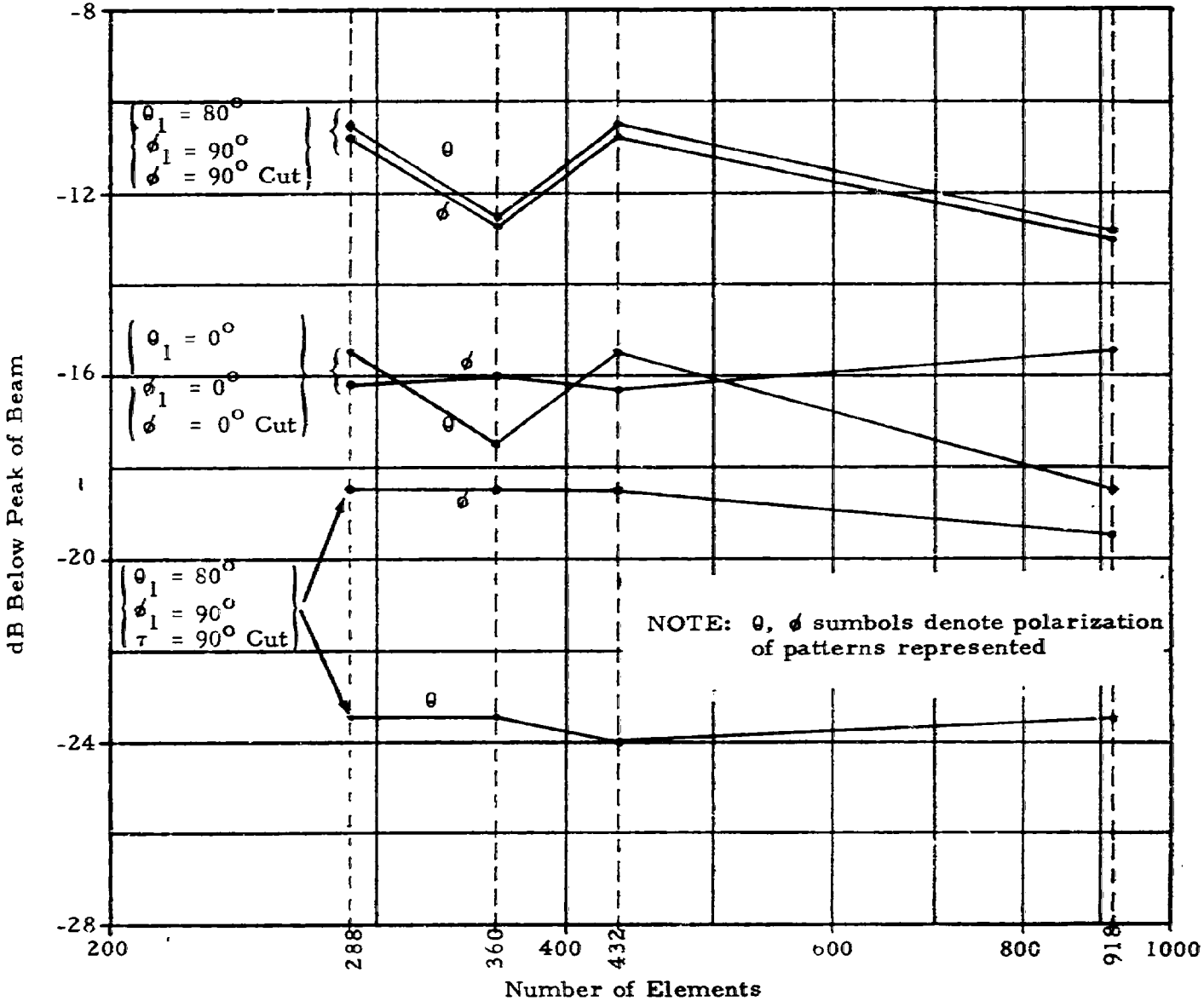

Figure 4.0-4. Highest Shoulder or First Sidelobe vs. Number of Elements on Cone for Two Beam Pointing Directions

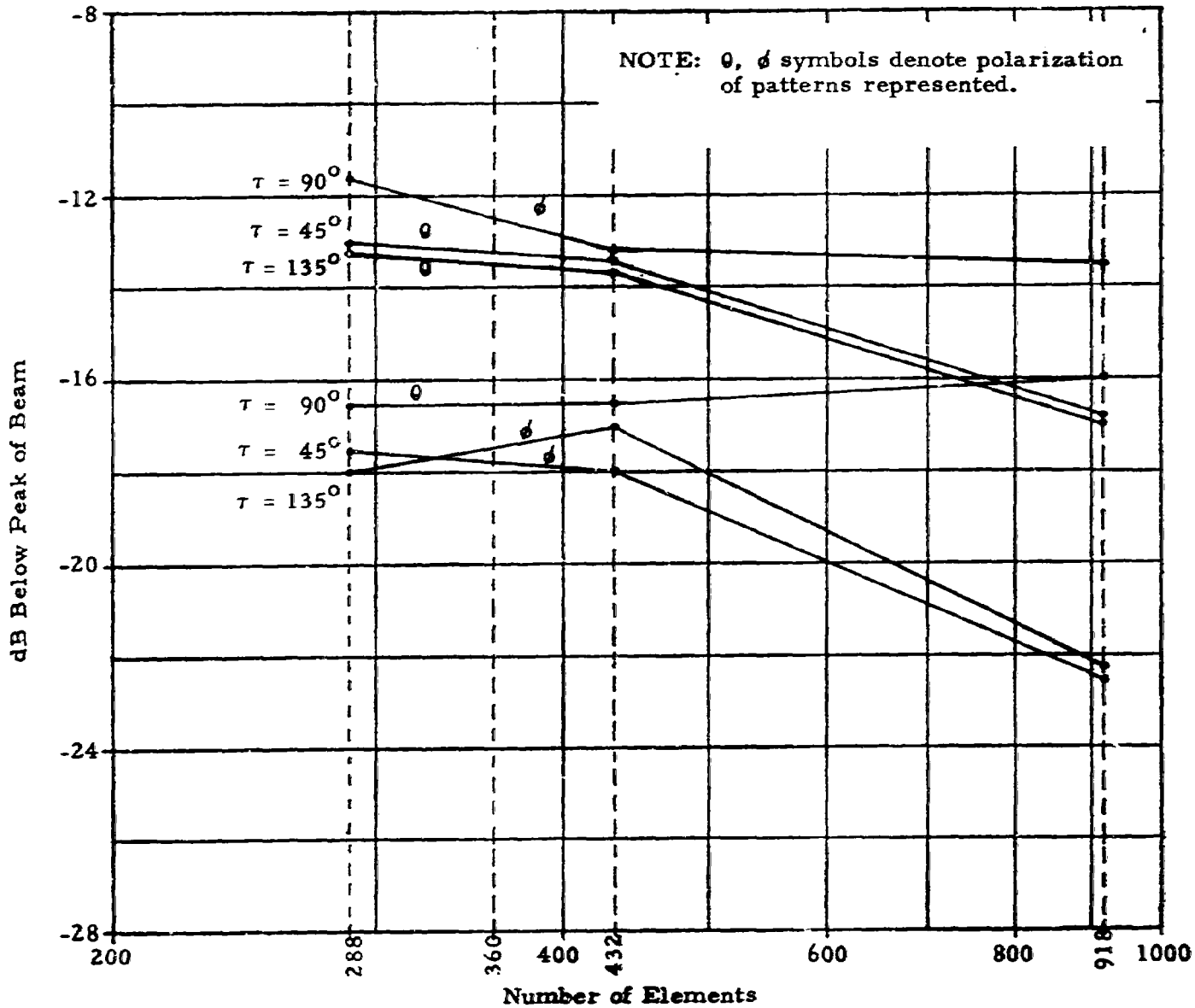

Figure 4.0-5. Highest Shoulder or First Sidelobe vs. Number of Elements on Cone for Beam Pointing Direction of $\theta_1 = 55^\circ$, $\phi_1 = 45^\circ$

When that situation occurred the level of the first sidelobe was plotted instead of that of the highest shoulder. Figure 4.0-4 gives the data for the beam pointing directions of $\theta_1 = 0^\circ$, $\phi_1 = 0^\circ$ and $\theta_1 = 80^\circ$, $\phi_1 = 90^\circ$; while, as was done for the grating lobes, the second figure presents only data for $\theta_1 = 55^\circ$, $\phi_1 = 45^\circ$. Overall there is a slight trend for lower shoulders (or first sidelobes) with an increasing number of elements. There were also a few cases where some degradation occurred with an increase in the number of elements so that, as with the grating lobes, it is difficult to set any rules.

The beamwidths of the patterns were measured but not plotted because no difference could be determined as a function of slot configuration. This fact, together with the inconclusive changes in shoulder level mentioned above, indicate that the smallest number of elements used, 288, is satisfactory from the standpoint of forming the main beam. However, 288 elements are not satisfactory in regard to the grating lobes and backlobes formed. Systematic element locations tend to cause grating lobes; hence, the introduction of judicious amounts of randomization may tend to break up such lobes. Such configurations can be readily investigated with the computer program that has been devised for this study.

5.0 IMPROVED ELEMENT PATTERNS FOR SLOTS ON CONES

The use of an improved element pattern is being restudied for computations of patterns of arrays on cones. A rigorous calculation of the θ-polarized electric field component of circumferential slots has recently appeared in the literature (Pridmore-Brown and Stewart, 1972). The computer program for that calculation has been ordered. The program can be modified to give the ϕ-polarized electric-field component as well.

An approximate method has also been developed for calculating the patterns of circumferential slots (Pridmore-Brown, 1972). This technique requires significantly less computation time than does the rigorous technique and gives good results for the θ-polarized component of the electric field strength, except near the cone axis. The discrepancy near the axis results from the use of an asymptotic expansion of the Legendre functions that is not valid on the axis. The possibility of modifying this approximate technique to apply in the neighborhood of the axis is being considered.

REFERENCES

1. Kummer, W. H., A. T. Villeneuve, J. E. Howard, and A. F. Seaton, (1970), "Integrated Conformal Arrays", Final Report on Contract N00019-69-C-0281, Report No. 2767.01/214, Hughes Aircraft Company, January, 1969 to March, 1970.

2. Kummer, W. H., M. C. Behnke, A. F. Seaton, A. T. Villeneuve, (1971), "Integrated Conformal Arrays", Final Report on Contract N00019-70-C-0397, Report No. 2767.01/266, Hughes Aircraft Company, March, 1970 to January, 1971.

3. Pridmore-Brown, D. C., (1972), "Diffraction Coefficients for a Slot Excited Conical Antenna", IEEE Trans. on Antennas and Propagation, Vol. AP-20, No. 1, January, 1972, pp. 40-49.

4. Pridmore-Brown, D. C. and G. Steward, (1972), "Radiation from Slot Antennas on Cones", IEEE Trans. on Antennas and Propagation, Vol. AP-20, No. 1, January, 1972, pp. 36-39.

5. Seaton, A. F., and W. H. Kummer, (April, 1972), "Conformal Antenna Arrays Study", Quarterly Report on Contract N00019-72-C-0212, Report No. 2765.31/353, Hughes Aircraft Company, 1 Jan. to 1 April 1972.

6. Seaton, A. F., A. T. Villeneuve, and W. H. Kummer, (July, 1972), "Conformal Antenna Arrays Study", Quarterly Report on Contract No. N00019-72-C-0212, Report No. 2765.31/380, Hughes Aircraft Co., 1 April to 1 July 1972.

7. Seaton, A. F., A. T. Villeneuve, and W. H. Kummer, (Oct. 1972), "Conformal Antenna Arrays Study", Quarterly Report on Contract N00019-72-C-0212, Report No. 2765.31/407, Hughes Aircraft Company, 1 July to 1 October 1972.

8. IRIG Standard, "Coordinate System and Data Formats for Antenna Patterns", Document 111-65, revised Aug., 1965, Published May, 1966 by Secretariat, Range Commanders Council, White Sands Missile Range, New Mexico 88002.

DISTRIBUTION

Activity

Commander,
Naval Air Systems Command
Department of the Navy
Washington, D. C. 20360
Attn: Code AIR-53321A
AIR-360 E
AIR-310 B (5)
AIR-604 A (4)

Commander, Naval Ordnance
Systems Command
Department of the Navy
Washington, D. C. 20360
Attn. Code ORD-034

Director
Office of Naval Research
800 North Quincy Street
Arlington, Virginia 22217

Raytheon Company
Hartwell Road
Bedford, Massachusetts 01730
Attn: Mr. Walter Jeros

Space-General Corporation
El Monte, California 91733
Attn: Mr. T. Falco

Department of the Air Force
Air Force Avionics Laboratory
(AFSC) Attn: Harold Weber
Air Force Systems Command
Wright-Patterson Air Force Base
Ohio 45433

Applied Physics Laboratory
The Johns Hopkins University
8621 Georgia Avenue
Silver Spring, Maryland 20910
Attn: Mr. R. Mallalieu

Activity

Commanding Officer
U.S. Naval Air Development Center
Johnsville, Pennsylvania
18974
Attn: Mr. Jerry Guarini

Director
U.S. Naval Research Laboratory
Washington, D. C. 20390
Attn: Code 5360

Commander
U.S. Naval Weapons Center
China Lake, California 93555
Attn: Code 35
Code 40
Code 601

Commanding Officer
U.S. Naval Avionics Facility
Indianapolis, Indiana 46218
Attn: Mr. Paul Brink

Commander
U.S. Naval Missile Center
Point Mugu, California 93041
Attn: Merle Oberg, Code 5351

Dr. E. B. McMillan
Resources Development Institute
P. O. Box 86
Greenlawn, N. Y. 11740

Naval Electronics
Laboratory Center
San Diego, California 92152
Attn: J. H. Provencher (2)
Code 2330

Activity

Dr. G. Tricoles
General Dynamics/Electronics Division
P. O. Box 81127
San Diego, California 92138

Director, ElectroSciences Lab.
Ohio State University
1320 Kinnear Road
Columbus, Ohio 43212

Professor A. Hessel
Polytechnic Institute of Brooklyn
Route 110
Farmingdale, N. Y. 11735

Teledyne Ryan Company
5650 Kearny Mesa Road
San Diego, California 92119
Attn: Mr. H. Penner

Dr. Sidney Alexander
ABMDA
Commonwealth Bldg.
1320 Wilson Boulevard
Arlington, Virginia 22209

Dr. Robert J. Tims
Sperry-Rand Corporation
Sperry Gyroscope Division
Microwave Engineering Department
Great Neck, New York 11020

Philip Blacksmith
Air Force Cambridge Research Laboratories
Laurence G. Hanscom Field
Bedford, Massachusetts 01730

McDonald Douglas Astronautics Company
5301 Bolsa Avenue
Huntington Beach, California 92647
Attn: Mr. John Wright
Mail Stop 9
Department A3-830/BB10

Activity

Advanced Sensor Laboratory
U.S. Army Missile Command
Redstone Arsenal
Huntsville, Alabama 35809
Attn: Mr. W. Lindberg

Mr. Howard S. Jones, Jr.
Harry Diamond Laboratories
Microwave Research & Development Br.
Connecticut Ave. and Van Ness St., N.W
Washington, D. C. 20438

Unclassified

Security Classification

DOCUMENT CONTROL DATA - R & D

(Security classification of title, body of abstract and indexing annotation must be entered when the overall report is classified)

1. ORIGINATING ACTIVITY *(Corporate author)*
Hughes Aircraft Company
Culver City, California

2a. REPORT SECURITY CLASSIFICATION
Unclassified

2b. GROUP

3. REPORT TITLE
Conformal Antenna Arrays Study

4. DESCRIPTIVE NOTES *(Type of report and inclusive dates)*
Final Report January 1972 to January 1973

5. AUTHOR(S) *(First name, middle initial, last name)*
Wolfgang H. Kummer Alfred T. Villeneuve
Arthur F. Seaton

6. REPORT DATE	7a. TOTAL NO. OF PAGES	7b. NO. OF REFS
January 1973	94	8

8a. CONTRACT OR GRANT NO.	9a. ORIGINATOR'S REPORT NUMBER(S)
N000 19-72-C-0212	2765.31/421 HAC Ref. No. C-4634
b. PROJECT NO	
c.	9b. OTHER REPORT NO(S) *(Any other numbers that may be assigned this report)*
d.	None

10. DISTRIBUTION STATEMENT
Distribution limited to U.S. Agencies only; (Test and Evaluation) (January 1973). Other requests for this document must be referred to Commander, Naval Air Systems Command, AIR-310B, Washington, D. C. 20360

11. SUPPLEMENTARY NOTES	12. SPONSORING MILITARY ACTIVITY
	Air Systems Command Department of Navy Washington, D. C.

13. ABSTRACT

Two methods of synthesizing patterns from conical arrays were investigated during this period. In the first method the equivalence principle was used to synthesize patterns that are approximate duplicates of the patterns of representative planar arrays. This is done by evaluating on the surface of the cone the near field of a centrally located and mechanically steered hypothetical planar array. These near fields are used to calculate the required complex excitations of real elements on the surface of the cone to nearly duplicate the pattern of the hypothetical planar array. Patterns are presented of the results for two beam pointing directions.

In the second method of synthesizing patterns from a conical surface, a heuristic approach was taken wherein the placement of the elements on the surface was based on extrapolations from linear and circular array theory and practice. Several element configurations are considered and numerous computed patterns are presented. The characteristics of these patterns are summarized by comparing in graphical form grating lobe levels, first sidelobe levels, and back-lobe levels for all of the patterns.

DD FORM 1 NOV 68 1473

Unclassified

Security Classification

14. KEY WORDS	LINK A		LINK B		LINK C	
	ROLE	WT	ROLE	WT	ROLE	WT
Antenna						
Conformal						
Conical						
Array						
Element						
Grating Lobe						
Pattern						
Equivalence						
Heuristic						